THERMAL AND MECHANICAL RESPONSES OF FIBER REINFORCED POLYMER COMPOSITES UNDER ONE-SIDED FIRE EXPOSURE

by

Ziqing Yu

A dissertation submitted to the faculty of
The University of North Carolina at Charlotte
in partial fulfillment of the requirements
for the degree of Doctor of Philosophy in
Mechanical Engineering

Charlotte

2012

Approved by:

_____
Dr. Aixi Zhou

_____
Dr. Qiuming Wei

_____
Dr. Russell G Keanini

_____
Dr. Jozef Urbas

ABSTRACT

ZIQING YU. Thermal and mechanical responses of fiber reinforced polymer composites in fire (Under the direction of DR. AIXI ZHOU)

This research investigated the thermal and mechanical responses of fiber reinforced polymer (FRP) composites in fire. The research focused on thermal decomposition and heat transfer, deformation, delamination, and structural integrity of FRP composites. The research was undertaken by thermal and fire testing, and fire dynamics and finite element modeling.

To simplify the modeling of the decomposition of FRP composites, an infinite-rate pyrolysis model was incorporated into heat transfer modeling to predict the thermal response of the composite panels under one sided heating. The thermal prediction by the infinite-rate model was compared to the finite-rate model, in which the decomposition was described by Arrhenius equation, and was validated with both bench and intermediate scale fire tests. A concept of shift temperature was introduced into the heat transfer to account for the effect of heating rate on the decomposition temperature.

With temperature results given by the heat transfer model, a simplified plane strain model was proposed to predict the mechanical response of FRP composites. Based on a bilinear traction-separation law, cohesive elements in commercial finite element software ABAQUS were incorporated in the mechanical model to consider the effect of delamination for sandwich panels.

In order to evaluate the effect of heat flux of a composite's own flame on its thermal response and fire properties, two-layer flame geometry was proposed to predict the effect of flame heat flux on the thermal response of char-forming materials. The total

flame heat flux in a typical cone test was estimated based on general turbulent flame temperature and combustible gas temperature.

All prediction results were validated with experimental data. It was demonstrated that (1) the modeling of decomposition reaction using the infinite-rate model required less input parameters, (2) a material's own flame had significant influent on its fire reaction properties at the beginning of flaming combustion, (3) the plane-strain model was capable of predicting deformation and time-to-failure with a good accuracy, and (4) cohesive elements can be used to model the delamination of sandwich FRP panels in fire

ACKNOWLEDGEMENTS

First of all, I would like to thank Dr. Aixi Zhou**,** my academic advisor, mentor, and friend during my study at UNC Charlotte. It is Aixi who introduced me into the field of fiber reinforced polymer composite materials and fire safety science and engineering. It has been a great pleasure working with Aixi over the past three years. His constant enthusiasm, encouragement, patience and optimism have always motivated me; whenever I had trouble with my research or personal issues, Aixi was always here helping me. I thank him very much.

I also want to thank Dr. Qiumin Wei, my committee member, for his time and encouragement when I have hard time in my daily life and PhD research. His PhD pursuing experience has been inspiring me all the way in my PhD research at UNC Charlotte.

My special thanks go to Dr. Russell Keanini, my committee member, for his knowledge and guidance for my research on fluid mechanics. I will never forget his kindness and compliments each time I see him.

I would like to thank Dr. Joel Urbas, my committee member, our fire expert, for his help and suggestions on our fire tests. I'm very impressed by his knowledge and experience on fire testing. I appreciate his careful review of my dissertation.

I learned so much about finite element analysis from the finite element course taught by Dr. Kingshuk Bose. I thank him for his help with my finite element modeling in my research.

I also appreciate assistances from Mr. William (Bill) Lindsey, our lab manager in the Department of Engineering Technology, in preparation of fire testing specimens. I was keeping him busy.

And finally, but most importantly, I want to thank my mother and father, my brothers and sisters, my wife, and my son and daughter who are always proud of me. Without their love, support, and encouragement, it is an impossible task to do my PhD study in the United States. I owe them too much.

TABLE OF CONTENTS

LIST OF TABLES

LIST OF FIGURES

LIST OF SYMBOLS

A	Rate constant (1/s)
A_{fl}	The bounding area of flame (m^2)
C_{app}	Apparent specific heat capacity (J/kg.K)
C_g	Gas specific heat capacity (J/kg.K)
C_p	Specific heat capacity (J/kg.K)
C_r	Resin specific heat capacity (J/kg.K)
D_{eff}	Equivalent diameter (m)
d	Thickness (m)
E	Activation energy (J/kg.mol)
E_c	Compressive modulus (Pa)
E_{c_0}	Virgin material compressive modulus (Pa)
E_t	Tensile modulus (Pa)
E_{t_0}	Virgin material tensile modulus (Pa)
F	The remaining virgin material fraction
f_v	Soot fraction
G	The shear relaxation modulus (Pa)
G_c	Fracture energy (N/m)
h	Enthalpy (J/kg)
h_c	heat transfer coefficient ($W/m^2.K$)
h_g	Gas enthalpy (J/kg)

I	Mean beam length (m)
K	The effective emission coefficient
k	Thermal conductivity (W/m.K)
k_r	Resin thermal conductivity (W/m.K)
k_{r_eff}	The effective resin thermal conductivity (W/m.K)
L_c	The unsupported length (m)
L_{fl}	Flame height (m)
L_g	Heat of gasification (kJ/g)
m	Instantaneous mass (kg)
m_0	Initial mass (kg)
$\dot{m}''$	Mass loss rate per unit area (kg/s.m²)
m_g	Gas mass (kg)
$\dot{m}_g''$	Gas mass flux (kg/s.m²)
N	The strain hardening parameter
n	Order of decomposition reaction
P	Pressure (N/m²)
P(T)	Temperature dependent material property
P_c	Euler buckling load (Pa)
P_R	The relaxed material property
P_t	Failure load under tension (Pa)
P_{t_0}	Virgin material failure load under tension (Pa)

P_{t_ch}	Char failure load under tension (Pa)
P_U	The un-relaxed material property
$\dot{Q}$	Heat release rate (W)
$\dot{q}''$	Heat release rate per unit area (W/m²)
$\dot{q}''_{conv}$	Convective heat flux (W/m²)
$\dot{q}''_{cr}$	The critical heat flux (W/m²)
$\dot{q}''_{e}$	Incident heat flux (W/m²)
$\dot{q}''_{fl}$	Flame heat flux (W/m²)
$\dot{q}''_{l}$	Heat loss (W/m²)
$\dot{q}''_{net}$	Net heat flux (W/m²)
$\dot{q}''_{pk}$	Peak heat release rate per unit area (W/m²)
$\dot{q}''_{rad}$	Radiation heat flux (W/m²)
Q	Decomposition heat (J/kg)
R	Universal gas constant (8.31 J/mol.K)
S_{ijkl}	Compliance tensor
T	Temperature (K)
T_g	Gas temperature (K)
T_p	The decomposition temperature (K)
T_p^{max}	Maximum decomposition temperature (K)
T_p^{min}	Minimum decomposition temperature (K)
T_{sh}	The shift temperature (K)
T_∞	Ambience temperature (K)

T_g'	Glass transition temperature (K)
t	Time (s)
t_n	Normal stress (Pa)
t_s	Shear stress (Pa)
t^0	The peak stress (Pa)
t_n^0	Peak normal stress (Pa)
t_s^0	Peak shear stress (Pa)
V	Volume fraction
V_{fl}	Flame volume (m^3)
v	Velocity (m/s)
W	Weight fraction

Greek symbols

α_{ij}	Thermal expansion coefficient
β	Heating rate (K/s)
β_{ij}	Moisture coefficient
γ_Y	The shear strain at the yield point
ΔA	Cross-section area (m^2)
ΔH_c	The effective heat of combustion (kJ/g)
$\Delta H_{c,ideal}$	The ideal heat of combustion (kJ/g)
$\Delta(MC)$	Moisture difference
ΔT	Temperature difference (K)
$\Delta \upsilon_c$	Char expansion

δ_f	Failure strain
ε	Emissivity
ε_{ij}	Strain tensor
Λ_{ij}	Pressure coefficient
ρ	Instantaneous density (kg/m³)
Φ	Porosity
$\overline{\emptyset}$	Initial fiber misalignment angle
χ_{ij}	Char expansion coefficient
σ	Stefan-Boltzmann constant ($W/(m^2K)$)
σ_{av}	Average strength (Pa)
σ_c	Compressive strength (Pa)

Subscripts

ch	Char
d	Decomposed state
f	Fiber
fl	Flame
r	Resin
s	Surface
v	Virgin state

CHAPTER 1: INTRODUCTION AND BACKGROUND

1.1. Introduction

1.1.1 Applications of fiber reinforced polymer composites

Fiber reinforced polymer (FRP) composites are high-performance materials that use fiber reinforcements for load resistance and a matrix for holding and protecting the fibers and transferring loading among fibers. The main advantages of FRP composites include high specific stiffness and strength, excellent corrosion resistance, good fatigue endurance, and tailorable mechanical properties.

FRP composites have been widely used in aerospace and aircraft structures, automobile structures, ships and boats, buildings, and civil infrastructures. FRP composites offer lower densities and higher specific strength than steel and aluminum used in the automobile industry. The main purpose of using FRP composites in the industry is to reduce the weight of automobile and increase the fuel efficiency. Hybrid technology, also known as plastic-metal composite technology, has long since established itself in the automotive industry as a method for manufacturing lightweight structural components. High-tech plastics now are used to produce a wide variety of automotive parts such as air intake manifolds, integrated oil filters, front end modules, headlamp bezels, pedal bearing blocks, brake pedals, door handle assemblies, mirror bases and airbag housings.

To reduce topside weight and minimize damage from corrosion and fatigue, US navy is expanding the use of FRP composites to superstructures, bulkheads, helicopter

hangers and other large shell-like structures. US Navy uses mainly thick sandwich structures with FRP laminate skins and balsa core. The structures have very light weight, high flexural rigidity, and excellent insulation characteristics.

The civil applications of FRP composites include building, bridge, pipeline, and storage tanks. For an example, FRP composites can be used to strength the beams, columns and slabs in buildings.

While the use of FRP composites is increasing in all applications, challenges remain due to poor fire performance of FRP composites. The thermal and mechanical response of FRP composites exposed to high temperature must be assessed before their applications. To ensure the fire safety of structures using FRP composites, the designer needs to satisfy either the prescriptive-based design requirements or the performance-based design requirements. In building applications, FRP materials must meet the performance criteria described in the standard fire tests, such as ASTM E84 [1], NFPA 286, and ASTM E119[2], when the prescriptive-based approach is used. US Navy has a stringent regulation [3] on the use of FRP composite in naval vessels. In aspects of the surface flammability, fire growth, smoke production and toxicity, test methods and acceptance criteria are described in details to ensure proper applications of FRP materials. Performance-based design provides an optional approach to meet fire safety goals and objectives based on quantitative assessment of design. For applications with FRP composites, their thermal and mechanical responses must be evaluated with thermal, fire, and mechanical models to satisfy performance objectives and performance criteria.

1.1.2 Fire damages of FRP composites

Fire damages [4] suffered by FRP structures are softening, degradation of the matrix, char formation, delamination, and matrix cracking. Softening and degradation of the matrix takes place around the glass transition temperature; Char formation is due to the thermal decomposition of the matrix; Delamination and cracking are due to misalignment deformation of plies or local kinking.

The fire damage experienced by sandwich FRP structures is somewhat different from laminate structures due to the core material. The interfaces between two face skins and core material are vulnerable to delamination when the decomposition of the core material occurs.

The char formation of FRP structures plays an important role in the thermal and mechanical response of FRP composites in fire. The char of FRP composites affects the thermal and mechanical responses in several ways. First, the char is a porous carbonaceous material with poor thermal conductivity and thus behaves as a thermal insulation layer to the remaining virgin material. Secondly, as the char layer becomes thicker, it limits the access of oxygen from ambience to the decomposition zone and consequently reduces the decomposition rate. Finally, the char can help keep the structural integrity of FRP structures in fire by holding fibers in place after the matrix has been degraded. The delamination and cracking reduces the resistance ability of a FRP structure to mechanical loading and eventually may lead to the collapse of the structure.

1.2. Background

1.2.1. Experimental techniques and standards to determine fire properties of FRP

Main apparatuses that can be utilized to determine basic thermal properties and the decomposition properties of FRP composites are Thermo-gravimetric Analyzer (TGA), Differential Scanning Calorimeter (DSC), and Hot-Disk.

TGA is used to determine the decomposition kinetics of polymer by measuring mass loss histories of polymer samples heated at a constant heating rate. Both powder and fragment samples can be used in a TGA test. The decomposition kinetics of FRP composites defines the relationship between the decomposition rate and temperature. The decomposition kinetics parameters include rate constant, activation energy, and the order of decomposition reaction. In the test, powder or fragment samples are heated up at a constant heating rate (ºC/min) and mass history is recorded. Decomposition kinetics can then be determined by curve fitting of TGA results.

Differential scanning calorimeter is the main equipment to measure specific heat capacity and the heat of decomposition of FRP composites. ASTM E1269 [5] provides a standard test method for the determination of specific heat capacity by differential scanning calorimeter. The test method consists of heating a sample and a reference material at a constant heating rate in a controlled atmosphere through a temperature range of interest. Heat flow histories into the sample and a reference material are monitored and recorded. Because the temperature-dependent specific heat capacity of the reference material is well known, the specific heat capacity and the heat of decomposition can be determined by comparing the heat flow of the sample to that of the reference material.

For the determination of fire properties of combustible materials, ASTM E1354 [6] provides a laboratory procedure with a cone calorimeter for measuring the response of materials exposed to controlled levels of radiant heating with or without an external igniter. The cone calorimeter is the most versatile bench-scale instrument for measuring the fire reaction properties of FRP composites. Fire tests with a cone calorimeter can be performed with specimen in a horizontal or vertical direction. The procedure is primarily used to determine the heat release rate, mass loss rate, time-to-ignition, the effective heat of combustion, and the smoke production.

To overcome the limitation of a cone calorimeter that is only applicable to test small flat specimens, ASTM E1623 [7] offers a technical procedure using intermediate scale calorimeter (ICAL) to determine fire properties of combustible materials in their end-use conditions in an intermediate size (1x1m), which is sufficiently large to allow fire tests to be performed on complex structural sections and components. In addition to fire properties that can be measured in a cone calorimeter, ICAL also can be conveniently used to measure the surface emissivity and temperature distribution of a combustible material with a thermal pyrometer and thermocouples.

Both Cone calorimeter and ICAL are based on the oxygen consumption principle [8], which states that the heat released per unit of oxygen consumed is near a constant of 13.1kJ/g for most organic materials.

The cone calorimeter and ICAL are mainly used to determine the fire reaction properties of a combustible material, such as time-to-ignition, mass loss rate, heat release rate, smoke production and development. To determine the fire resistance properties of a FRP structure, such as structural integrity, thermal insulation, burn-through resistance, a

furnace test can be used for that purpose [2]. The test method involves heating a large composite panel commonly in its end-use conditions by a gas or electric furnace [10]. A tensile, compressive and/or bending load can be applied to the panel during the thermal exposure. Temperature, heat flux, and deformation of the panel are monitored and recorded. Different from the heating conditions in a cone calorimeter or an ICAL where a controlled heat flux is applied to a specimen, the furnace temperature in a furnace test follows a standard temperature-time curve.

The furnace test method [9] is often used for large FRP panels. Radiant heat flux test [89] offers a test method to determine compressive or tensile strength of FRP beams under one-sided heating. The test method involves irradiating one-side of a specimen with a constant heat flux while simultaneously a compressive or tensile loading is axially applies to the specimen. Temperatures, strains, and time to failure of the specimen are recorded. Thermal insulation and strength of the composite can then be evaluated based on experimental data.

1.2.2 Heat transfer models for the predictions of thermal response of FRP composites

When a FRP composite is exposed to fire, it receives the combined heat flux of thermal radiation and convection. Before the decomposition temperature of the FRP composite is reached, the composite undergoes only heat conduction with thermal expansion. Thermal expansion has negligible effect on heat transfer because it costs fractional energy. Once the decomposition temperature is reached, the matrix resin, organic fibers, and/or core material for a sandwich structure of the composite will decompose with char formation for thermosets and the generation of heat for an exothermic reaction or absorption of heat for an endothermic reaction, which acts as a

heat source or heat sink inside the composite. Meanwhile, the decomposition reaction will generate volatiles, including combustible and inert gases that initially are trapped in the composite due to low permeability. As the volatile gases accumulate in the composite, internal pressure builds up in gas-filled pores that complicates the heat transfer process in terms of internal gas convection and so called cavity radiation. When the permeability is larger enough due to char formation, cracking, or delamination, the volatiles make their way out of the composite. The movement of the internal volatiles has a cooling effect on the composite because in general gas products have higher specific heat capacity. Once the released combustible gases meet the combustion conditions, such as a minimum concentration of combustible gases, the composite will be ignited and flame will form at the surface with thermal feedback into the composite, which in turn drives the composite to decompose at a higher rate until the composite is completely decomposed.

In the whole thermal process, heat energy loses into ambience through all possible boundaries of the composite by means of thermal radiation, heat convection, and heat conduction if the composite shares boundaries with other solids.

In predicting the thermal response of FRP composites, numerous heat transfer model can be found in the literature. Those thermal models differ in capability and accuracy to account for the effects of the decomposition reaction and fire damages on heat transfer. The simplest model to calculate temperature in an FRP panel is the standard one-dimensional heat conduction equation, where decomposition's effects are neglected. The equation is good for temperature prediction before the occurrence of decomposition. Mouritz and Gibson [10] provided a good review of thermal models of FRP composites

exposed to fire or high temperature. As stated in their book, the first heat transfer model that can account for the thermal decomposition of polymer matrix was developed by Pering, Farrell and Springer [11]. In the one dimensional model as shown in Equation (1.1), a source term equal to the product of the decomposition by the theoretical mass loss rate was added to consider decomposition's effects.

$$\rho C_p \frac{\partial T}{\partial t} = \frac{\partial}{\partial x}\left(k \frac{\partial T}{\partial x} \right) + \frac{\partial m}{\partial t} Q \tag{1.1}$$

A more sophisticated model, which is capable of taking into account the diffusion of decomposition induced gas in addition to the decomposition heat, was presented by Henderson and colleagues [12],

$$\rho C_p \frac{\partial T}{\partial t} = \frac{\partial}{\partial x}\left(k \frac{\partial T}{\partial x} \right) - \dot{m}_g'' C_g \frac{\partial T}{\partial x} - \frac{\partial \rho}{\partial t}(Q + h - h_g) \tag{1.2}$$

where the cooling effect of internal gases was calculated based on convective mass transfer theory and the decomposition reactions were modeled with Arrhenius equation.

Based on the original work by Henderson et al. [12], Florio, Henderson, Test and Hariharan [13] developed a remarkable model (Equation (1.3))in which not only the heat conduction, pyrolysis, diffusion of decomposition gas, but also the effects of thermal expansion and internal pressure were considered.

$$\begin{aligned} m_g C \frac{\partial T}{\partial t} = \dot{m}_g'' \Delta A \Delta x C \frac{\partial T}{\partial t} + \Delta A \Delta x \frac{\partial}{\partial x}\left(k \Phi \frac{\partial T}{\partial x} \right) + h_r \Delta A \Delta x (T_s - T_g) + \Delta A \Delta x \frac{D(\Phi P)}{Dt} \\ - \frac{\partial m}{\partial t}\left(h(T_s) - h_g + v^2/2 \right) \end{aligned} \tag{1.3}$$

However, as shown by the researcher himself, taking expensive computation cost to consider the effects of thermal expansion and internal gas pressure cannot significantly improve the temperature prediction in decomposing composite materials.

In literature, other heat transfer models for composite structures can also be fund but with little difference from the models mentioned above [10]. Because too many factors affect heat transfer in the chemical reaction of decomposition and no accurate temperature, heating rate, and/or temperature gradient dependent thermal properties as well as thermal boundaries are available, it is acknowledged that there is no single heat transfer model suitable for all applications even though some models are mathematically capable of accounting for many phenomena in decomposition.

The decomposition of FRP composition has a remarkable influence on the process of heat and mass transfer. A common way for modeling the decomposition of FRP composites takes advantage of Arrhenius equation to relate the decomposition rate with temperature. The decomposition kinetics parameters in the Arrhenius equation can be determined with a series of TGA tests as described in the introduction section. Pyrolysis models using the Arrhenius equation or other analytical functions are referred as to finite-rate pyrolysis models. Another way to consider the decomposition is based on the assumption that decomposition takes place at infinite rate at a single decomposition temperature point. Pyrolysis models based on this assumption can be referred as to infinite-rate pyrolysis models.

Thermal boundary conditions define the heat and mass exchange through all boundaries and thus affect the whole heat transfer process inside the material of interest. Thermal boundary conditions must be accountable for thermal exposure to fire, thermal insulation, and heat loss. The thermal exposure to a fire is typically modeled as a heat flux boundary condition. The heat flux from a fire includes convection and radiation, which is described by

$$-k\frac{dT}{dt} = \varepsilon_{fl}\sigma T_{fl}^4 - \varepsilon_s\sigma T_s^4 + h_c\left(T_{fl} - T_s\right) \tag{1.4}$$

where ε_{fl} and ε_s are the emissivities of the flame and the exposed surface, respectively; T_{fl} and T_s are the temperatures of the flame and the exposed surface, respectively; h_c is the convective heat transfer coefficient. The first term on the right side of the above equation is the radiation from fire, second term is re-radiation heat loss from the exposed surface; last term is convective heat transfer.

In applications where the external heat flux is measured with a water cooled heat flux, the thermal boundary condition is given by

$$-k\frac{dT}{dt} = \dot{q}_e^{"} + \varepsilon_s\sigma(T_s^4 - T_\infty^4) + h_c(T_s - T_\infty) \tag{1.5}$$

where $\dot{q}_e^{"}$ is the heat flux from an external heat source measured by the heat flux gauge and T_∞ is the ambient temperature. It is noted that the thermal feedback of a material's own flame is not considered in the boundary condition.

Thermal insulation boundary can be described by

$$-k\frac{dT}{dt} = h_c(T_s - T_\infty) \tag{1.6}$$

where h_c is the conductive heat transfer coefficient defining the heat transfer rate between the material of interest and the insulation layer. The coefficient can be determined based on the thermal conductivity of the insulation material and insulation thickness. h_c*=0* defines an ideal thermal insulation boundary.

1.2.3. Mechanical models in literature to predict structural response of FRP in fire

With knowledge of temperature profile and thermal decomposition from thermal response models, the mechanical response of FRP composites in the combined thermal and mechanical loading can be assessed with a mechanical model.

The first analytical mechanical model by McManus and Springer [14] used the following governing equation to include the influence of thermal expansion, internal gas pressure, moisture as well as charring expansion.

$$\varepsilon_{ij} = S_{ijkl}\sigma_{kl} + \alpha_{ij}\Delta T + \Lambda_{ij}\Delta P + \beta_{ij}\Delta(MC) + \chi_{ij}\Delta v_c \tag{1.7}$$

where $\alpha, \Lambda, \beta, \chi$ are the thermal, pressure, moisture, and charring expansion coefficients, and $\Delta T, \Delta P, \Delta(MC), \Delta v_c$ are the temperature, pressure, moisture content and char volume differences, respectively. The model was remarkable but expensive or less practical since all the coefficients must be experimentally determined before stress and strain can be calculated.

By describing the progressive reduction of mechanical properties of FRP composites over temperature increase with an analytic function, the progressive softening model can be used to calculate the loss of stiffness, strength and time to failure. In the model, the properties, including Young's modulus, shear modulus, and compressive strength, can be described with the error function or the hyperbolic function as shown in the following

$$P(T) = \frac{P_U + P_R}{2} - \frac{P_U - P_R}{2}\,\mathrm{erf}\left(\varphi\left(T - T_g'\right)\right) \tag{1.8}$$

$$P(T) = \frac{P_U + P_R}{2} - \frac{P_U - P_R}{2}\tanh\left(\varphi\left(T - T_g'\right)\right) \tag{1.9}$$

where P(T) is the particular mechanical property; P_U and P_R are the un-relaxed (low temperature) and the relaxed (high temperature) value of the property, respectively; T_g' is the mechanically determined glass transition temperature; φ is a constant describing the breath of the distribution. To account for thermal decomposition, a power law factor based on the residual resin content is used to predict the mechanical properties upon the onset of thermal decomposition.

Mouritz and Mathys [15] developed a two-layer model that can be used to estimate the residual strength and time to failure of a FRP laminate under combined tensile loading and one-sided heating. The model assumes that a fire damaged laminate consists of a char layer and a virgin layer. The tension and compression modulus are given, respectively, by

$$E_t = \left(\frac{d - d_{ch}}{d}\right) E_{t\_0} + \frac{d_{ch}}{d} E_{t\_ch} \tag{1.10}$$

$$E_c = \left(\frac{d - d_{ch}}{d}\right) E_{c\_0} + \frac{d_{ch}}{d} E_{c\_ch} \tag{1.11}$$

The failure load under tension and the Euler buckling load are

$$P_t = \left(\frac{d - d_{ch}}{d}\right) P_{t\_0} + \frac{d_{ch}}{d} P_{t\_ch} \tag{1.12}$$

$$P_c = \frac{C\pi^2 E_c b (d - d_{ch})^3}{12 L_c^2} \tag{1.13}$$

where d and d_{ch} are the total thickness and char layer thickness, respectively; L_c is the unsupported length of FRP beams.

Based on the Budiansky and Fleck kinking failure model [16], Boyd SE [17] and coworkers used the time-temperature superstition principle to develop a time-temperature dependent compression strength model:

$$\sigma_c(t,T) = G(t,T)\left[1 + N\left(\frac{3}{7}\right)^{\frac{1}{N}}\left(\frac{\overline{\emptyset}/\gamma_Y}{N-1}\right)^{\frac{N-1}{N}}\right]^{-1} \tag{1.14}$$

where G is the shear relaxation modulus, N is the strain hardening parameter, γ_Y is the shear strain at the yield point, and $\overline{\emptyset}$ is the initial fiber misalignment angle. The model considers the visoelastic effect as well as the initial local shear yield due to the initial fiber misalignment.

1.3 Challenges and Research Objectives

Despite the knowledge gained into the fire behavior of FRP composites, significant gaps remain in our understanding of their fire properties. The main challenges for predicting fire behavior of FRP composites are:

(1) The heat transfer and mass transfer through the boundaries and inside the FRP composite are very complicated and only can be approximated to some degree,

(2) It is difficult to obtain accurate temperature and heating rate dependent mechanical, thermal, and chemical properties for model input, and

(3) The complexity of failure mechanisms involved when an FRP structure is subjected to simultaneous fire and mechanical loads.

The validation of the fire response predictions of FRP composites depends on fire tests. Laboratory fire tests have a limited representation to that an FRP composite undergoes in case of fire. The limitations are:

(1) The thermal loading applied has a limited representation to real fire scenarios,

(2) Specimens have a limited representation to FRP structures in end-use conditions, and

(3) Only simple ventilation, fire growth and spread modes can be replicated in a laboratory environment through fire testing apparatus.

Most thermal models for the predictions of fire response of FRP composite are one-dimensional (1D) heat transfer models. The current three-dimensional (3D) fire assessment model is only applicable for the cases where the decomposition reaction does not occur. The reason is that there is no simple way, if not impossible, to define the movement of internal decomposition volatiles and their corresponding mass boundary conditions in 3D. For example, the most accepted thermal model to predict the thermal response of FRP composite, Henderson's 1D model, in which the modeling of internal gas convection rests on the assumption that there is no mass flux at the back surface all the time and all decomposition gases escape out of the material through the exposed surface. The assumption is reasonable for an FRP panel is exposed to one-sided heating before the back surface reaches the decomposition temperature where. However, for a FRP structure engulfed in a fire, it is not possible to obtain well-defined mass flux boundary conditions. On the other hand, most available models were validated only with small scale fire tests.

Another drawback of most current thermal models is the ignorance of thermal feedback from an FRP composite's own flame, which may disguise the fire hazard of a FRP structure.

Thus, the overall objective of this research was to improve the predications of the thermal and mechanical responses of FRP composites under one-sided heating. To achieve this goal, specific objectives were:

1. To quantify the significance of the convection effect of internal decomposition volatiles.
2. To validate 1D heat transfer models with bench-scale and intermediate-scale fire tests.
3. To develop simplified decomposition model to predict mass loss rate.
4. To propose a flame model to evaluate the effect of thermal feedback of an FRP composite's own flame.
5. To simplify current mechanical models that incorporate the modeling of thermal response and fire damages into the model.
6. To validate the simplified mechanical models with structural fire test data.

1.4. Organization

The dissertation consists of five chapters. The first chapter is literature review. The second to fourth chapters are based on three research papers, respectively. Each of the three chapters includes literature review, research methodology, test results, and conclusion. The second chapter describes fire testing for thermal and fire properties of FRP composites and evaluates the effects of pyrolysis modeling, internal gas convection, and thermal boundary conditions on thermal response of FRP composites. The third chapter focuses on the modeling of lateral deflection, in-plane deformation, and delamination with a plane-strain mechanical model. The fourth chapter presents a two-layer flame model and investigates the effects of a FRP composite's own flame on fire

properties. The fifth chapter summarizes conclusions of this research and provides directions for future research on the thermal and mechanical responses of fiber reinforced polymers in fire.

CHAPTER 2: VALIDATING THERMAL RESPONSE MODELS USING BENCH-SCALE AND INTERMEDIATE-SCALE FIRE EXPERIMENT DATA[1]

2.1 Abstract

The thermal response of fiber reinforced polymer composite was measured by bench-scale Cone Calorimeter and Intermediate-scale Calorimeter (ICAL) fire experiments. Finite-rate and infinite-rate pyrolysis models were used to predict the response of the composite panels under the same thermal boundary conditions as in the fire tests. It was shown that both models can give acceptable temperature, mass loss and effective char thickness predictions. The effect of internal gas convection on thermal response prediction was determined insignificant at low heat flux levels. The thermal insulation at the back surface significantly increases both temperature and mass loss predictions.

2.2 Introduction

Fiber Reinforced Polymer (FRP) composites are being increasingly used in many engineering structures where fire safety requirements are stringent, such as aircrafts, automobiles and trains, buildings, and ships. When exposed to sustained heating or fire conditions, FRP materials will degrade, decompose, generate heat and flame, and yield

---

[1] This chapter is based on a manuscript with the same title that has been accepted for publication by Mechanics of Advanced Materials and Structures. Chapter 2 provides more details than the manuscript due to page limit of a journal article.

smoke and gases. The structure will possibly collapse under combined mechanical and thermal loads. As a result, FRP composites may be dangerous and even deadly to passengers or occupants. Concerns about the fire performance of FRP materials have affected their wider applications in structures where fire risk is high.

To ensure the fire safety of structures using FRP composites, the designer needs to satisfy either the prescriptive-based design requirements or the performance-based design requirements [18-19]. When using the prescriptive-based approach in the International Building Code [18], FRP materials are required to meet the performance criteria described in the referred standard fire tests, such as ASTM E84, NFPA 286, and ASTM E119. When using a performance-based approach, the behavior of the designed FRP materials and structures in fire must be evaluated against design fire scenarios to meet all performance criteria set by the project stakeholders [19]. For non-load bearing applications, a fire growth analysis must be performed to estimate fire development and fire products generation. When used for load-carrying applications, a thermo-mechanical (or thermo-structural) analysis should be performed to examine the mechanical and structural response of FRP structures in fire. Both the fire growth analysis and the thermo-mechanical analysis require a thermal analysis to predict the thermal response of FRP structures in fire, such as the temperature rise in structures and the rate of decomposition (or pyrolysis) of the material. The thermal analysis is the first critical step since many physical and mechanical properties are affected by the decomposition process. In fact, the understanding of the thermal response of the composites provides the basis for all following tasks analyzing and designing FRP composites in fire.

The thermal response of FRP composites can be determined directly by thermal and fire tests. Common thermal tests include Thermo-gravimetric Analysis (TGA) for determining decomposition (or pyrolysis) kinetics, Differential Scanning Calorimeter (DSC) for determining phase transition and heat capacity, and instruments for measuring temperature-dependent thermal conductivity and other material properties. In addition to thermal tests, fire tests are used to determine the thermal response and fire behavior of FRP materials in fire conditions, including bench-scale fire tests using a Cone Calorimeter [20] and intermediate-scale fire tests using an Intermediate-scale Calorimeter (ICAL) [21]. Fire tests in the Cone Calorimeter use flat squared 10cmx10cm specimens typically at a horizontal orientation with the back surface thermally insulated. The ICAL tests use flat squared samples in the size of 100cm x 100cm. The ICAL was developed primarily to measure fire properties for products in a manner representative of their end use that cannot be tested in the Cone Calorimeter.

Alternatively, mathematical models may be used to estimate the thermal response of FRP composites in fire. A thermal response model in general includes two parts: a part for heat and mass transfer prediction and another part for pyrolysis (or decomposition) prediction. Although there are many heat transfer and pyrolysis models for combustible solids [22-23] in general and for FRP composites particular [11-13, 23-37], depending on how the rate of pyrolysis is described, these models can be categorized as finite-rate pyrolysis kinetics models and infinite-rate pyrolysis kinetics models [38-39]. A finite-rate model usually uses an Arrhenius reaction equation to describe the pyrolysis rate. An infinite-rate model assumes that a pyrolysis front with zero thickness separates the char layer from the virgin material and pyrolysis occurs at an infinite rate at a single pyrolysis

temperature point instead of a temperature range [38-39]. These two types of pyrolysis models have been widely used for predicting the thermal response of FRP composites in fire [11-13, 23-36]. In these studies, thermal properties obtained from TGA and DSC tests are usually used to predict the thermal response of the composites in fire conditions. However, the heating conditions in TGA and DSC tests [40-41] are quite different from Cone and ICAL fire conditions [20-21]. Samples in TGA or DCS are either in powder form or small fragment (a few grams in weight). Tests are done without ignition and flaming of the sample in a small enclosed space. While in Cone or ICAL tests, specimens are in plate forms and heated beyond ignition and flaming under well ventilated conditions. When performing validation, the key parameters are mass loss and temperature history data and the growth of char layer, because many other properties are dependent on the mass loss and temperature profiles as well as char thickness. For example, heat release rate can be estimated using mass loss rate and the heat of combustion of the material. The decomposition process and residual strength and stiffness properties are temperature and char thickness dependent. Although there are some validations of these models against mass loss and temperature data measured from small-scale fire tests [12-13, 25-36], there was no validation of these thermal models against both mass loss and temperature history data obtained from intermediate-scale fire tests. The effects of specimen size and boundary conditions on the fire performance of materials are significant. The lack of experimental validation of these thermal response models against fire experiment data across different scales motivated this study.

The purpose of this study was to validate two types of thermal response models using bench-scale Cone calorimeter and intermediate-scale ICAL fire testing results. The

key parameters in the validation work are mass loss and temperature histories as well as the char thickness growth of the composite material in fire. Fire tests using Cone and ICAL calorimeters were carried out to measure temperature histories, mass loss and mass loss rate histories, and the char growth of E-glass/polyester composite under constant heat fluxes. Then, thermal and fire dynamics parameters such as decomposed density and pyrolysis kinetics were determined with TGA tests. A finite-rate pyrolysis kinetics model and an infinite-rate pyrolysis kinetics model were used to predict the temperature and mass loss characteristics of the composite panels under the same thermal boundary conditions as in the Cone and ICAL fire tests. Temperature, mass loss (and mass loss rate) and char thickness predictions from both models were compared with experimental data from the fire tests for model validations. In addition, the significance of internal gas convection in predicting the thermal response of FRP composites in fire was also investigated, and the influence of thermal insulation on thermal response was evaluated.

2.3. Bench-Scale and Intermediate-Scale Fire Experiments

2.3.1. Experimental material and methods

The specimens in cone calorimeter tests and ICAL tests in the study were cut from 6.35mm (¼") thick pultruded E-glass/polyester panels. The fiber faction of the composite was 28.7% by volume and 40% by weight.

A Cone Calorimeter was used for bench-scale fire tests. The specimens of E-glass/polyester were tested in the horizontal orientation according to ASTM E1354 [20]. Specimen size was 10cm x10cm. Tests were conducted at heat flux levels of 25, 35, 45, 55, and 65kW/m^2. Mass loss histories were obtained for all tests. Due to the small size of the specimens and sensitivity of the equipment, to ensure the mass loss measurement

accuracy, no thermocouple was implemented to measure the temperature histories of Cone Calorimeter specimens.

An ICAL was used for testing the intermediate-size specimens of the same material. Specimen size was 100cmx100cm. ICAL tests were conducted at three heat flux levels: 25, 35, and 45kW/m^2 (the maximum heat flux is 50kW/m^2 for the ICAL). The apparatus is shown in Figure 2.1 and test procedures are described in details in ASTM E1623 [21]. Since the ICAL specimens are much larger, in addition to mass loss measurement, thermocouples and an infrared pyrometer were used to measure temperatures for both the exposed and the back surfaces of all ICAL specimens. The locations and layout of eight thermocouples for the exposed and the back surfaces were shown in Figure 2.2.

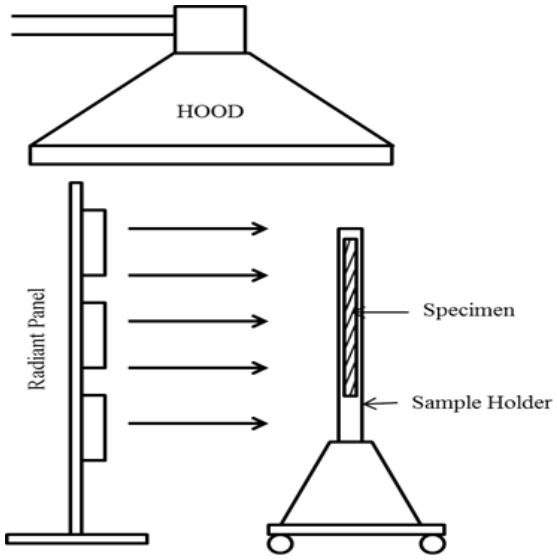

Figure 2.1: The schematic of ICAL (side view)

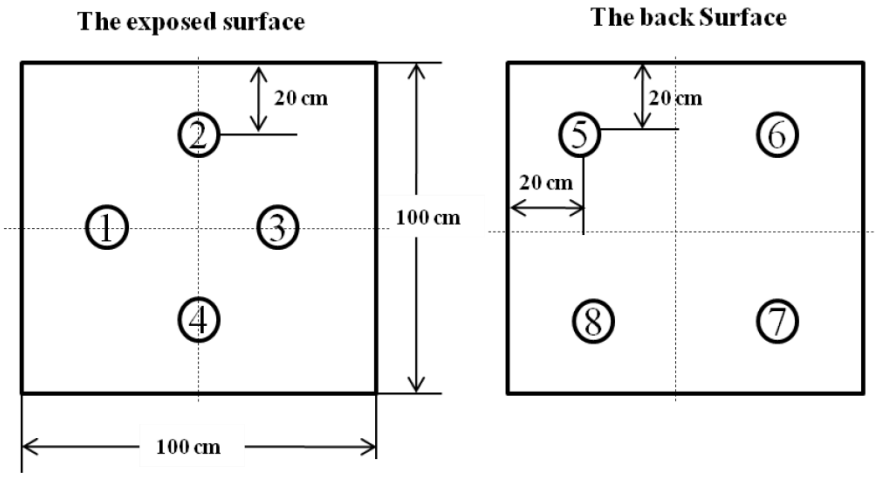

Figure 2.2 Thermocouple layout

A Heitronics infrared pyrometer, Model KT19.81 with a 0–1000°C temperature range and wavelength band of 8–10 mm was positioned behind a slot in the ICAL radiant panel and was aimed just above the thermocouple junction of thermocouple #2 to provide validation temperature data for thermocouple temperature measurement of the exposed surface. The spectral emissivity setting of the pyrometer was maintained at 1.0 during all ICAL tests [42]. The infrared pyrometer was calibrated at the factory with a blackbody furnace. Its limit of error is 0.5°C.

2.3.2. Specimen preparation

The specimens were cut directly from the pultruded E-glass/polyester panels. Cone Calorimeter specimens were conditioned in an environmental chamber at 23 ± 3°C and 50 ± 5% relative humidity per ASTM E1354 requirements. ICAL specimens were maintained in a conditioned room at 23 ± 3°C and 50 ± 5% relative humidity per ASTM E1623 requirements.

To measure the temperatures of the exposed surface of ICAL specimens, two holes 17.5 mm apart and 0.7 mm in diameter were drilled for each of the four thermocouples through specimens along the thickness direction. Thermocouple leads were then pulled through the holes such that the thermocouple junction on the exposed surface was positioned approximately in the middle of the holes.

To keep good contact between the thermocouple junction and the exposed surface during testing, approximately 5 g of weight was hung on the thermocouple lead wires as shown in Figure 2.3. The thermocouples were the bare 0.127 mm diameter type K with error limit of 2.2 °C or 0.75% of the temperature in °C.

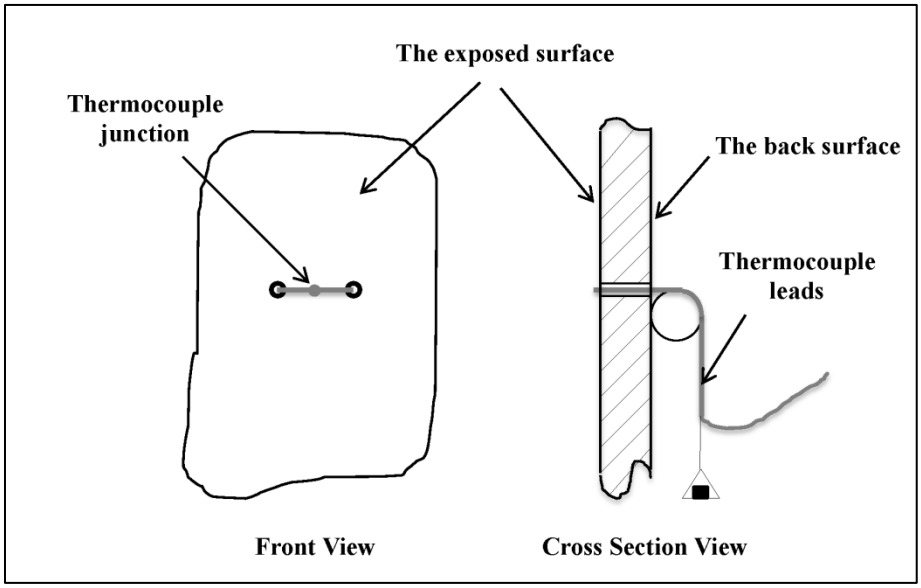

Figure 2.3: Thermocouple instrumentation at the exposed surface

To measure temperatures at the back surface, four thermocouples were attached to the surface using epoxy adhesive to ensure that thermocouple junction had good contact with the surface all time during the fire tests.

2.4. Thermal Response Models

2.4.1. Finite-rate pyrolysis model

Finite-rate pyrolysis models describe the pyrolysis rate with kinetics parameters. These parameters define pyrolysis reaction as a gradual process over a temperature range with finite pyrolysis rates. Mass loss prediction with the finite-rate model requires a heat transfer model to obtain temperature profile. Many researchers [12, 25, 28-32] based their models on the one presented in [12] for predicting the thermal response of FRP composites in fire. The finite-rate model in this work was based on Henderson's model [12] as shown in Equations (2.1)-(2.4). It is a one-dimensional model for a one-sided heating condition, and assumes that (1) no accumulation of decomposed volatiles in the composite, (2) heat and mass transfer take place only in the through-thickness direction, and (3) the mass flux at the unexposed surface is zero.

$$\rho C_p \frac{\partial T}{\partial t} = \frac{\partial}{\partial x}\left(k \frac{\partial T}{\partial x}\right) - \left(Q + h - h_g\right)\frac{\partial \rho}{\partial t} - \dot{m}_g'' C_g \frac{\partial T}{\partial x} \tag{2.1}$$

$$\frac{\partial \dot{m}_g''}{\partial x} = -\frac{\partial \rho}{\partial t} \tag{2.2}$$

$$\frac{\partial \rho}{\partial t} = -A(\rho_v - \rho_d)\left(\frac{\rho - \rho_d}{\rho_v - \rho_d}\right)^n \exp\left(-\frac{E}{RT}\right) \tag{2.3}$$

$$\dot{m}'' = -\int_0^d \frac{\partial \rho}{\partial t} dx \tag{2.4}$$

where ρ, ρ_v, ρ_d are the instantaneous, virgin, and decomposed density, respectively; the enthalpy of composite is $h = \int_0^T C_p \, dT$. The three terms on the right hand side of Equation (2.1) relate to heat conduction, resin pyrolysis and volatile convection, respectively; the enthalpy of decomposed gases is $h_g = \int_0^T C_g \, dx$. Equation (2.3) is the

n^{th} order Arrhenius equation to describe the pyrolysis reaction where E is the activation energy, A is a constant, and n is the order of decomposition reaction; $\dot{m}''$ in Equation (2.4) is mass loss rate per unit area. The finite-rate model requires that certain pyrolysis kinetics parameters must be known for the calculation. The determination of these kinetics parameters will be shown in the following section.

TGA tests were performed with powder samples to obtain the decomposed density, pyrolysis kinetics, and heating-rate dependence of pyrolysis temperature of the composite. The samples were ground from the pultruded E-glass/polyester panels and had weight of about 4 mg. The tests were run at heating rates of 5, 10, 15, 20, and 25°C/min under air ambience. The air ambience condition was used to determine pyrolysis kinetics because it represents a well-ventilated fire scenario, e.g. in cone calorimeter test and ICAL test.

By introducing normalized remaining resin mass $w = \frac{\rho - \rho_d}{\rho_v - \rho_d}$, Equation (2.3) can be rewritten as

$$\frac{dw}{dt} = -Aw^n \exp\left(-\frac{E}{RT}\right) \tag{2.5}$$

$$\frac{d^2w}{dtdT} = -Anw^{n-1}\frac{\mathrm{dw}}{\mathrm{dT}}\exp\left(-\frac{E}{RT}\right) - Aw^n \exp\left(-\frac{E}{RT}\right)\frac{E}{RT^2} \tag{2.6}$$

At the temperature point corresponding to peak mass loss rate, $\frac{d^2w}{dtdT} = 0$. Then we have

$$\frac{1}{\beta}Anw^{n-1}\exp\left(-\frac{E}{RT}\right) = \frac{E}{RT^2} \tag{2.7}$$

where $\beta = \partial T/\partial t$ is the heating rate. Using results from three TGA tests at different heating rates, Equation (2.7) can be solved for Arrhenius parameters *A*, *n*, and *E*. Because the temperature point corresponding to the peak MLR is the best indicator for decomposition, this method is mathematically capable of catching decomposition temperatures provided TGA curves are smooth enough.

Using the analytic method described above with TGA data at heating rates of 5, 15, 25°C/min, the pyrolysis kinetics of the composite was determined as *A*=34377066771s^{-1}, *n*=4.4463, and *E*=149026 $Jmol^{-1}$.

The density of virgin the E-glass/polyester composite is ρ_v =1,888 kg/m³. The density of decomposed composite, an important input in the analysis of pyrolysis kinetics, was determined from TGA tests. Final mass was measured at about 600°C, at which the matrix is completely decomposed. It was shown that the remaining mass ratios after pyrolysis had an average value of 0.6. Assuming that the effect of thermal expansion on density is negligible, the decomposed density is then estimated by $\rho_d = 0.6 \times \rho_v = 1133$ kg/m³.

In cone calorimeter and ICAL tests, when the effect of flame heat flux from the combustion of the specimen is not considered, the thermal boundary condition at the exposed surface is:

$$-k\frac{\partial T}{\partial x} = \dot{q}_e^{"} - \varepsilon_s \sigma (T_s^4 - T_\infty^4) - h_c (T_s - T_\infty) \tag{2.8}$$

where $\dot{q}_e^{"}$ is the heat flux applied by the cone heater or the radiant panel; ε_s is the emissivity of the exposed surface; σ is Stefan-Boltzmann constant; T_s, T_∞ are the surface and ambience temperature, respectively; The convective heat transfer coefficient h_c is

taken as 10 W/m².K [42, 44]. General thermal boundary condition at the back surface is given by:

$$-k\frac{\partial T}{\partial x} = \varepsilon_s \sigma (T_s^4 - T_\infty^4) + h_c (T_s - T_\infty) \tag{2.9}$$

If thermal insulation is present at the back surface, the first term on the right side of Equation (2.9) is zero and the second term defines a heat conduction boundary, in which the heat transfer coefficient h_c can be estimated based on the thermal conductivity of insulation material and its thickness. This case represents the thermal boundary condition of the unexposed surface of a cone calorimeter specimen. If no insulation at the back surface, h_c was taken as 10 W/m².K [44]. This represents the thermal boundary condition of the unexposed surface of an ICAL specimen. Emissivity ε_s in Equations (2.8)-(2.9) was taken as unity [42, 44].

In addition to thermal boundary conditions, the model is subject to mass transfer boundary conditions at the exposed surface and the back surface as shown in Equations (2.10)-(2.11), respectively. Note that the mass boundary conditions are reasonable and the model is valid until the composite becomes thermally thin when pyrolysis gases escape out of the back surface as well as the exposed surface.

$$\dot{m}_g'' = \int_0^d \frac{\partial \rho}{\partial t}\, dx \tag{2.10}$$

$$\dot{m}_g'' = 0 \tag{2.11}$$

The composite used in this study was E-glass/polyester. Material properties for the composite and its components are listed in Table 2.1.

The effect of porosity on the thermal conductivity of polyester was accounted for with an asymmetrical model for porous materials with two phases [46]. The two phases here are polyester and pore, which is left behind by the decomposition reaction.

$$k_{r\_eff} = k_r(1-\Phi)^{1.5} \tag{2.12}$$

$$F = \frac{(\rho_v - \rho)}{(\rho_v - \rho_d)(1 - V_f)} \tag{2.13}$$

Assuming that the effect of thermal expansion is negligible, the thermal conductivity of the composite is given implicitly by

$$\frac{1}{k} = \frac{1 - V_f}{k_{r\_eff}} + \frac{V_f}{k_f} \tag{2.14}$$

Table 2.1: Material Properties of the E-glass/Polyester Composite Material [45]

The origin density $\boldsymbol{\rho_v}$ (kg/m³)	1888
The decomposed density $\boldsymbol{\rho_d}$ (kg/m³)	1133
Fiber heat capacity $\boldsymbol{C_f}$ (J/kg.K)	$760 + 3.88 \times 10^{-2}T$
Resin heat capacity $\boldsymbol{C_r}$ (J/kg.K)	$1600 + 0.8T$
Fiber thermal conductivity $\boldsymbol{k_f}$ (W/m².K)	$760 + 2.05 \times 10^{-4}T$
Resin thermal conductivity $\boldsymbol{k_r}$(W/m².K)	$0.2 - 1.356 \times 10^{-4}T$ $(T \ll 200°C)$ $0.2 + 2 \times 10^{-4}T$ $(T > 200°C)$
Fiber volume fraction $\boldsymbol{V_f}$	0.2872
Fiber weight fraction $\boldsymbol{W_f}$	0.4

and the specific heat of the composite is determined as

$$C = \frac{W_f C_f}{W_f + (1 - W_f)(1 - \Phi)} + \frac{(1 - W_f)(1 - \Phi) C_r}{W_f + (1 - W_f)(1 - \Phi)} \tag{2.15}$$

In the FEA implementation in COMSOL [47], 24 fifth-order Lagrange elements (Larange-Quintic) were used through the thickness. Temperature and MLR in test conditions in ICAL tests were predicted with the finite-rate model (Equations (2.1)-(2.4)) and then with the model in which volatile convection term in Equation (2.1) was neglected. Using these two sets of results, comparison can be made to investigate the effect of volatile convection on thermal response modeling. The results and comparisons are presented in Figures 2.4 and 2.5.

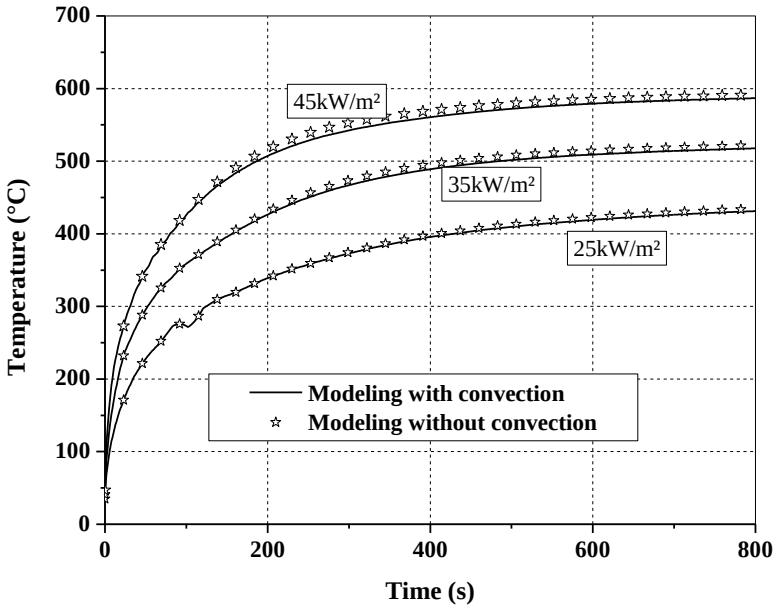

Figure 2.4: Effect of the internal gas convection term on temperature prediction (ICAL data)

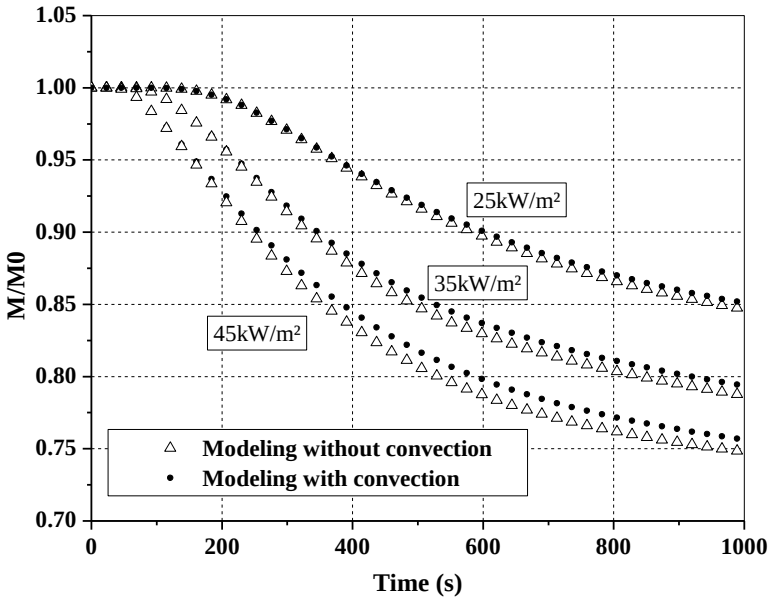

Figure 2.5: Effect of the internal gas convection term on mass loss prediction (ICAL data)

The last term on the right side of Equation (2.1) in the finite-rate model accounts for the effects of internal gas convection. Internal gas convection has cooling effects on the material because pyrolysis gases in general have larger heat capacity than the material itself. Figure 2.4 shows temperature predictions from the finite-rate model with and without consideration of internal gas convection compared to temperature measurements with pyrometer. It is seen that temperature predictions with and without the convection term at 25kW/m² are almost the same, and temperature predictions at 45kW/m² are a little higher without the consideration of internal gas convection. Figure 2.5 shows that the effect of internal gas convection on mass loss is insignificant but gradually increase as heat flux level increase. The modeling results show that the effect of internal gas convection can be neglected at the heat flux level up to 45kW/m².

2.4.2. Infinite-rate pyrolysis model

The pyrolysis of polymers consists of a series of chemical reactions that occur over a range of temperature. Based on the assumption of infinite pyrolysis rate at an existing pyrolysis temperature point, finite-rate pyrolysis models can be reduced to infinite-rate pyrolysis model with a pyrolysis front of zero thickness that separates char layer from the virgin material. Since polymers in general absorb heat during pyrolysis, only endothermic pyrolysis needs to be considered. The endothermic pyrolysis process from virgin material to char material takes a constant amount of enthalpy per unit volume, equal to $(\rho_v - \rho_d)Q$ at pyrolysis temperature point [38].

The implementation of the infinite-rate pyrolysis model using the finite element method needs to use caution at the pyrolysis temperature point at which the sudden change of enthalpy occurs. The rate of enthalpy change at the pyrolysis temperature point is infinite and will cause convergence problem. To overcome the convergence difficulty in finite element implementation, instead of a single point of pyrolysis temperature T_p, a small temperature range $(T_p - \Delta T) \ll T \ll (T_p + \Delta T)$ for pyrolysis was introduced. The selection of ΔT depends on mesh size and temperature gradient. Mesh sensitivity should be checked for convergence.

In Equation (2.16), apparent specific heat C_{app} was used to account for enthalpy change over the pyrolysis front, therefore only two terms on the right hand side of the equation. The equations (2.17)-(2.20) show the implementation of the infinite-rate model with commercial software COMSOL [47].

$$\rho C_{app}\frac{\partial T}{\partial t}=\frac{\partial}{\partial x}\left(k\frac{\partial T}{\partial x}\right)-\dot{m}_g''C_g\frac{\partial T}{\partial x} \tag{2.16}$$

$$\rho C_{app}=\begin{cases}\rho_v C_v \;\; if\; T<\left(T_p-\Delta T\right)\\ \frac{(\rho_v-\rho_d)Q}{2\Delta T}+\frac{1}{2}(\rho_v C_v+\rho_d C_d)\;\; if\;\left(T_p-\Delta T\right)\le T\le\left(T_p+\Delta T\right)\\ \rho_d C_d \;\; if\; >\left(T_p+\Delta T\right)\end{cases} \tag{2.17}$$

$$T_p=f(\beta);\;\; \beta=\frac{1}{d}\int_0^d\frac{dT}{dt}\,dx \tag{2.18}$$

$$\delta_{ch}=\frac{m_0-m}{(\rho_v-\rho_d)\Delta A} \tag{2.19}$$

$$\dot{m}''=\frac{d\delta_{ch}}{dt}(\rho_v-\rho_d) \tag{2.20}$$

where the dependence of pyrolysis temperature T_p was determined as an exponential function as in the section of characterization of pyrolysis. Equation (2.19) defines effective char thickness δ_{ch}, in which $m=\Delta A\times Int(\rho)$ and $Int(\rho)$ represents the integral of instantaneous density ρ over the whole domain (which is the thickness of the panel here) whose value is easy to obtain each time step in COMSOL. Same as the finite-rate model, 24 Larange-Quintic elements were used through the thickness. Compared to the finite-rate model, the infinite-rate model does not need pyrolysis kinetics parameters.

The equations (2.16)-(2.20) were solved for MLR with $\Delta T=1°C$ and with $\Delta T=0.5°C$ respectively. Mass loss and temperature results showed that the solutions were convergent. From Figures 2.4 and 2.5, internal gas convection has negligible effect on thermal response modeling; therefore, the third term in Equation (2.16) can be neglected in computation. It should be noted that the definition of effective char thickness in Equation (2.19) can be used to estimate effective char thickness in fire tests if one dimensional heat and mass transfer can be assumed.

Higher heating rates can delay the occurrence of pyrolysis and increase the pyrolysis temperature. In this work, pyrolysis temperature was defined as the temperature point corresponding to the maximum MLR point, which was determined in TGA tests. The heating-rate dependence of pyrolysis temperature was obtained by curve fitting with an exponential function. The relationship was determined as

$$T_p = T_p^{max} - \left(T_p^{max} - T_p^{min}\right)e^{-\beta/9.21586} \tag{2.21}$$

where the maximum pyrolysis temperature T_p^{max} is 639.4 K and the minimum T_p^{min} is 579.7 K when heating rate approaches zero.

2.5. Results and Discussion

2.5.1. Effect of pyrolysis modeling on thermal response predictions

Figures 2.6(a)-(c) show temperature measurements from both pyrometer and thermocouples at the exposed surface in ICAL tests at 25, 35, and 45kW/m². All tests were started at the time of 120 seconds when the shield panel was open and the specimen began to receive heat flux from the radiant panel. It is shown that agreement between pyrometer and thermocouple measurements is excellent, indicating the surface temperatures were correctly measured by thermocouples.

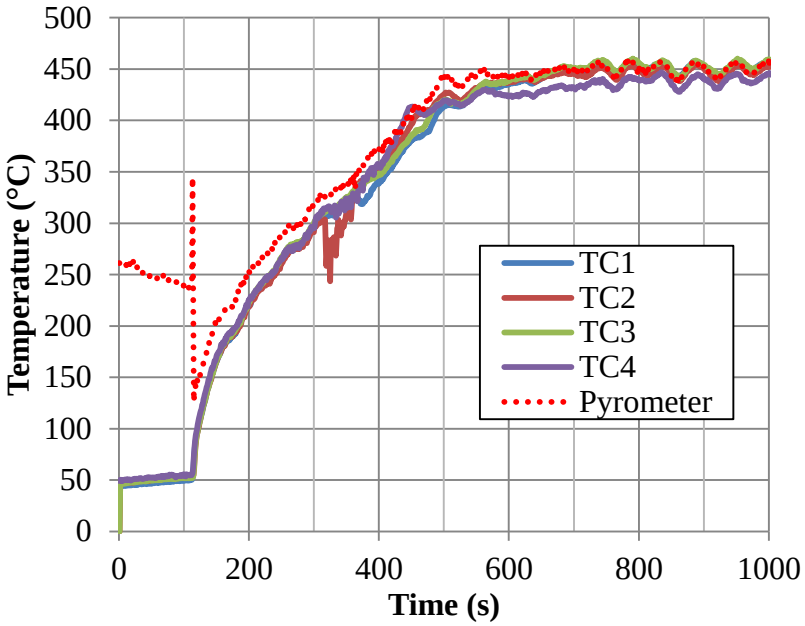

Figure 2.6 (a): Temperatures at the exposed surface at 25kw/m²

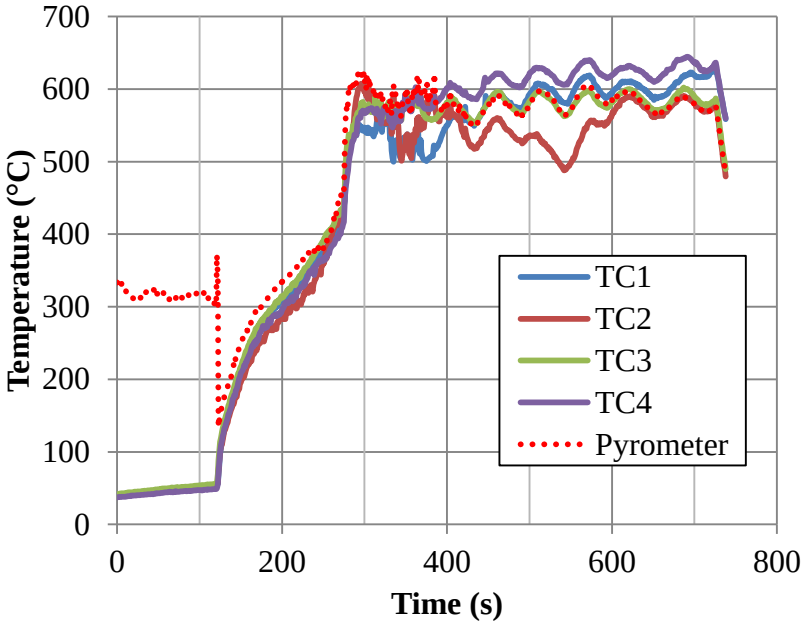

Figure 2.6 (b): Temperatures at the exposed surface at 35kw/m²

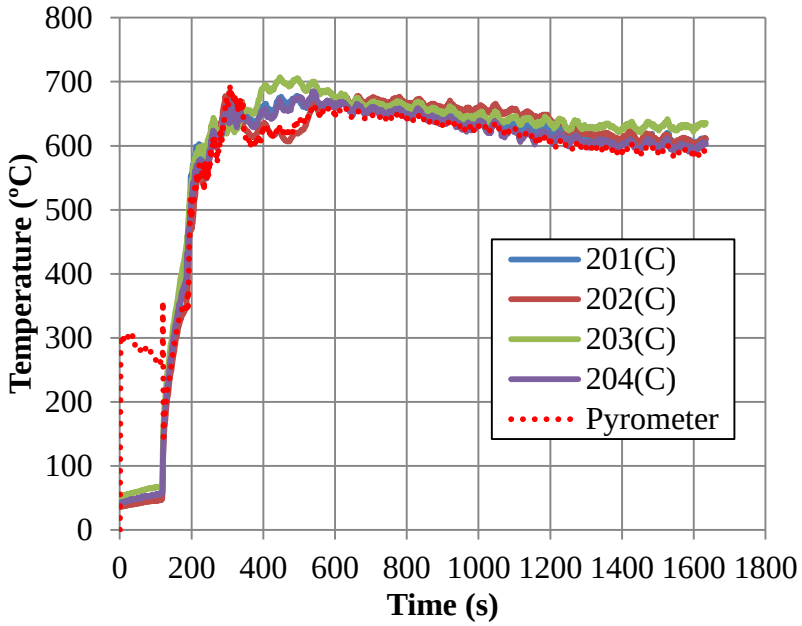

Figure 2.6 (c): Temperatures at the exposed surface at 45kw/m²

Figures 2.7 (a)-(c) show the comparisons of temperatures between ICAL tests and predictions from the finite-rate and the infinite-rate models. Experimental temperature results in the figures were from thermocouple measurements.

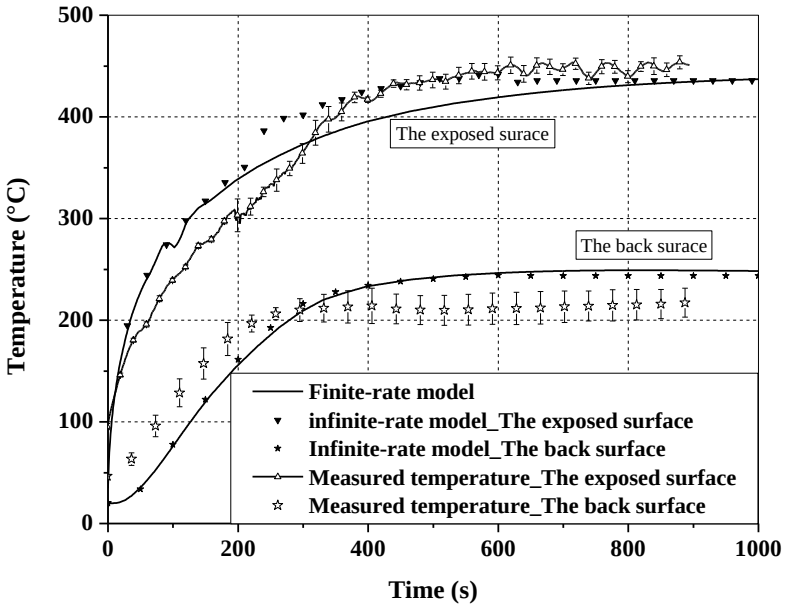

Figure 2.7(a): Comparisons of predicted and measured temperatures at 25kW/m²

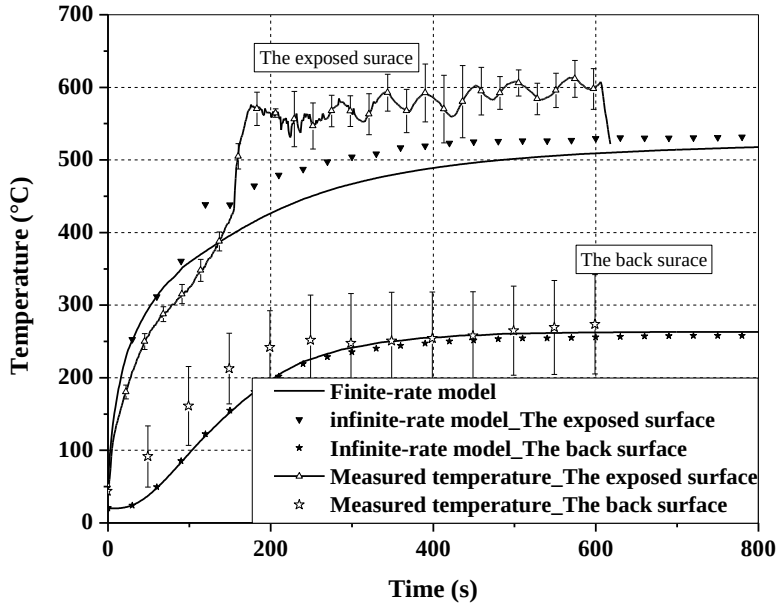

Figure 2.7(b): Comparisons of predicted and measured temperatures at 35kW/m²

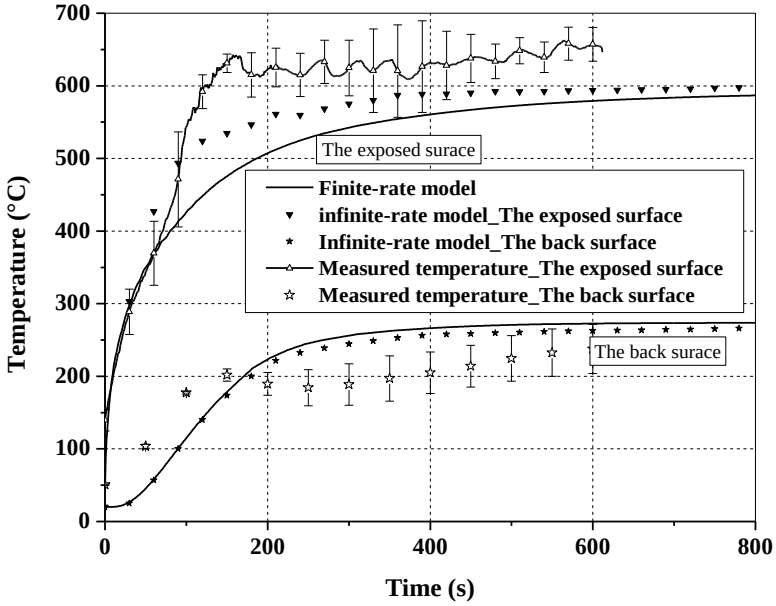

Figure 2.7(c): Comparisons of predicted and measured temperatures at 45kW/m²

Overall, the temperature predictions of the back surface with two models are in acceptable agreement with temperature measurements. The Temperature predictions of the exposed surface are good at heat flux of 25kW/m² and are poor at heat flux levels of 35 and 45kW/m². The reason is flame heat flux. Flame heat flux caused temperature jumps from measurements at about 150s for 35kW/m² irradiance level and at 80s for 45kW/m² irradiance level, which started at time-to-ignition. No ignition was observed in ICAL tests at 25kW/m² irradiance level. Compared to experimental data, the infinite-rate model gave better temperature predictions at the exposed surface than the finite-rate model. Two models gave similar temperature predictions at the back surface.

Figures 2.8-11 show mass loss and MLR predictions with the two models compared to the results obtained by the cone calorimeter tests and the ICAL tests, respectively. Mass loss predictions are in good agreement with test results except in cone calorimeter at 25kW/m² heat flux level.

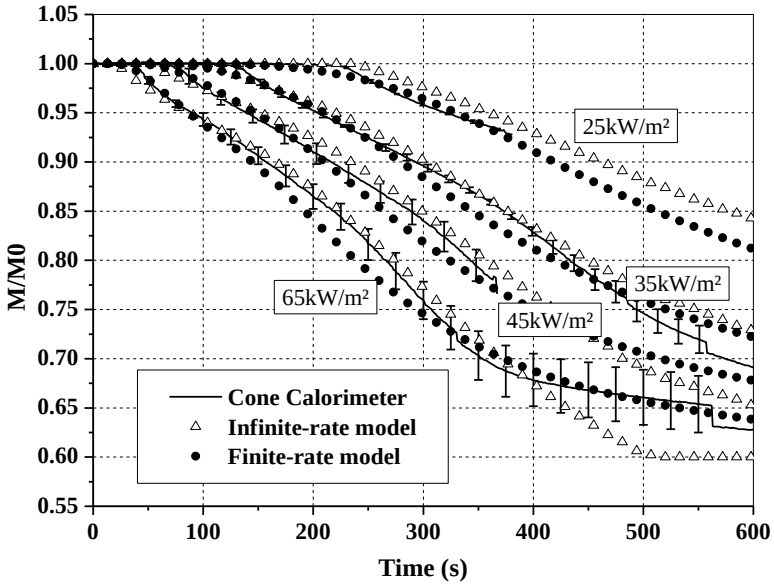

Figure 2.8: Comparisons of predicted and measured mass loss (cone data)

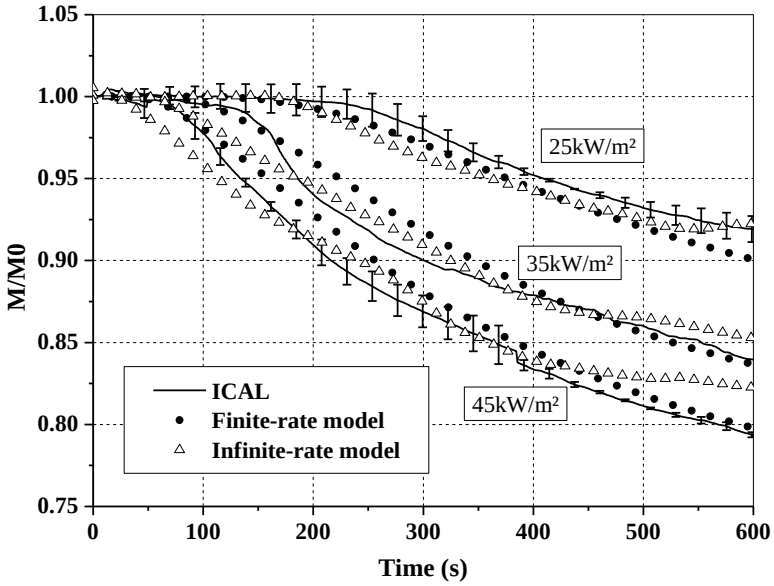

Figure 2.9: Comparisons of predicted and measured mass loss (ICAL data)

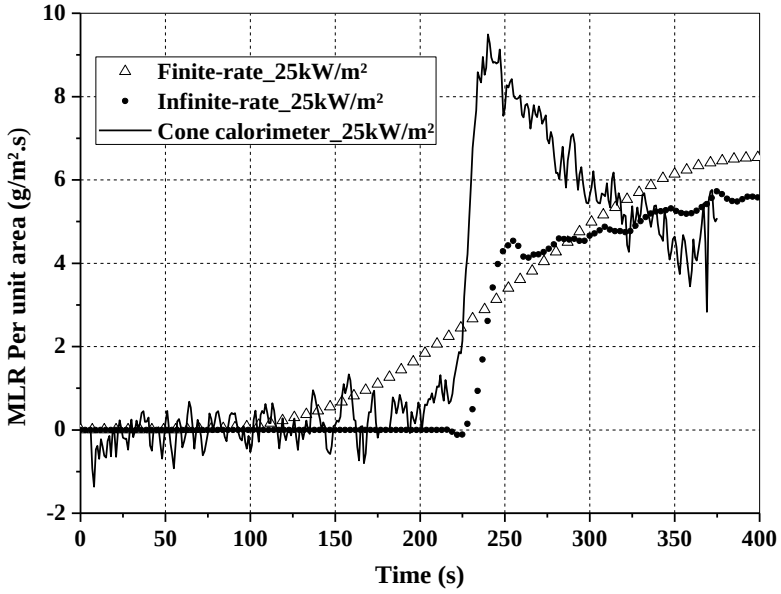

Figure 2.10(a): Comparisons of predicted and measured mass loss rate at 25kW/m² (Cone data)

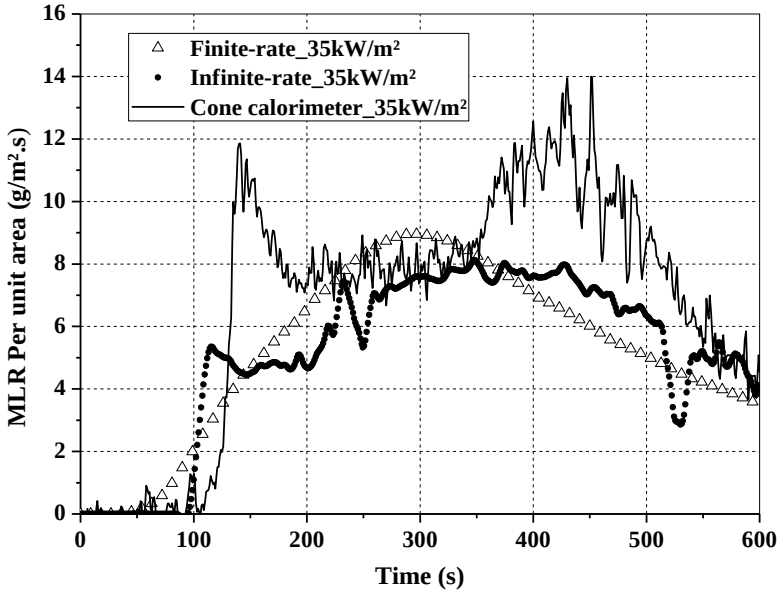

Figure 2.10(b): Comparisons of predicted and measured mass loss rate at 35kW/m² (Cone data)

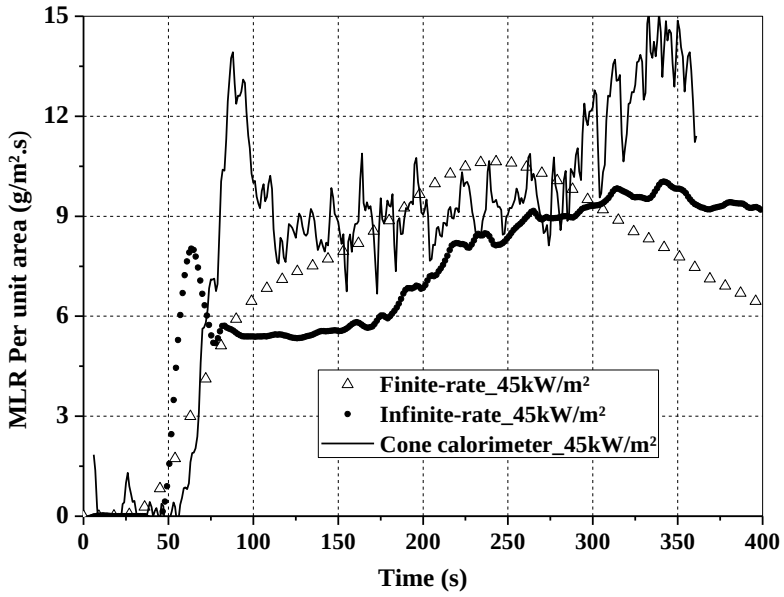

Figure 2.10(c): Comparisons of predicted and measured mass loss rate at 45kW/m² (Cone data)

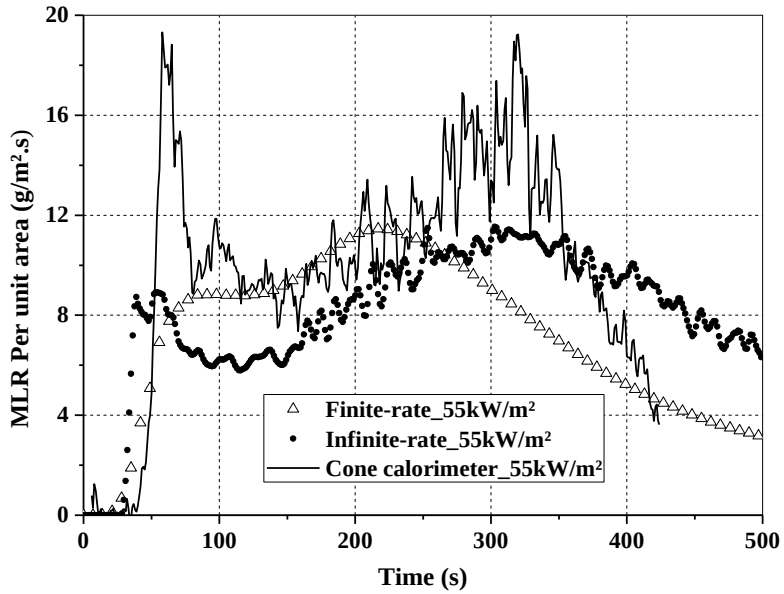

Figure 2.10(d): Comparisons of predicted and measured mass loss rate at 55kW/m² (Cone data)

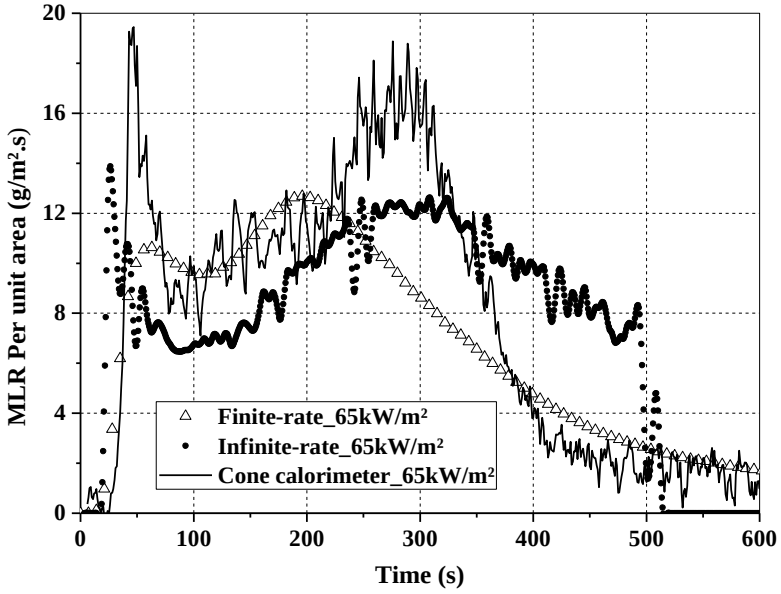

Figure 2.10(e): Comparisons of predicted and measured mass loss rate at 65kW/m² (Cone data)

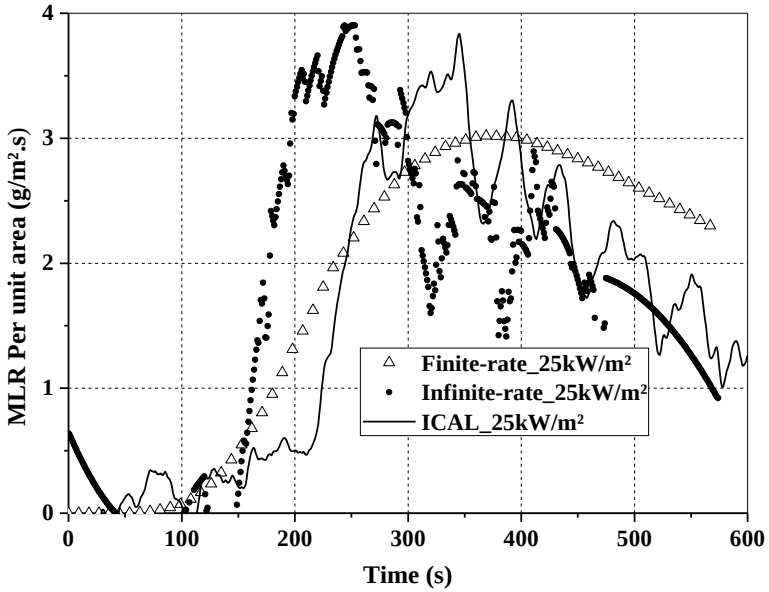

Figure 2.11(a): Comparisons of Predicted and measured mass loss rate at 25kW/m² (ICAL data)

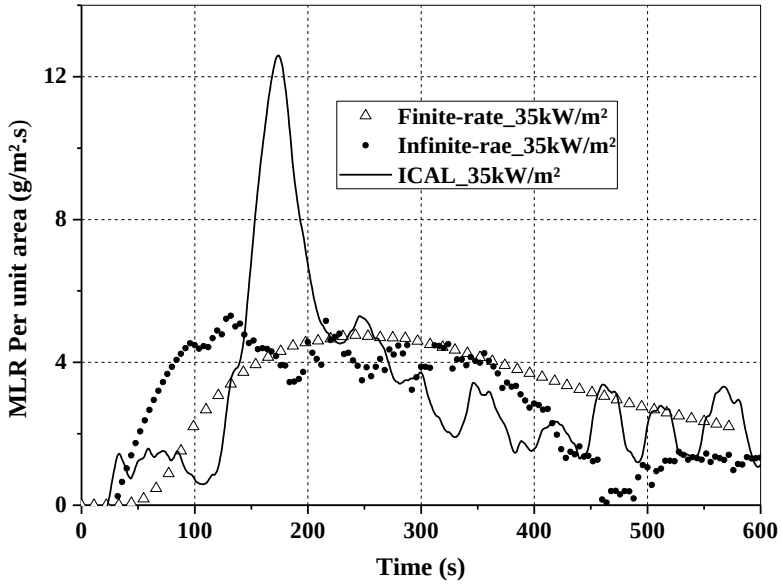

Figure 2.11(b): Comparisons of Predicted and measured mass loss rate at 35kW/m² (ICAL data)

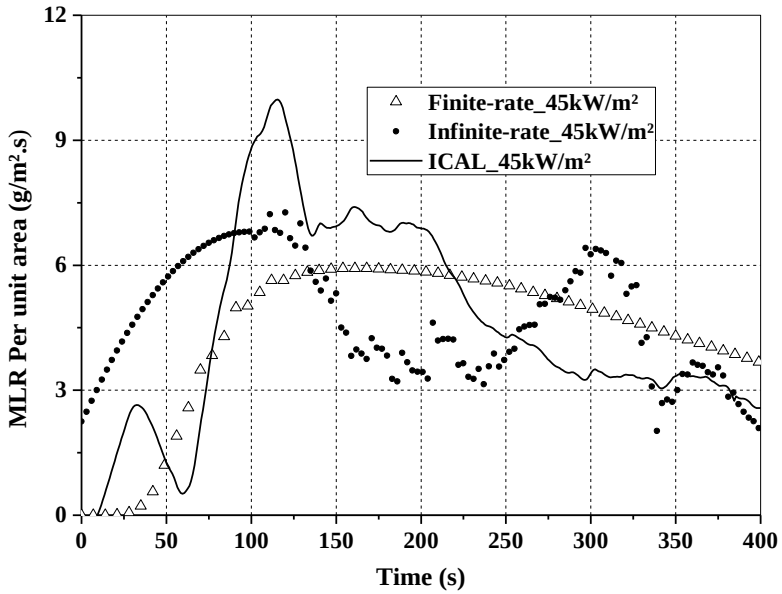

Figure 2.11(c): Comparisons of Predicted and measured mass loss rate at 45kW/m² (ICAL data)

As shown in Figures 2.10(b)-(e), the infinite-rate model gave MLR predictions around two MLR peaks of test results from cone calorimeter; the finite-rate model

performed better between two MLR peaks. Overall, two models underestimated MLR. The underestimation was caused by flame heat flux. For the finite-rate model, another reason that caused the underestimation at the second MLR peak is one major deficiency of the model. For char forming materials like FRP, the second peak takes place when the material become thermally thin as the pyrolysis front approaching the back surface. In the case, pyrolysis gases will escape out of both the exposed surface and the back surface instead of only the exposed surface at the beginning, which makes the finite-rate model valid only for thermally thick condition.

Char thickness comparisons between cone calorimeter tests and modeling are shown in Figure 2.12. The effective char thickness of the specimen in a cone calorimeter was estimated with mass loss data and the decomposed density using Equation (2.19). It is illustrated that overall the infinite-rate model predicted better char thickness results at all heat flux levels than the finite-rate model.

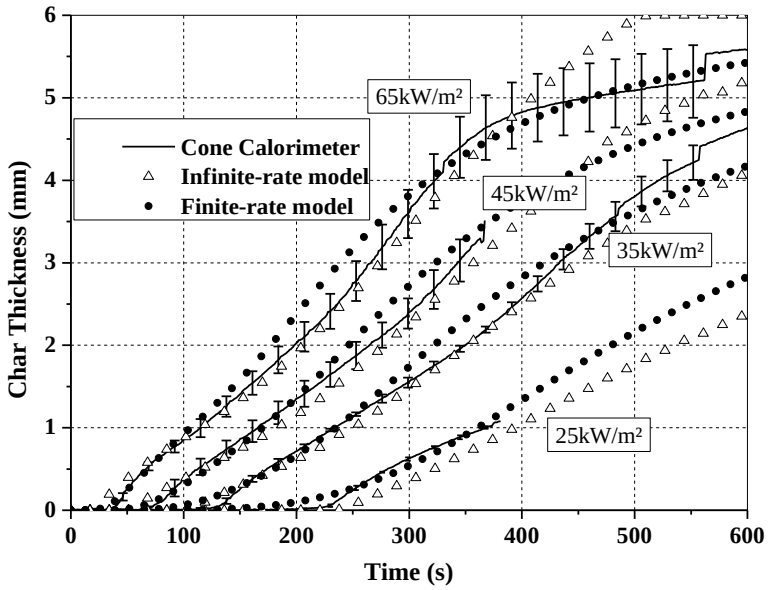

Figure 2.12: Comparisons of predicted and measured char thickness (cone data)

2.5.2. Influence of thermal insulation on thermal response

The effect of thermal insulation at the back surface on the thermal response of the composite was investigated with the finite-rate model. Temperature and mass loss predictions with and without thermal insulation were compared to ICAL test results. As shown in Figure 2.13 and Figures 2.14(a)-(c), the thermal insulation at the back surface significantly increases both mass loss and temperature predictions. Different thermal boundary conditions at the back surface of specimens between the cone calorimeter and the ICAL appear to be the main reason that mass loss and MLR measured using the ICAL are lower than those obtained from cone calorimeter tests.

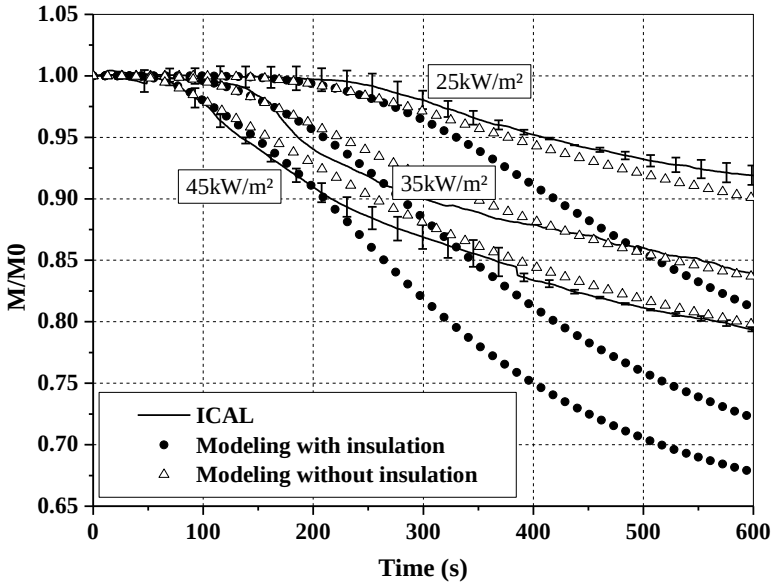

Figure 2.13: Effect of back surface insulation on mass loss

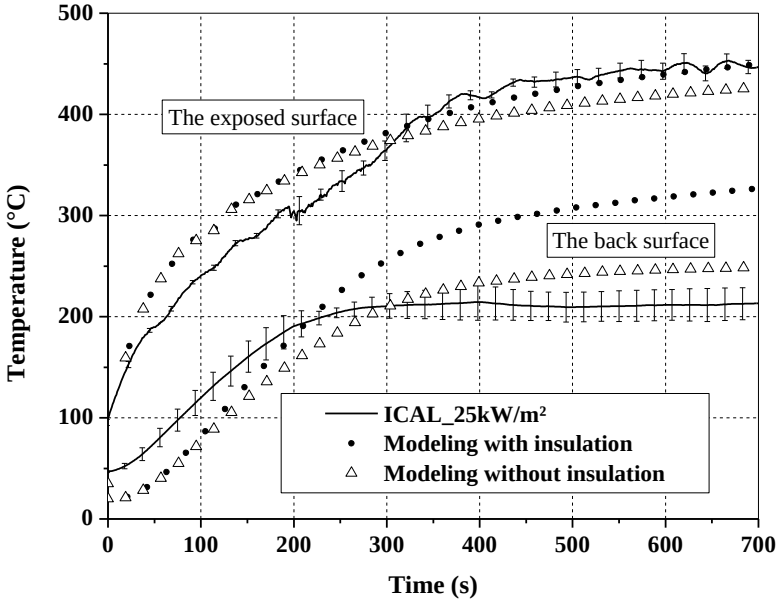

Figure 2.14(a): Effect of back surface insulation on temperature rise at 25kW/m²

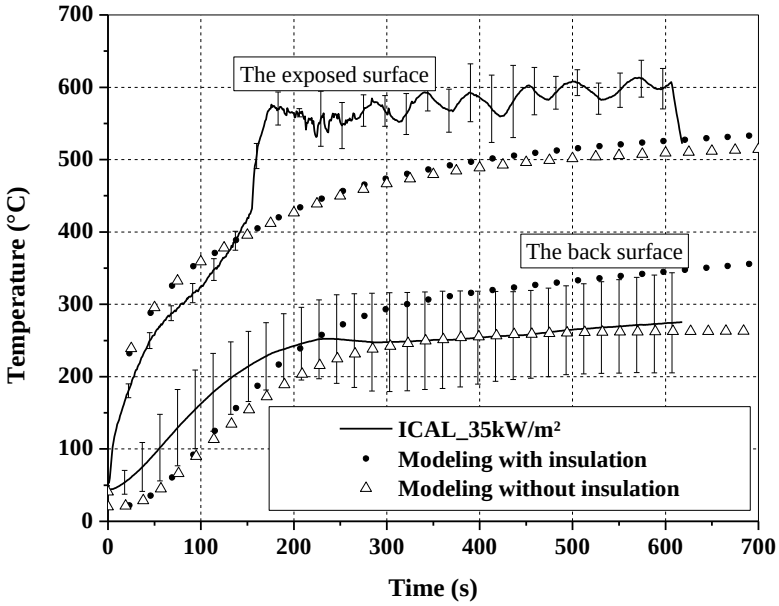

Figure 2.14(b): Effect of back surface insulation on temperature rise at 35kW/m²

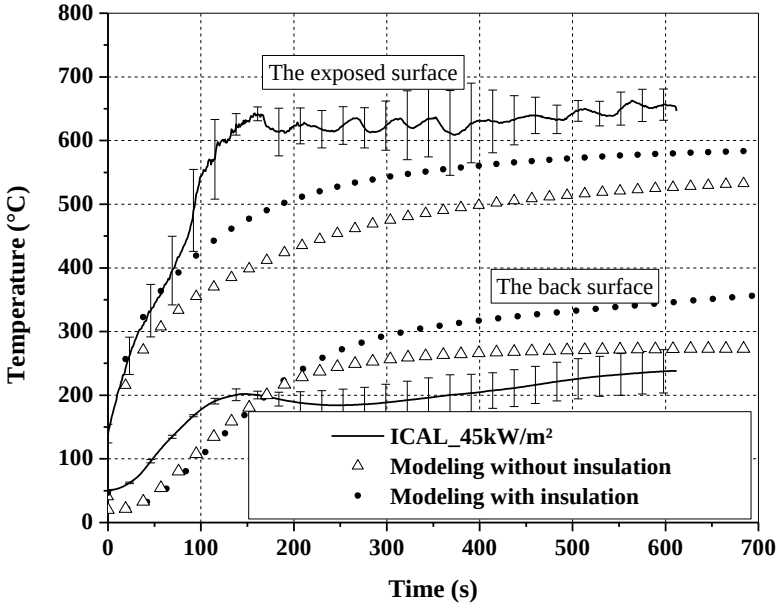

Figure 2.14(c): Effect of back surface insulation on temperature rise at 45kW/m²

2.6. Conclusions

The thermal response of FRP composites exposed to one-sided heating fire condition was measured by bench-scale and intermediate-scale fire tests. A finite-rate pyrolysis kinetics model and an infinite-rate pyrolysis kinetics model were used to predict temperature and mass loss characteristics as well as the char depth of FRP composite panels under the same thermal boundary conditions as in the cone calorimeter and ICAL fire tests. Temperature, mass loss, mass loss rate and char thickness predictions from the thermal response models were compared with experimental data from the Cone and ICAL fire tests. It was shown that both the finite-rate and infinite-rate pyrolysis models can give acceptable mass loss, the effective char thickness, and the back surface temperature predictions. Flame heat flux significantly increases the exposed surface temperature after ignition and should be considered. The infinite-rate model works well

for both thermally-thin and thermally-thick conditions and is easier to implement with fewer parameters. The effect of internal gas convection on thermal response prediction was determined insignificant up to heat flux level of 45kW/m². The thermal insulation at the back surface significantly increases both temperature and mass loss predictions.

CHAPTER 3: FIBER REINFORCED POLYMER COMPOSITE STRUCTURES IN FIRE: MODELING AND VALIDATION[2]

3.1. Abstract

This paper presents a thermo-mechanical model for predicting the behavior of fiber reinforced polymer (FRP) composite structures subject to simultaneous thermal and compressive loading. The model includes a thermal sub-model to calculate the temperature history of the structure and a structural sub-model to predict the mechanical performance of the structure. Both thermal and mechanical properties in the two sub-models were temperature dependent. The effect of heating rate on decomposition was considered through a shift temperature factor in the thermal sub-model. Cohesive elements were incorporated in the structural sub-model to consider the effect of delamination for sandwich panels. The model was implemented by the finite element method and was validated by comparing the numerical results with a one-sided heating test on FRP laminate strips and furnace structural fire tests on FRP laminate and sandwich panels.

[2]This chapter is based on a manuscript with the same title that has been accepted for publication by Mechanics of Advanced Materials and Structures. Chapter 3 provides more details than the manuscript due to page limit of a journal article.

3.2. Introduction

Fiber reinforced polymer (FRP) composites have been widely used in various structural applications. FRP composites offer many advantageous physical and mechanical properties, such as high specific strength, light weight, and good fatigue and corrosion resistance. However, since FRP composites contain polymer matrices, the composites and their structures are combustible. FRP composites will degrade, decompose, and sometimes yield toxic gases at high temperatures or when subject to fire conditions. Due to their combustible nature, fire safety and fire protection of FRP composites are of great concern. The evaluation of the performance of materials and structures in fire includes reaction to fire and fire resistance studies. The reaction-to-fire study examines fire growth (e.g., ignitability, flame spread, and heat release) and fire effluents (e.g., smoke opacity and toxicity). The fire resistance study examines how a structure resists fire and usually measures three parameters: insulation, integrity, and load bearing capacity (for load-bearing elements). The intention of this paper was to address the fire resistance of FRP composite structures with a focus on developing and validating an integrated thermo-mechanical method for predicting the response of FRP structures in fire.

Analyzing the fire resistance of FRP structures requires at least three analyses: (1) a heat transfer analysis to predict the temperature profile in the structures as a function of time and location; (2) a decomposition (or pyrolysis) analysis to estimate the rate of decomposition under certain fire conditions; and (3) a structural analysis to examine the mechanical and structural response of FRP structures in fire. The heat transfer analysis is critical since estimating the response of a structure in fire requires temperature-dependent

thermal properties and mechanical properties of the material (e.g., specific heat, mass loss, thermal conductivity, thermal expansion, residual stiffness and strength, fracture toughness, etc.). The effect of insulation can also be estimated based on heat transfer analysis. The decomposition analysis is important since many physical and mechanical properties are affected by the decomposition process. The structural analysis will give fire protection engineers or structural engineers critical information related to structural integrity and fire resistance, such as deflection and strain as a function of time, residual stiffness and strength of the structure, stability and integrity of the structure, and time-to-failure estimation of the structure.

For temperature prediction, the simplest model is the standard one-dimensional heat conduction equation without heat source term, where decomposition effects are neglected. The first heat transfer model that can account for the thermal decomposition of the polymer matrix was developed by [11]. In the one dimensional model, a source term equal to the product of the decomposition by the theoretical mass loss rate was added to consider decomposition's effects. A more sophisticated model, which is capable of taking into account the diffusion of decomposition induced gas in addition to the decomposition heat, was presented in [12], where the cooling effects of internal gases were calculated based on convective mass transfer theory, and the decomposition reactions were modeled with the Arrhenius equation. Based on the work in [12], Florio et al. [13] developed a model in which not only the heat conduction, pyrolysis, and diffusion of decomposition gas, but also the effects of thermal expansion and internal pressure are considered. However, as shown by the authors, taking expensive computation cost to consider the

effects of thermal expansion and internal gas pressure could not significantly improve the temperature prediction in decomposing composites.

In the literature, other heat transfer models for composite structures can also be found but with little difference from the models mentioned above [10, 48-49]. Because too many factors affect heat transfer in the chemical reaction of decomposition and no accurate temperature, heating rate, and/or temperature gradient dependent thermal properties as well as thermal boundaries are available, it is acknowledged that there is no single heat transfer model suitable for all applications even though some models are mathematically capable of accounting for all phenomena in the decomposition process. In this study, the model developed in [11] will be used as a base for thermal analysis.

For structural analysis, a simplified "two-layer model" which divides the cross section of composite panel into a virgin layer and char layer can be used to estimate the residual strength and time-to-failure of a laminate panel under combined mechanical loading and one-sided heating. Mouritz and Mathys [15] formulated the two-layer model based on rule-of-mixtures to predict the residual tensile strength of polymer laminates under fire. For simplicity, the tensile strength through the char layer is assumed negligible, and the strength through the virgin layer has the value at room temperature. Based on the two-layer model, a simplified three-layer model includes one more layer with partially degraded mechanical properties between the virgin layer and the char layer, and might be able to give more accurate strength and time-to-failure prediction upon more modeling effort and computational cost [50]. To account for the effects of delamination in structural analysis, Lua [51] developed a finite element model that predicts the delamination failure in the sandwich composites in addition to the diffuse

damage caused by the fiber/tow/matrix failure. A recent review on modeling the structural response of polymer composites in fire is presented in [35].

The first analytical model that was capable of predicting the thermal and mechanical response of a composite structure under fire and loading was developed by McManus and Springer [14]. The model can account for effects from thermal expansion, decomposition gas induced pressure, moisture, and charring expansion. Other analytical models based on beam theory, bending theory, and/or buckling theory can also be found in the literature [52-53], but appear less practical than the models above because when taking into account the effects of decomposition, they are numerically difficult to implement.

This paper presents a finite-element (FE) based thermo-mechanical method for modeling the response of FRP composite structures in fire. The model includes a heat transfer analysis sub-model (with decomposition included) and a structural analysis sub-model. The model provides a finite element method to model FRP composites in one-sided heating and compressive loading. A novelty in the heat transfer analysis sub-mode was the introduction of a factor to consider the effect of heating rate on decomposition and mass loss in fire conditions [43]. The novelty in the structural analysis sub-model was that the modeling of delamination was introduced and temperature-dependent fracture properties were implemented in the model. All temperature predictions were compared with experimental data from FRP laminate coupons under one-sided constant heat flux fire and intermediate scale FRP laminate and sandwich panels under a one-sided furnace fire. In the structural analysis section, the predicted in-plane deformation, transverse deflections, and time to failure were compared with experimental observations

from the same FRP laminate coupons under one-sided heating and FRP laminate and sandwich panels under a one-sided furnace fire. The models were implemented in FE modeling software, so the focus was on the modeling aspects of the research rather than programming implementation. The last section is an assessment of fire resistance based on temperature profile and deformation histories from the heat transfer model and the structural model using structural failure criteria.

3.3. Heat Transfer Model

3.3.1. One dimensional heat transfer

The following one-dimensional heat transfer model has been developed by Henderson et al. [12] for degrading material with the instantaneous, unidirectional flow of gases toward the heated surface:

$$\rho C \frac{\partial T}{\partial t} = \frac{\partial}{\partial x}\left(k \frac{\partial T}{\partial x}\right) - \left(h - h_g\right)\frac{\partial \rho}{\partial t} - \dot{m}_g'' C_g \frac{\partial T}{\partial x} \tag{3.1}$$

$$\frac{d(\dot{m}_g'')}{dx} = -\frac{\partial \rho}{\partial t} \tag{3.2}$$

$$h_g = \int_0^T C_g \, dT; \;\; h = Q + \int_0^T C dT \tag{3.3}$$

where x is the coordinate along the thickness direction; T is temperature; t is time; ρ, C, k, h are density, specific heat, thermal conductivity, and enthalpy for composites, respectively; and $\dot{m}_g'', h_g, C_g$ are mass flow, enthalpy and specific heat for gases generated from the decomposition of resin, respectively. The three terms on the right hand side of Equation (3.1) relate to heat conduction, resin decomposition and volatile convection, respectively. The resin decomposition term is negative when the decomposition process is endothermic and positive when exothermic. The decomposition reaction for vinyl ester

in the study is endothermic. The last term is negative because of the convective cooling effect of the volatiles due to decomposition.

3.3.2. Modeling decomposition

The Arrhenius equation can be used to describe the effect of temperature on the rate of chemical reaction [10]. In this study, only the decomposition of resin was considered, which is given by:

$$\frac{d\rho}{dt} = -A(\rho_v - \rho_d)\left[\frac{\rho - \rho_d}{\rho_v - \rho_d}\right]^n \exp\left(-\frac{E}{RT}\right) \tag{3.4}$$

where ρ, ρ_v, ρ_d are the instantaneous density, the virgin density, and the decomposed density respectively; *A*, *E*, and *n* are rate constant, activation energy, and the order of decomposition reaction that are main parameters describing the decomposition process.

The Arrhenius parameters *A*, *n*, and *E* can be determined using Thermogravimetric Analysis (TGA) or Differential Scanning Calorimeter (DSC) tests and are generally dependent on heating rate and sample scales. As we know, higher heating rates increase the decomposition temperature. An FRP panel exposed to a constant heat flux of 50kW/m² can undergo an initial heating rate up to 1000°C/minute at the exposed surface, and the decomposition temperature at the exposed surface could be significantly higher than other locations. A concept of shift temperature was introduced here to account for heating rate's effects on decomposition. The modified Arrhenius equation is given by:

$$\frac{d\rho}{dt} = -A(\rho_v - \rho_d)\left[\frac{\rho - \rho_d}{\rho_v - \rho_d}\right]^n \exp\left(-\frac{E}{R(T - T_{sh})}\right) \tag{3.5}$$

where the shift temperature T_{sh} is a function of heating rate and can be determined from TGA/DSC tests. To determine the shift temperature, series of TGA/DSC tests need to be conducted at a practically wide range of heating rates. Since higher heating rates can increase the temperature of decomposition; and therefore, each TGA/DSC test at a specific heating rate will give its own temperature of decomposition, the shift temperature can be determined by fitting a function of heating rate for the decomposition temperature.

3.3.3. Thermal properties at different material states

Thermal conductivity and specific heat capacity depend on temperature and the decomposition state of the material. At three material states, virgin material, decomposing material, and decomposed material, a material has different thermal properties. While thermal properties at virgin and decomposed states can be determined by thermal tests such as DSC and Hot Disk. The rule of mixture [10] can be used to compute thermal properties at decomposing state, as shown in Equations (3.6)-(3.8):

$$k = Fk_v + (1 - F)k_d \tag{3.6}$$

$$C = FC_v + (1 - F)C_d \tag{3.7}$$

$$F = (\rho - \rho_d)/(\rho_v - \rho_d) \tag{3.8}$$

where k_v, k_d, C_v, C_d are thermal conductivities and specific heat capacities at virgin and decomposed states, respectively. F is the residual weight fraction of resin to original resin.

3.3.4. Thermal boundary conditions

If fire is defined by temperature, the thermal boundary at the exposed surface is then given by

$$-k\frac{\partial T}{\partial x} = \varepsilon_s \sigma (T_{fl}^4 - T_s^4) + h(T_{fl} - T_s) \tag{3.9}$$

For a furnace fire, the temperature difference between furnace gas and the exposed FRP surface is within 10°C; therefore, for simplicity, the temperature at the exposed surface can be assumed to be the same as the furnace gas temperature:

$$T_{fl} = T_s \tag{3.10}$$

If fire is defined by heat flux, the thermal boundary at the exposed surface is:

$$-k\frac{\partial T}{\partial x} = \dot{q}_e^{"} - \varepsilon_s \sigma (T_s^4 - T_\infty^4) - h(T_s - T_\infty) \tag{3.11}$$

The thermal boundary condition at the unexposed surface is given by Equation (3.12) as suggested by ASTM E1591 [44]:

$$-k\frac{\partial T}{\partial x} = \varepsilon_s \sigma (T_s^4 - T_\infty^4) + h_c(T_s - T_\infty) \tag{3.12}$$

In boundary equations above, ε_s is the emissivity of the exposed surface; σ is Stefan-Boltzmann Constant ($5.67 \times 10^{-8} W.m^{-2}.K^{-4}$); and T_{fl}, T_s, and T_∞ are the temperatures of fire, the exposed surface, and ambience (air temperature on the cold side of the specimen surface), respectively. According to ASTM E1591 [44], convective heat transfer coefficient h_c can be set at a constant value of 10W/m².K. For organic material such as FRP composite, emissivity ε_s is 0.95-0.99, and 0.99 is used in the study.

3.4. Structural Model

In the study, the FRP composite panels are considered elastic. Most FRP structures, such as those pultruded and VARTMed, can be considered as orthotropic in

structural analysis, and are assumed to be orthotropic during the whole duration of fire exposure.

3.4.1. Constitutive equation

The first analytical mechanical model by McManus and Springer [14] used the following governing equation to include the influence of thermal expansion, internal gas pressure, and moisture as well as charring expansion.

$$\varepsilon_{ij} = S_{ijkl}\sigma_{kl} + \alpha_{ij}\Delta T + \Lambda_{ij}\Delta P + \beta_{ij}\Delta(MC) + \chi_{ij}\Delta v_c \tag{3.13}$$

where $\alpha, \Lambda, \beta, \chi$ are the thermal, internal gas pressure, moisture, and charring expansion coefficients, respectively, and $\Delta T, \Delta P, \Delta(MC), \Delta v_c$ are the temperature, internal gas pressure, moisture content and char volume differences, respectively. This model is remarkable because it can account for additional effects from fire (such as internal gas pressure, moisture, and charring) but less practical since all the coefficients must be experimentally determined before the equations can be solved to calculate stress and strain. For all five terms on the right side of Equation (3.13), compliance and thermal expansion are the two dominant factors affecting stress and strain all the time. The other three factors (internal gas pressure, moisture, and char expansion) have no effect on the laminate until vaporization or decomposition occurs at corresponding temperatures. High internal gas pressure and high moisture content may have significant effects on delamination. However, composites made from the Vacuum Assisted Resin Transfer Molding process usually have low moisture content. While the composite decomposes under intensive external heat, volatile and moisture will diffuse to the burned surface and thus help reduce the internal gas pressure and moisture buildup. In general, their

influence on deformation is complicated and it is expensive to experimentally determine and numerically calculate the effect. Char formation significantly affects thermal and mechanical responses. The effect of decomposition and charring on thermal and mechanical properties has already been considered in the thermal model using a decomposition factor. The contribution from the char itself to mechanical resistance is negligible because of its very low Young's modulus. Therefore, the char expansion term can be removed for simplicity. The overall effects of decomposition and charring were included in the mechanical property model by introducing a power law factor as shown later in the Temperature-Dependent Mechanical Properties section (Equations (3.16)-(3.17)). Therefore, only the material compliance and thermal expansion will be included in the numerical calculation, and the constitutive equation is then reduced to:

$$\varepsilon_{ij} = S_{ijkl}\sigma_{kl} + \alpha_{ij}\Delta T \tag{3.14}$$

where i,j,k,l=1,2,3. ε_{ij} is the strain tensor, S_{ijkl} is elastic compliance and $S_{ijkl} = S_{klij}$ for orthotropic materials, σ_{kl} is the stress tensor, α_{ij} are the thermal coefficients of expansion, and $\Delta T = T - T_{\infty}$ is the temperature difference. The above equation assumes $\sigma_{kl} = 0$ initially (i.e., zero initial stress prior to loading and fire).

Because in this study compressive load was applied only along longitudinal direction (x-direction) with a uniform distribution over width direction (y-direction) and the panel was very thin, we can assume that strain oriented in y-direction is negligible and panels only experience plane strain in x-z plane, then $\varepsilon_{yy} = \varepsilon_{yz} = \varepsilon_{xy} = 0$ and the problem is reduced to be two dimensional. The compliance matrix **D** for orthotropic material becomes:

$$[D_{IJ}] = [S_{ijkl}] = \begin{bmatrix} \frac{1}{E_x'(T)} & -\frac{v_{zx}'}{E_z'(T)} & 0 \\ -\frac{v_{xz}'}{E_x'(T)} & \frac{1}{E_z'(T)} & 0 \\ 0 & 0 & \frac{1}{2G_{zx}(T)} \end{bmatrix} \tag{3.15}$$

where $E_x' = \frac{E_x}{1-v_{yx}v_{xy}}$, $E_z' = \frac{E_z}{1-v_{yz}v_{zy}}$, $v_{zx}' = \frac{v_{yx}v_{zy}+v_{zx}}{1-v_{yz}v_{zy}}$, $v_{zx}' = \frac{v_{yz}v_{xy}+v_{xz}}{1-v_{yx}v_{xy}}$; *I, J*=1,2,3; *i, j, k, l*=1,2; Young's modulus and shear modulus E_x, E_z, G_{zx} are the functions of temperature, and Poisson's ratios are assumed independent of temperature. Coupled thermal/mechanical analysis can be achieved through the temperature-displacement step in ABAQUS [54] by solving Equation (3.14) numerically using four-node plane strain element CPE4RT.

3.4.2. Temperature-dependent mechanical properties

The analysis of composite structures in fire requires that each elastic constant or strength value is expressed as a function of temperature. For composites with thermosetting resin systems, glass transition occurs before decomposition. A suitable mechanical property vs. temperature relationship can be obtained through fitting experimental data of a composite at different temperature levels under isothermal conditions [10]. A number of empirical functions can be used for fitting the mechanical properties of thermoset composites. As demonstrated in [10], particular success was achieved with functions based on a hyperbolic tangent function:

$$P(T) = \frac{P_U + P_R}{2} - \frac{P_U - P_R}{2} tanh\left(k'(ln(a_T) + \frac{H}{R}(\frac{1}{T_g} - \frac{1}{T}))\right) \tag{3.16}$$

where k' is a constant describing the breadth of the relaxation and T_g is the temperature of the mechanically observed glass transition. The function describes mechanical behaviors as a function of both temperature and time-scale, and thus viscoelastic effects are considered in the model. When applying this equation for this study, we should realize that the experimental data used for fitting the model are from tests that have the same time-scale as in the validation case studies later. Therefore, creep measurement shift factor is zero and the expression simplifies to:

$$P(T) = \frac{P_U + P_R}{2} - \frac{P_U - P_R}{2}\tanh(\varphi(T - T'g)) \tag{3.17}$$

where P(T) is the particular mechanical property, P_U and P_R are values of that property at the room and at high temperatures, respectively. T'_g is the mechanically determined glass transition temperature, at which mechanical properties are half reduced compared with those at room temperature. In general, T'_g is not the same for all properties; φ is a constant describing the breadth of the distribution. Except for Poisson's ratios, Equation (3.17) works for all mechanical properties, including elastic modulus, strength, and fracture energies provided that all coefficients are determined correctly based on experimental data. The temperature-dependent mechanical model is valid until the initiation of decomposition since it cannot account for decomposition effects on mechanical properties. To consider the effects of decomposition, a power law factor F^n is multiplied to Equation (3.17)

$$P(T) = \left\{\frac{P_U + P_R}{2} - \frac{P_U - P_R}{2}\tanh\left(\varphi\left(T - T'_g\right)\right)\right\}F^n \tag{3.18}$$

$$F = (\rho - \rho_d)/(\rho_v - \rho_d) \tag{3.19}$$

where F relates the mass loss of resin to mechanical properties and in general is temperature as well as heating rate-dependent. Equation (3.19) does not show explicitly the effect of heating rate. However, when calculating instantaneous density using Equation (3.5), the effect of heating rate is included in the model. Since in Equation (3.5), a shift temperature T_{sh} is introduced in modeling mass loss. The shift temperature is a function of heating rate and considers the effect of heating rate on decomposition. The exponent n is a constant dependent on the relationship between the mass loss of the resin matrix and the mechanical property, and must be determined by tests.

3.4.3. Modeling delamination

Delamination is a very common damage in FRP sandwich structures under simultaneous one sided heating and mechanical loading. Typical FRP sandwich panels consist of FRP skins and core. In ABAQUS, cohesive elements can be used to model the delamination of interface between FRP skins and core. Bilinear traction-separation law is selected for the constitutive response of interface [54]. The constitutive response is initially linear elastic, followed by damage initiation and damage propagation [55]. The traction separation response is reversible until the peak stress, t^0, is reached. Damage modeling includes damage initiation based on either stress or strain, and damage evolution based on either displacement, δ_f, or fracture energy, G^C. In ABAQUS, options are available on deletion of damaged elements according to maximum degradation, which should be defined with material imperfections considered. In this study, temperature-dependent fracture properties were used in delamination modeling, and more details will be given in Validation Problem III.

3.5. Fire Resistance and Failure Criteria

Fire resistance describes the ability of a material or structure to restrict the spread of fire and to retain mechanical and physical integrity. In the study, the following four criteria were used to assess fire resistance of FRP composites. The temperature limit criterion measures the thermal insulation of FRP panels; the other three criteria measure the ability of FRP structures to resist collapse.

3.5.1. Temperature limit

Fire resistance is very often defined by the time taken for the unexposed surface temperature to reach 160°C, at which point the fire is likely to spread to neighboring rooms [2].

3.5.2. Buckling failure

Buckling failure is indicated by the sudden change of deformations and can be determined using deformation histories, such as transverse deflection and in-plane deformation.

3.5.3. Load bearing capacity

In structural fire testing, according to ISO 834 (which is very similar to ASTM E-119), failure to support the load is deemed to have occurred for an axially loaded structure when both of the following limits have been exceeded [56]:

$$C = H/100 \text{ and } dC/dt = 3H/1000 \tag{3.20}$$

where C in mm and dC/dt in mm/min are the limits of axial contraction and axial contraction rate. H is the initial height in millimeters. The criterion is similar to buckling failure criterion but is based on quantitative measurement of deformation and works for

non-buckling cases as well. It should be noted that the load bearing criterion in Equation (3.20) is intended to ensure safety during furnace fire tests. Because two validation problems in this study (to appear in Model Validation section) involve furnace fire tests, this criterion is introduced here.

3.5.4. Compressive strength criterion

Failure is assumed to occur once the average compressive strength ($\boldsymbol{\sigma_{av}}$) is reduced to the compressive stress applied to the laminate [57]. The failure criterion does not account for lamina-level effects and treats composite panels as bulk materials. The average compressive strength is determined by integrating the strength values over the entire thickness of the laminate using the Simpson integration technique:

$$\sigma_{av} = \frac{1}{b-a}\int_{a}^{b} = \frac{1}{3m}\left[\sigma(x_0) + 4\sigma(x_1) + 2\sigma(x_2) + \cdots + 2\sigma(x_{k-2}) + 4\sigma(x_{k-1}) + \sigma(x_k)\right] \tag{3.21}$$

where m is an even number of locations along the thickness of panels where the residual compressive strength is calculated. The criterion is valid for failures caused by compression or tension but not by buckling or bending failure because it cannot account for thermal moment due to thermal expansion and eccentric moment due to movement of neutral axis.

3.6. Model Validation

3.6.1. Validation problem I: FRP laminate under one-sided heat flux

In the first validation study, a one-sided heating test [57] was modeled. As in the test, a glass/vinyl ester laminate of size 560x50x9 mm was exposed directly to a constant

heat flux of 50kW/m² at one side and thermally insulated at another side. Material properties for the glass/vinyl ester [57] composite are provided in Table 3.1.

The top end of the laminate was roller-guided (i.e., clamped but can move in vertical direction) and the bottom end was completely clamped. Constant compressive loading of 80% of the Euler buckling load was applied at top of the laminate. In FEA implementations, one-dimensional thermal analysis was conducted in COMSOL. The same thermal analysis can be conducted in ABAQUS, but COMSOL is easier to implement. 30 elements of size 0.3 mm are uniform through thickness direction. A time-dependent solver was used with a time step of 1 second. Mesh and time-step sensitivity studies were performed and showed that temperature results converged very well. Mesh and time-step sensitivity studies were also performed for all flowing thermal and structural analyses. Temperatures at hot face, middle, and cold face from modeling are compared with experimental results. With the temperature profile from thermal analysis, two-dimensional structural analysis was carried out in ABAQUS. When modeling a structure that bending or buckling is expected using reduced-integration elements, at least four elements along thickness are needed in ABAQUS to overcome hourglass numerical problem. For that reason, the thickness of the panel was uniformly discretized with 12 elements of size 0.75mm. ABAQUS/Standard with an initial time step of 10 seconds was used to solve the constitutive equation (an initial time step is needed to get ABAQUS started and has little influence on convergence and results), subsequent time steps were determined automatically by ABAQUS based on built-in converge criteria. Thermal boundary condition as in Equation (3.10) was used on the hot face, and the condition as in Equation (3.12) was used on the cold face.

Table 3.1: FRP material properties in validation problem I

Density [kg/m³]	1921	Manufacturer
Compressive Modulus [GPa]	28	In-house test
Shear Modulus [GPa]	3.8	In-house test
Fiber volume fraction	0.55	Burn off test
Heat of decomposition [J/kg]	378800	DSC/TGA
Specific heat [J/kg.K] (45°C)	960	DSC
Specific heat [J/kg.K] (140°C)	1210	DSC
Specific heat [J/kg.K] (290°C)	1360	DSC
Thermal Conductivity [W/m.K]	0.43	In-house test
Rate constant [1/s]	5.59E13	TGA
Activation energy [J/kg.mol]	212705	TGA
Order of decomposition reaction	1	TGA

Mesh sensitivity studies with double elements were performed for both thermal and structural modeling in this and the following two validation studies, temperature and deflection results were found converged very well.

The temperature comparisons of modeling with tests in Figure 3.1 show that the agreement is excellent, revealing that the model can reasonably predict the thermal effects of heat conduction, endothermic decomposition of vinyl ester, and convection flow of the volatiles as shown in the three terms on the right side of Equation (3.1). In Equation (3.5), a shift temperature is included to consider the effect of heating rate on

decomposition. However, as temperature results shown in Figure 3.1, the effect of high heating rates occur only in the first few minutes (about 4 minutes) on the heated surface only

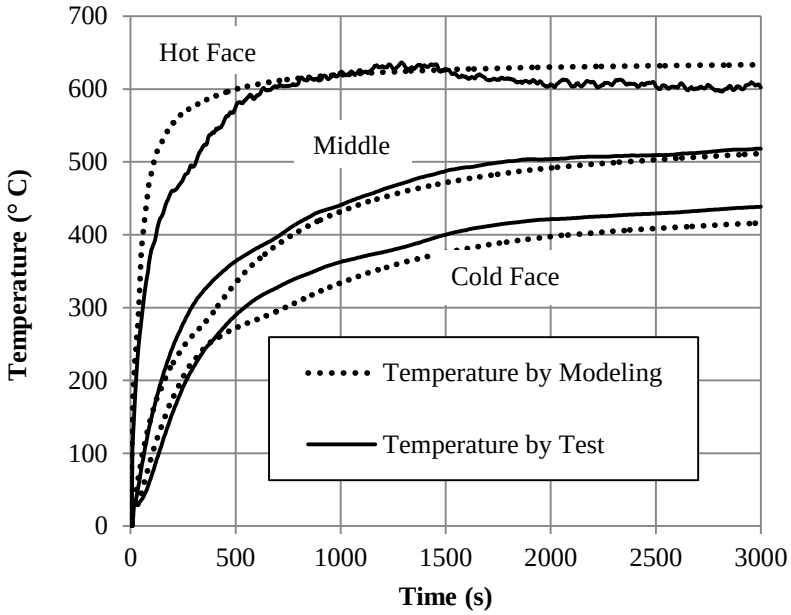

Figure 3.1: Temperatures at Different Locations

After about 4 minutes the heating rate decreased quickly. This holds true in general for one sided heating. Therefore, heating rate in this case study has minor influence on the predictions of temperature and thus decomposition rate.

Included in Figure 3.2 are deflection comparisons at center point. Both results from modeling and tests indicate that the laminate bends initially toward the heat source due to thermal moment caused by uneven thermal expansion over thickness, then the eccentric moment reverses the laminate away from the heat source because the neutral axis moves away from the heat source due to larger stiffness loss at the exposed surface. Modeling predicts correct deflection tendency and the agreement is good.

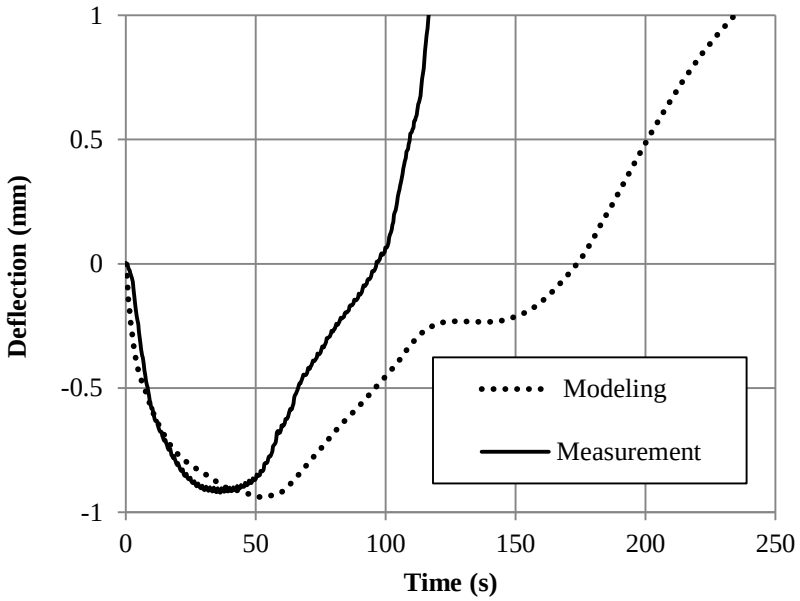

Figure 3.2: Comparison of Deflection at Center Point

Based on axial contraction and axial contraction rate results by modeling, time to failure according to load bearing capacity is 8 minutes when both limits of axial contraction and axial contraction rate are met. It is noted that buckling failure cannot be determined based on deformation history, including axial contraction and deflection at center point because no sudden deformation change was detected.

3.6.2. Validation problem II: FRP laminate panel under furnace fire

In the second validation study, a structural test [58] was modeled. In this test, a glass/vinyl ester laminate of size 910x710x12 mm with 25.4 mm thick superwool as thermal insulation was exposed to IMO A. 754 furnace fire. Glass/vinyl ester laminate [58-59] used in this validation study had less fiber content than in the first validation study and has different thermal and mechanical properties, as shown in Table 3.2.

The top end of the laminate was roller-guided (i.e., clamped but can move in the vertical direction), while bottom end was simply supported. A constant force of 9.7kN

was applied on top of the laminate. The full mechanical load was applied prior to thermal loading and kept constant during testing. Thermocouple TC1 was located at the exposed surface of superwool, while thermocouples TC2-TC5 were positioned 4 mm apart along the thickness of the laminate for temperature measurement. Deflections at 160, 310, and 620 mm away from the bottom surface and in-plane deformation of top surface were measured in the test. One-dimensional thermal analysis was conducted in COMSOL. Thickness direction, including superwool insulation and laminate, uses 60 elements of size 0.62mm. A time-dependent solver was used with an initial time step of 10 seconds. In the 2D structural analysis in ABAQUS, element size was 2x2 mm with 19 elements through the thickness (including superwool). The solver was ABAQUS/Standard and the initial time step was 10 seconds. A prescribed temperature boundary defined by IMO A. 754 standard time-temperature curve was used on the hot face, and the condition as in Equation (3.12) was used on the cold face.

Figures 3.3(a)-(d) compare temperature results from modeling with experimental data, which was obtained by averaging temperature results of the test used in this validation study and two other structural fire tests conducted in [58]. The three tests used the same samples subject to the same thermal load (IMO A.754) and boundaries but different mechanical loading. Mechanical deformations before failure from all three tests were very small compared to length and width of panels and were assumed to have no effects on heat transfer, which was verified reasonable by error bars of test temperatures. Overall, the test and modeling are in good agreement. The temperature difference between test and modeling is mainly caused by unreliable thermal properties at high temperature and an increasing uncertainty on measurement of high temperatures, as show

Table 3.2: FRP material properties in validation problem II and III

Density [kg/m³]	1682	Manufacturer
Compressive Modulus [GPa]	20.67	In-house test
Fiber weight fraction	0.7	-
Heat of decomposition [J/kg]	378800	DSC/TGA
Virgin Specific heat [J/kg.K]	$1080 + 0.0452T$	DSC
Decomposed Specific heat [J/kg.K]	$1041 + 0.259T$	DSC
Virgin Thermal Conductivity [W/m.K]	$0.312 + 4.405 \times 10^{-5}T$	TDA
Decomposed Thermal Conductivity	$0.0949 + 2.83 \times 10^{-4}T$	TDA
Rate constant [1/s]	5.59E13	TGA
Activation energy [J/kg.mol]	212705	TGA
Order of decomposition reaction	1	TGA

by error bars in Figures 3.3(a)-(d). On the other hand, our current thermal model does not explicitly account for the effects of internal gas pressure, thermal expansion, and volatile gas accumulation on thermal properties. While thermal expansion only consumes little energy and has little influence on heat transfer, internal gas pressure and volatile gas accumulation can affect heat transfer considerably by increasing the porosity (and permeability) of the composite, which can reduce thermal conductivity and increase specific heat. In the current model, thermal properties at the decomposing state are highly dependent on the measurements of thermal properties at the virgin state and the decomposed state, and the interpolation method (Equations (3.6)-(3.8)). From the

comparisons in Figures 3.3(a)-(d), the estimated magnitude of error is between 5-20% by ignoring these factors, although reliable experimental data are needed to examine this issue. Further research is needed to obtain more accurate thermal properties for a decomposing composite, especially the effect of changing porosity (permeability) on heat transfer.

Figures 3.4(a)-(d) shows deflection results by modeling compared to test data. Agreement in general is good, except for deflection at location 620mm, as shown in Figure 3.4(c). The differences are primarily due to the change of mechanical boundary conditions of the top end during fire tests. Figure 3.4(c) shows the deformation close to the top end.

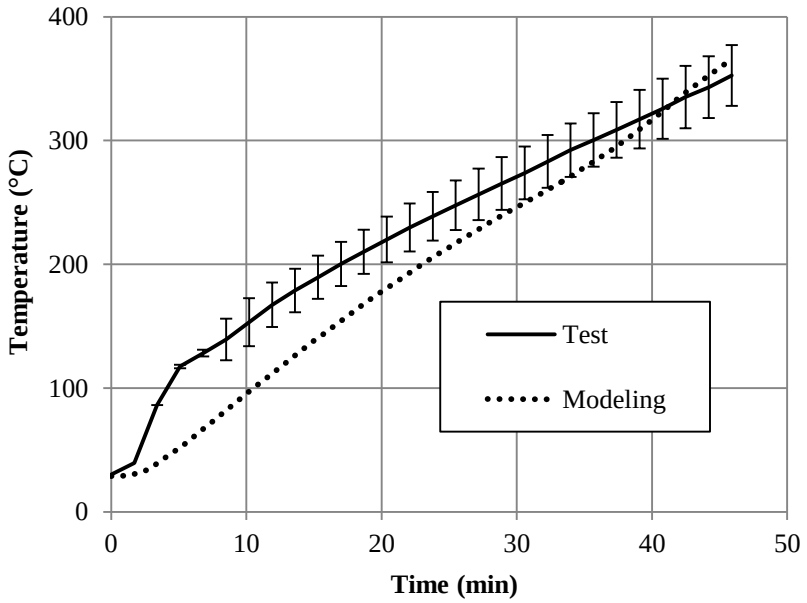

Figure 3.3(a): Temperatures at TC2

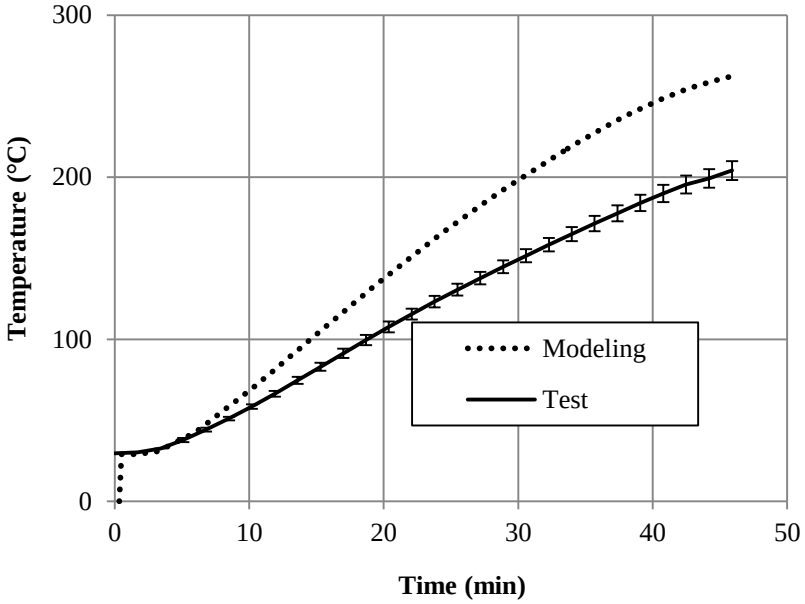

Figure 3.3(b): Temperatures at TC3

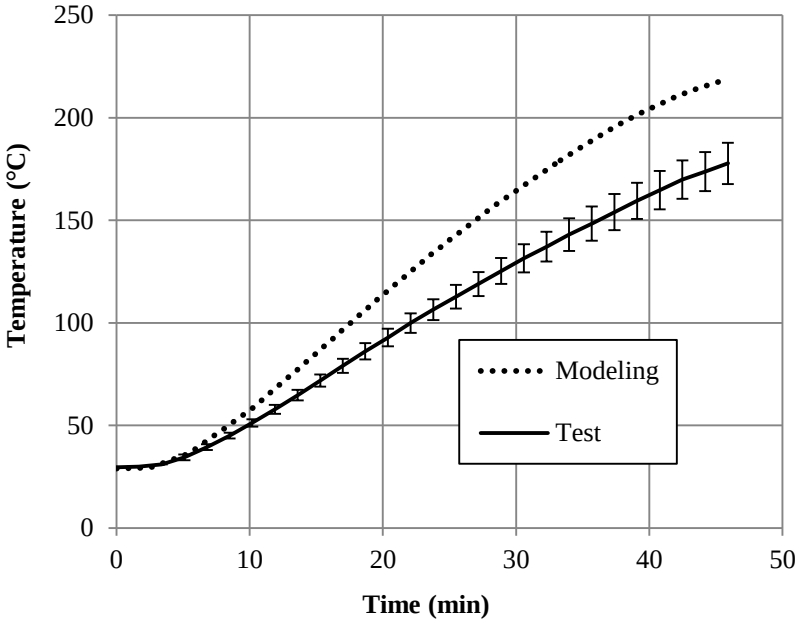

Figure 3.3(c): Temperatures at TC4

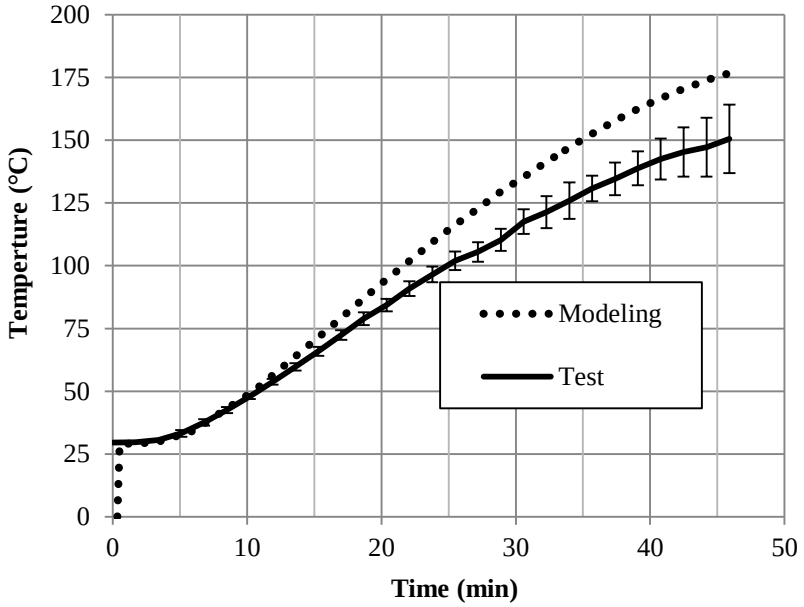

Figure 3.3(d): Temperatures at TC5

The boundary condition on the top end has significant effects on deflection. The top end had an initial "roller-guided" boundary condition, but this condition was changing during fire testing because of the heating of the steel fixtures and the softening and thermal expansion of the composite at high temperature. No information was available detailing the exact boundary condition as a function of time during the fire tests. However, our model suggests the effect of heating changed the boundary condition from the initial "roller-guided" to somewhere between "roller-guided" and "simply supported." Our modeling results further show that for locations far from the top end, this effect is less significant, as shown in Figures 3.4(a), (b) and (d). Modeling successfully predicts global buckling failure, which is indicated by a sudden change of deflection. Both deflection history and time to failure from modeling are in good agreement with test results, indicating that the mechanical property model works well and plain strain assumption is reasonable. Based on in-plane deformation, time to failure given by

criterion of load bearing capacity is 42 minutes, which is very close to test results and time to buckling failure.

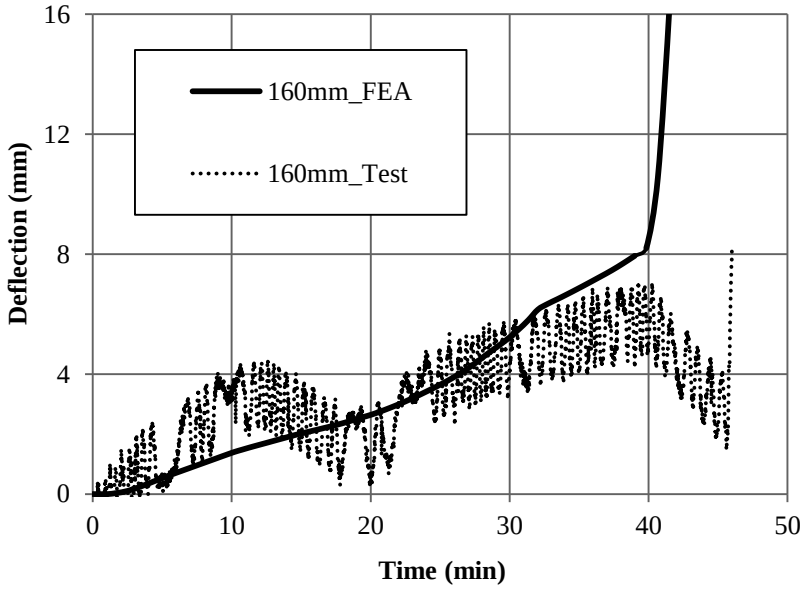

Figure 3.4(a): Deflections at 160mm

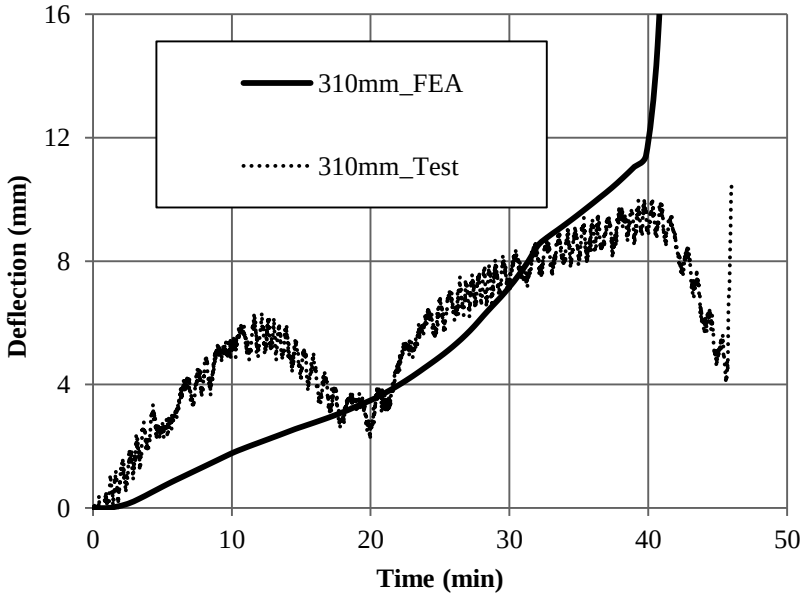

Figure 3.4(b): Deflections at 310mm

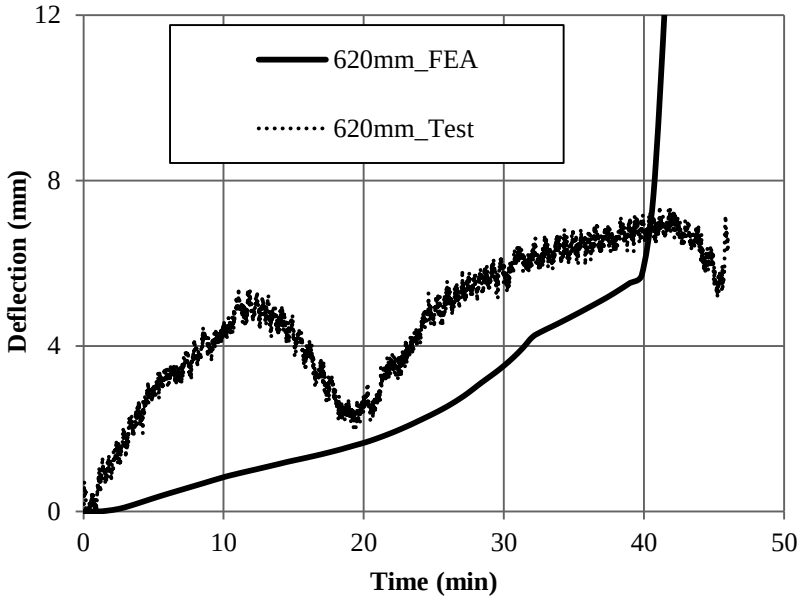

Figure 3.4(c): Deflections at 620mm

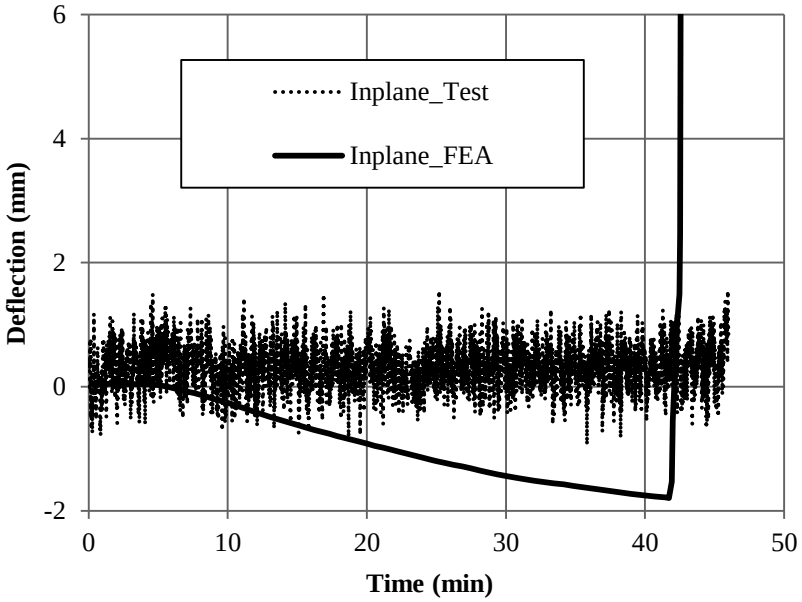

Figure 3.4(d): In-Plane Deformation

3.6.3. Validation problem III: FRP sandwich panel under furnace fire

In the last validation, a structural test [58] on sandwich panel was modeled. Test setup, and thermal and mechanical boundaries were the same as the structural test in Validation Problem II, except that the compressive load on the top was 21.8kN, and the

sample was a sandwich panel which had two 3mm thick skins and a 12 mm thick balsa wood core, for an overall thickness of 18 mm. Two skins were made of glass/vinyl ester as the laminate panel in validation problem II. Material properties for balsa wood [58-59] are provided in Table 3.3.

Table 3.3: Material properties for balsa wood

Density [kg/m³]	178	Manufacturer
Modulus of elasticity[GPa]	0.175	In-house test
Heat of decomposition [J/kg]	500000	DSC/TGA
Virgin specific heat [J/kg.K]	$1420 + 0.68T$	DSC
Decomposed specific heat [J/kg.K]	$3194 + 1.33T$	DSC
Virgin thermal conductivity	$0.06 + 9.211 \times 10^{-8}T^{2.503}$	TDA
Rate constant [1/s]	2.2E5	TDA
Activation energy [J/kg.mol]	88000	TGA
Order of reaction	2	TGA

Thermocouple 1 (TC1) still measured the temperature of the exposed surface of superwool, TC2 measured the interface between superwool and FRP skin, TC3 and TC5 the two interfaces between FRP skin and balsa core, TC4 the middle of balsa, and TC6 the back surface of panel, respectively. Since temperature prediction had been well validated in Validation Problems I and II, in Problem III, only TC2 and TC6 measurements were used for validating temperature prediction. Deflections/deformations at the same locations as the test in Validation Problem II were measured. A temperature

boundary as in Equation (3.10) using the IMO A. 754 standard time-temperature curve was used on the hot face and a heat flux boundary as in Equation (3.12) was used on the cold face. Similar to Validation Problem II, a one-dimensional thermal analysis was conducted in COMSOL. The thickness direction, including superwool thermal barrier, laminate skins, and balsa core, was uniformly discretized with 60 elements of size 0.72mm. Time-dependent solver was used with time step of 1 second. The 2D Structural analysis in ABAQUS was conducted with element size of 3x3 mm for superwool and balsa, 1.5x3 mm for FRP skins, 0.0001x 3mm for the cohesive layer; a total of 18 elements (including cohesive layer). The solver was ABAQUS/Standard using an initial time step of 10 seconds.

Delamination modeling on two interfaces between FRP skin and balsa core used one single layer of cohesive elements. The following quadratic stress criterion was used for damage initiation:

$$\left(\frac{\langle t_n \rangle}{t_n^0}\right)^2 + \left(\frac{t_s}{t_s^0}\right)^2 = 1 \tag{3.22}$$

where t_n, t_n^0, t_s, t_s^0 are the normal stress, peak normal stress, first shear stress, and peak shear stress of interface, respectively; damage evolution was based on fracture energy. All material properties for delamination modeling, such as peak stress and fracture energy as shown in Table 3.4, were temperature dependent and were fitted to Equation (3.17) as other mechanical properties [51].

Figure 3.5 shows temperatures at locations TC2 and TC6 compared to test results. Temperature predictions at FRP skins (TC2 and TC6) are good.

Table 3.4: Delamination model parameters for FRP/balsa interface

Mode I fracture energy $\boldsymbol{G_I}$ [N/m]	450
Mode II fracture energy $\boldsymbol{G_{II}}$ [N/m]	1060
Normal peak stress [MPa]	11
Shear peak stress [MPa]	16

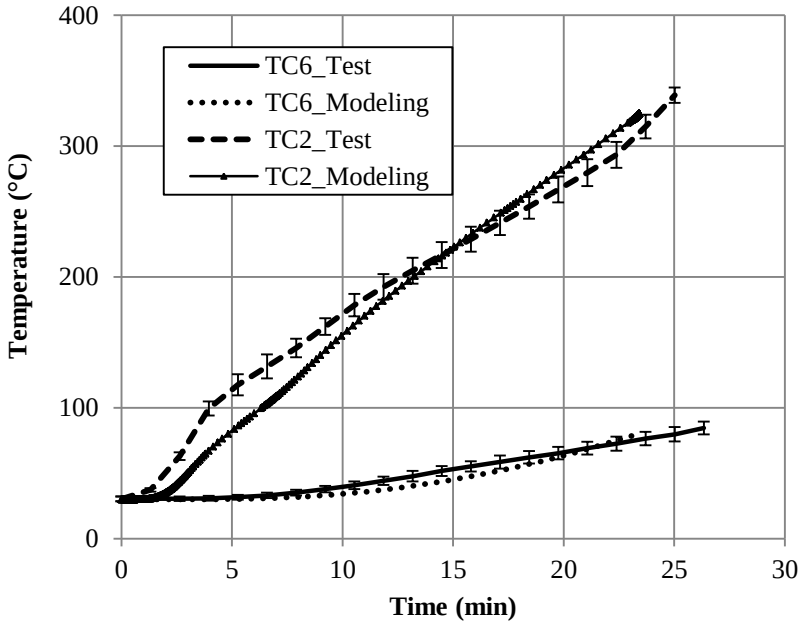

Figure 3.5: Comparison of Temperatures in Validation Problem II**I**

In-plane deformation and deflection results are shown in Figures 3.6(a)-(d). The agreement between modeling and test is excellent, except for the deflection history at 620mm, which can be explained by the same reason mentioned in validation problem II.

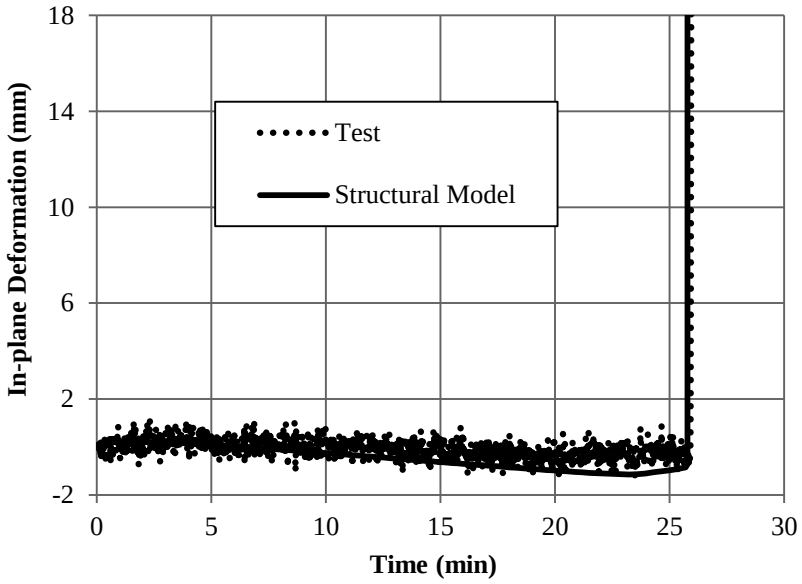

Figure 3.6 (a): In-Plane Deformation

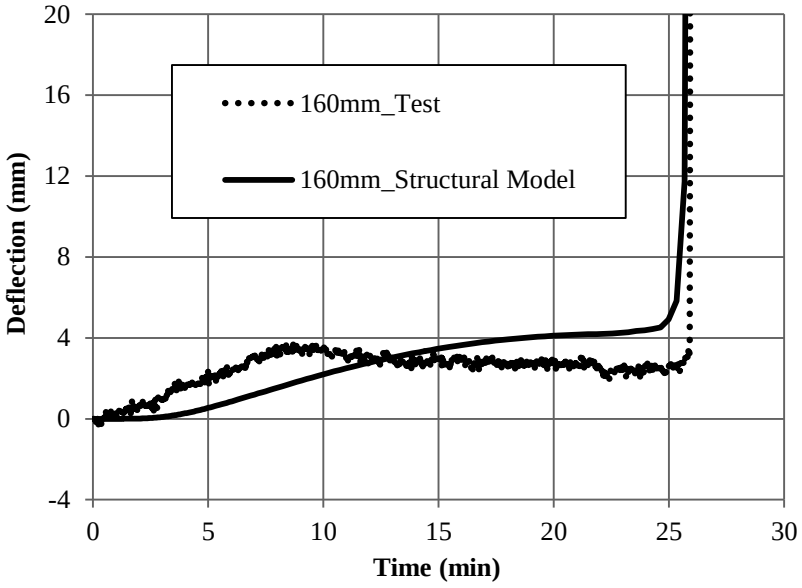

Figure 3.6 (b): Deflection at 160mm

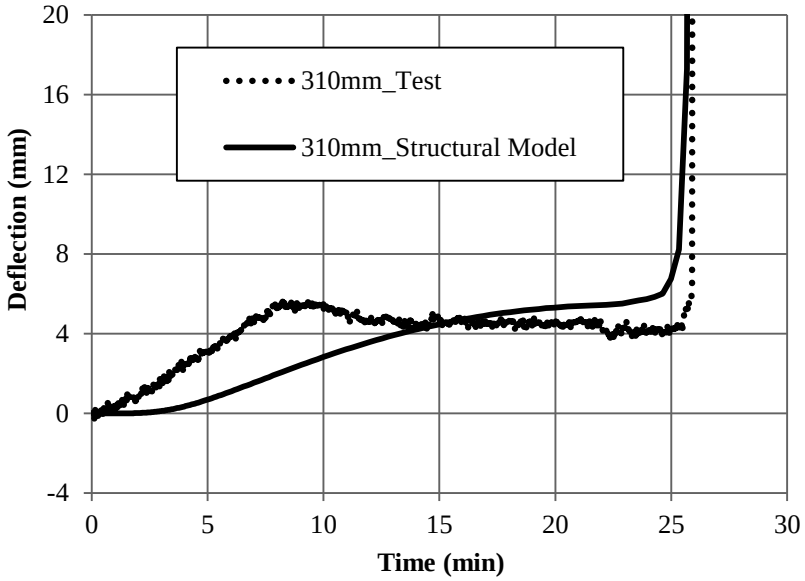

Figure 3.6 (c): Deflection at 310mm

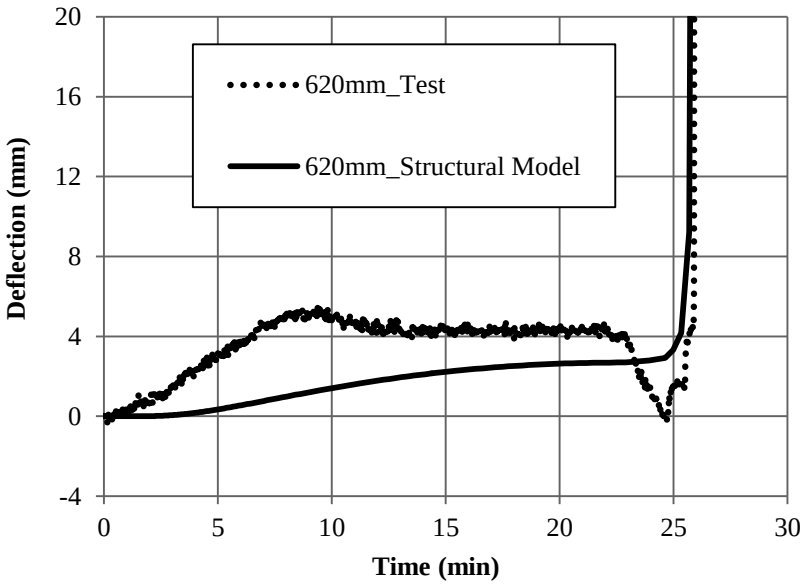

Figure 3.6 (d): Deflection at 620mm

Delamination modeling is good compared to test results, as shown in Figure 3.7. It is seen in modeling that delamination occurred at the upper part of the FRP/balsa

interface on the hot side, and no delamination at the interface on the cold side, which is consistent with test results.

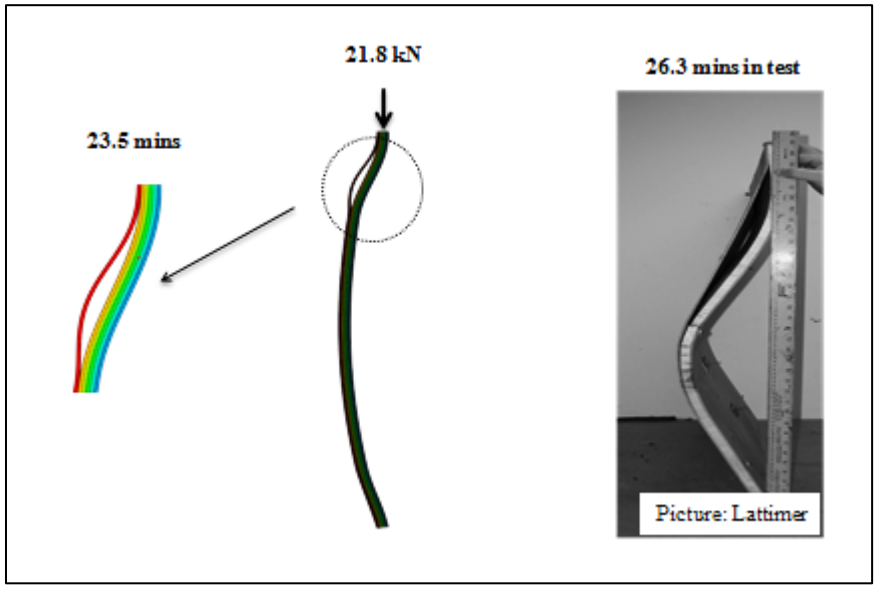

Figure 3.7: Delamination in sandwich structure

Both temperature limit and average strength gave no failure in 30 minutes because of good thermal insulation provided by superwool. Time to failure given by both bucking failure and load bearing capacity is 25.7 minutes, which is almost the same as in the test.

3.7. Conclusion

In this paper, a finite element based method was presented to predict the temperature and deformation histories of FRP structures under one-sided heating and simultaneous compression. The model included 1D heat transfer modeling and 2D mechanical modeling. The model considered temperature-dependent mechanical and thermal properties. The effects of decomposition on both temperature and deformation were included in the model. A concept of shift temperature was introduced to account for heating rate's effect on the decomposition temperature and therefore behavior of

laminates in fire. Assuming bilinear traction-separation response, cohesive elements can be incorporated in the thermo-mechanical model to consider the effect of delamination in the response of sandwich panels in fire. The model was validated with three case studies: a single FRP laminate strip under one-sided constant heat flux and compression, a single FRP laminate panel under furnace fire and compression, and an FRP/Balsa sandwich panel under furnace fire and compression. Deformation and structural response predictions compared well with experimental data. Although validation was conducted with cases of compressive loading, the model can be extended to tensile loading when it is validated with tensile loading in the future. Temperature prediction can be improved if more accurate temperature-dependent material properties are available. With temperature profile and deformation histories calculated from the model, fire resistance of FRP panels can be assessed. Results from the numerical modeling showed that the failure of FRP structures in fire is more likely controlled by the structure's stability (resistance to buckling). The proposed model is useful for predicting the response of FRP structures in fire in the performance-based fire safety design of FRP structures.

CHAPTER 4: EFFECT OF FLAME HEAT FLUX ON THERMAL RESPONSE AND FIRE PROPERTIES OF CHAR-FORMING COMPOSITE MATERIALS[3]

4.1 Abstract

This study evaluates the effect of flame heat flux on the prediction of thermal response and fire properties of a char-forming composite material. A simplified two-layer flame model was proposed and incorporated into a heat transfer thermal model to predict the thermal response and fire reaction properties of a burning material. A typical char-forming material, E-glass reinforced polyester composite, was used in the study. A cone calorimeter was used to measure the fire reaction properties of the composite. The flame heat flux in a cone calorimeter test setting was estimated using the simplified flame model. Thermal response and fire property predictions with and without the effect of flame heat flux were compared to experimental data obtained from the cone calorimeter tests. Results show that the average flame heat flux of the composite in a cone calorimeter was 19.1±6kW/m² from model predictions and 23.2±4kW/m² from experimental data. The flame had a significant effect on the thermal response and fire properties of the composite around the first heat release peak but the effect decreased rapidly afterwards.

---

[3]This chapter is based on a manuscript with the same title that has been submitted for publication by Fire and Materials. Chapter 4 provides more details than the manuscript due to page limit of a journal article.

4.2 Introduction

When exposed to a heat source, a combustible material will be heated up, once the flaming combustion conditions are met, the material will be ignited with flame covering its exposed surface. The combustion is sustained when a positive net heat flux into the material is maintained. Before ignition, the material receives heat flux only from the external heat source. After ignition, the flame adds additional heat flux to the material. The heat flux from a material's own combustion flame plays an important role in the determination of fire properties because it contributes a major part of the driving force causing flame spread to occur and drives the material to burn at a higher level [62].

The flame heat flux from flaming materials can be determined either by direct experimental measurement or predictions from analytical or numerical models. Quintiere [62] developed a semi-quantitative model to predict the steady burning rate of both thermoplastic and char-forming materials, from which the flame heat flux could be estimated, but the model could not predict transient burning rate. Babrauskas and Wetterlund [2] studied the flame spread data of six materials using the LIFT apparatus with additional instrumentation for measuring heat fluxes. The heat fluxes obtained experimentally in [2] showed much less variation among materials than other comparable data from the literature. Beaulieu et al. [63] measured the flame heat fluxes of samples of 105mm in diameter and showed that the total flame heat fluxes of black polymethylmethacrylate (PMMA), propylene, and black polymethylene (POM) in normal oxygen concentration are 20, 15, and 11kW/m^2, respectively. They also used a surface emitter model to calculate the flame heat fluxes in the tests with measured flame temperature and flame emissivity. Petrella [64] used sample diameters of 71-113mm in

horizontal orientation to predict the flame heat fluxes of eight wood-based materials by measuring the steady-state mass burning rate, the average flame heat flux for the eight wood-based materials was determined as 30.9±11 kW/m². Azhakesan et al. [65] addressed the effect of flame heat flux on the opposed flow flame spread and provided a good review on methods to estimate flame heat flux from both calorimetric data and numerical modeling. Rhodes and Quintiere [66] developed a transient burning model for thermoplastic materials and showed that the flame heat flux of black PMMA was approximately a constant value of 37kW/m². Most previous research focused on determining flame heat flux from thermoplastic materials that exhibit a steady burning rate soon after ignition. A char-forming material typically exhibits more complicated burning behaviors with increasing surface temperature. Very limited work was done to examine the flame heat flux from the burning of char-forming materials. Luo et al. [7-8] and Chen et al [69] used computational fluid dynamics (CFD) models to estimate flame temperature and the effect of flame on boundary conditions of char-forming composite materials. The modeling of turbulent flame is always with uncertainty and at expensive computation cost [7-9], thus fire modeling based on CFD principles is still a challenging task despite available advanced computing techniques and technologies. There is a need of simplified physics-based flame models for estimating flame heat flux from char-forming materials for fire safety design purpose.

While much research has been given to measuring or modeling the flame heat flux from burning materials, little attention has been paid to examining the effect of a material's own combustion flame on the transient thermal response and fire properties of the material. Most thermal models [11-13, 25, 70-74] that have been used to predict the

thermal and thermo-mechanical responses of a material ignored the effect of a material's own flame after flaming ignition. However, the flame heat flux from a burning material in general is in the same order of magnitude as the irradiance heat flux applied in small-scale fire tests [6]. While the ignorance of flame heat flux can simplify the model and its numerical simulation, it will underestimate mass loss rate and heat release rate predictions and may disguise the actual fire hazard of a combustible material. A thorough quantitative study is needed to investigate the effect of flame heat flux from a burning char-forming material on its thermal response and fire property determination.

The objective of the study is to evaluate the effect of flame heat flux on the prediction of transient thermal response and fire properties of a char-forming composite material. A simplified two-layer flame model was proposed and validated. To have a general flame model, typical turbulent flame properties (such as fuel gas temperature, flame temperature and flame height) were used to estimate the flame heat flux. The simplified flame model was incorporated into a heat transfer thermal model to predict the thermal response and fire reaction properties of a burning material with the consideration of the effects from flame heat flux. A typical char-forming material, E-glass reinforced polyester composite, was chosen in this study. E-glass/polyester composite has been widely used in building construction, where fire safety measures are stringent. In addition, many needed material thermal and fire properties were known [37, 75-76] for this study. Cone calorimeter tests were performed to determine the fire reaction properties of the E-glass/polyester composite. The prediction of the effect of flame heat flux on thermal response and fire properties was evaluated by comparing the modeling results with experimental data.

4.3 Heat Transfer Model

The model for predicting the thermal response and fire reaction properties of the composite in fire is based on the mass and heat transfer model developed by Henderson et al [11]. This model has been widely used to calculate the temperature distribution and mass flux in composites exposed to fire [35]. The model offers a good balance between capability and accuracy [12, 25, 37, 75-76]. Based on the assumptions that pyrolysis gases are transported instantaneously to the surfaces and the mass flux at the unexposed surface is zero, the one-dimensional model is given by:

$$\rho C \frac{\partial T}{\partial t} = \frac{\partial}{\partial x}\left(k \frac{\partial T}{\partial x}\right) - \left(Q + H - H_g\right)\frac{\partial \rho}{\partial t} - \dot{m}_g'' C_g \frac{\partial T}{\partial x} \tag{4.1}$$

$$\frac{\partial \dot{m}_g''}{\partial x} = -\frac{\partial \rho}{\partial t} \tag{4.2}$$

$$\frac{\partial \rho}{\partial t} = -A(\rho_v - \rho_d)\left(\frac{\rho - \rho_d}{\rho_v - \rho_d}\right)^n \exp\left(-\frac{E}{RT}\right) \tag{4.3}$$

where three terms on the right hand side of Equation (4.1) relate to heat conduction, resin pyrolysis, and volatile convection, respectively; the enthalpy of a composite $H = \int_0^T C\, dT$; the enthalpy of pyrolysis gases $H_g = \int_0^T C_g\, dx$; Equation (4.3) is Arrhenius equation to describe the pyrolysis reaction.

The E-glass/polyester composite in the study has a 28.72% fiber volume fraction. Material properties of the composite are listed in Table 4.1 [45]. Using an analytic method described in [43] with TGA data at heating rates of 5, 15, 25°C/min, the pyrolysis kinetics of the composite was determined as the rate constant A=34377066771s^{-1}, the order of reaction n=4.4463, and the activation energy E=149026 Jmol^{-1}.

Table 4.1: Material Properties of the E-glass/Polyester

The origin density $\boldsymbol{\rho_v}$ (kg/m³)	1888
The decomposed density $\boldsymbol{\rho_d}$ (kg/m³)	1133
Fiber heat capacity $\boldsymbol{C_f}$ (J/kg.K)	$760 + 3.88 \times 10^{-2}T$
Resin heat capacity $\boldsymbol{C_r}$ (J/kg.K)	$1600 + 0.8T$
Fiber thermal conductivity $\boldsymbol{k_f}$ (W/m².K)	$760 + 2.05 \times 10^{-4}T$
Resin thermal conductivity $\boldsymbol{k_r}$(W/m².K)	$0.2 - 1.356 \times$
Fiber volume fraction $\boldsymbol{V_f}$	0.2872
Fiber weight fraction $\boldsymbol{W_f}$	0.4

The effect of porosity on the thermal conductivity of polyester was accounted for with an asymmetrical model for porous materials with two phases. The two phases here are polyester and pore, which is left behind by pyrolysis reaction.

$$k_{r\_eff} = k_r(1 - F)^{1.5} \tag{4.4}$$

$$F = \frac{(\rho_v - \rho)}{(\rho_v - \rho_d)(1 - V_f)} \tag{4.5}$$

Assuming that the effect of thermal expansion is negligible, the thermal conductivity of the composite is given implicitly by

$$\frac{1}{k} = \frac{1 - V_f}{k_{r\_eff}} + \frac{V_f}{k_f} \tag{4.6}$$

and the specific heat of the composite is determined as

$$C = \frac{W_f C_f}{W_f + (1 - W_f)(1 - F)} + \frac{(1 - W_f)(1 - F) C_r}{W_f + (1 - W_f)(1 - F)} \tag{4.7}$$

In a cone calorimeter test, the thermal boundary condition at the exposed surface is:

$$-k\frac{\partial T}{\partial x} = \dot{q}_e'' + \dot{q}_{fl}'' - \varepsilon_s \sigma (T_s^4 - T_\infty^4) - h(T_s - T_\infty) \tag{4.8}$$

In Equation (4.8), the effect of the flame heat flux $\dot{q}_{fl}''$ is considered here as an additional heat flux to the irradiance heat flux $\dot{q}_e''$. The convective heat transfer coefficient in Equation (4.8) is taken as 10 W/m².K [42, 44, 46].

Thermal insulation condition is applied at the back surface in a cone calorimeter test, which is described by:

$$-k\frac{\partial T}{\partial x} = 0 \tag{4.9}$$

4.4 Flame Heat Flux in a Cone Calorimeter Test

For a typical cone calorimeter test in horizontal mode, the flame can be approximated with a simplified two-layer model as shown in Figure 4.1. The two layers refer to a layer of fuel core and a layer of flame sheet.

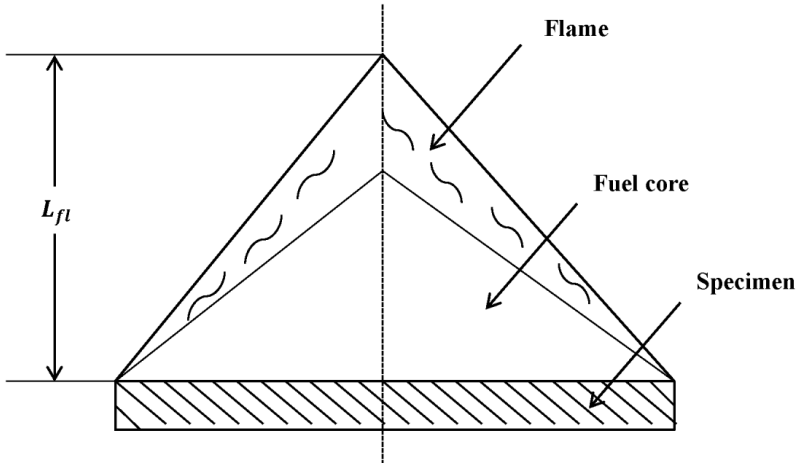

Figure 4.1: Two-layer flame model

Although a sample used in a cone calorimeter test is a square, the shape of the flame over the sample after ignition is approximately a cone as observed in a cone calorimeter test. It is assumed that the flame sheet can be modeled as surface emitter [64] for radiation, and the fuel core is responsible only for convective heat transfer. The reason for neglecting the radiation from fuel core is that the radiation energy is a strong function of temperature and the fuel core has a much lower temperature than the flame sheet.

The flame heat flux includes two parts: convective heat flux and radiative heat flux. The total flame heat flux $\dot{q}''_{fl}$, radiative flame heat flux $\dot{q}''_{rad}$ [63] and convective flame heat flux $\dot{q}''_{conv}$ [63] are given respectively by

$$\dot{q}''_{fl} = \begin{cases} \dot{q}''_{rad} + \dot{q}''_{conv} & if\ \dot{m}'' \geq \dfrac{5g}{m^2.s} \\ 0 & otherwise \end{cases} \tag{4.10}$$

$$\dot{q}''_{rad} = \varepsilon_{fl}\varphi\sigma T_{fl}^4 \tag{4.11}$$

$$\dot{q}''_{conv} = h(T_g - T_s) \tag{4.12}$$

In Equation (4.10), it is assumed that when mass loss rate per unit area $\dot{m}''$ is below 5g/m².s the flame is not stable and has no contribution to net heat flux into the sample. The reason for this is that extinguishment can occur if mass loss rate is below the empirical threshold [77].

The stoichiometric polymer flame temperatures are approximately 1250ºC [78]. This is the maximum temperature a solid polymer flame can reach in a normal ventilation condition. The measured lowest flame temperature for polyester was 750°C [78]. Solid polymer flame temperatures [79-81] fell in a range 917-1127ºC under normal ventilation condition. Test conditions in a cone calorimeter represent an over-ventilated condition in which additional air will reduce flame temperature. In this study, 1022°C (the average of 917-1127ºC) was used as the flame temperature T_{fl} in calculations. The gas temperature T_g was taken as 822°C (about 200°C below the flame temperature) [82]. For a thin flame in a cone calorimeter test, the flame emissivity ε_{fl} [77] is given by

$$\varepsilon_{fl} = 1 - \exp(-KI) \tag{4.13}$$

$$K = 3.72 C_0 f_v T_{fl} / C_2 \tag{4.14}$$

$$I = 3.6 V_{fl} / A_{fl} \tag{4.15}$$

Equation (4.14) is an empirical formula [90] to estimate the effective emission coefficient; the mean beam length I [91] is calculated based on flame volume and flame bounding area as in Equation (4.15); C_0 is a constant between 2 and 6, a value of 4 is used here; f_v is the soot fraction in flame, a value of 1×10^{-6} is used here [83]; C_2 is the

Planck's second constant (1.4388×10^{-2} m.K); The flame volume V_{fl} and the bounding area A_{fl} were calculated with the equivalence diameter D_{eff} of the square specimens and the flame height L_{fl} [84].

$$V_{fl} = \frac{1}{12}\pi D_{eff}^2 L_{fl} \tag{4.16}$$

$$A_{fl} = \frac{1}{2}\pi D_{eff}\sqrt{D_{eff}^2/4 + L_{fl}^2} + \frac{1}{4}\pi D_{eff}^2 \tag{4.17}$$

$$L_{fl} = 0.23\ \dot{Q}^{2/5} - 1.02 D_{eff} \tag{4.18}$$

$$D_{eff} = 2\sqrt{a/\pi} \tag{4.19}$$

In Equation (4.18), $\dot{Q}$ is heat release rate in kW; the view factor φ is given by

$$\varphi = \frac{1}{\sqrt{1 + 4\,L_{fl}^2/D_{eff}^2}} \tag{4.20}$$

4.5 Modeling of Fire Reaction Properties

Equations (4.1)-(4.3) can be solved for the density change rate. Assuming instantaneous release of decomposition gas to the exposed surface, MLR per unit area is given by

$$\dot{m}'' = -\int_0^L \frac{\partial \rho}{\partial t}\, dx \tag{4.21}$$

Heat release rate per unit area then can be calculated using

$$\dot{q}'' = \dot{m}'' \Delta H_c \tag{4.22}$$

The effective heat of combustion ΔH_c can be either determined with fire tests or be estimated through a chemical reaction equation. In this study, the effective heat of combustion of E-glass/polyester was obtained from cone calorimeter tests and was equal to 11.5kJ/g.

The heat of gasification is another important fire property because it is used in CFD fire growth models to calculate the mass flux of volatile products from a burning surface. The ratio of the effective heat of combustion to the heat of gasification is an important parameter in assessing the flammability of a material because the ratio is the energy released per energy required to gasify the material [77]. With the knowledge of the net heat flux and MLR, the heat of gasification L_g is given by

$$L_g = \dot{q}''_{net}/\dot{m}'' \tag{4.23}$$

$$\dot{q}''_{net} = \dot{q}''_e + \dot{q}''_{fl} - \dot{q}''_l \tag{4.24}$$

$$\dot{q}''_l = \varepsilon_s \sigma (T_s^4 - T_\infty^4) + h(T_s - T_\infty) \tag{4.25}$$

4.6 Cone Calorimeter Tests

A cone calorimeter was utilized to determine the fire reaction properties of mass loss rate, heat release rate, and time to ignition for the glass/polyester composite specimens. The specimens were 10 cm squares with a thickness of 6 mm. Totally 20 tests were conducted in accordance with ASTM E1354 at heat fluxes of 15, 25, 35, 45, 55, and 65kW/m². Figure 4.2 is a picture of a cone calorimeter test.

Figure 4.2: Cone calorimeter test with E-glass/polyester

Flame heat flux can be determined based on cone calorimeter data [87]. Peak HRR $\dot{q}''_{pk}$ can be described by

$$\dot{q}''_{pk} = \left(\Delta H_c / L_g\right)\dot{q}''_e + \dot{q}''_0 \tag{4.26}$$

$$\dot{q}''_0 = \left(\Delta H_c / L_g\right)(\dot{q}''_{fl} - \dot{q}''_{cr}) \tag{4.27}$$

As shown in Figure 4.3, by plotting peak HRR against applied irradiance $\dot{q}''_e$, the flame heat flux $\dot{q}''_{fl}$ can be obtained from the slope $\Delta H_c / L_g$ and the intercept $\dot{q}''_0$ in which the critical heat flux is assumed to equal to the irradiance at which it takes 20 minutes [83] to ignite a material. Using peak HRR data from cone calorimeter tests, the flame heat flux of E-glass/polyester specimens in cone calorimeter tests is estimated as 23.2kW/m².

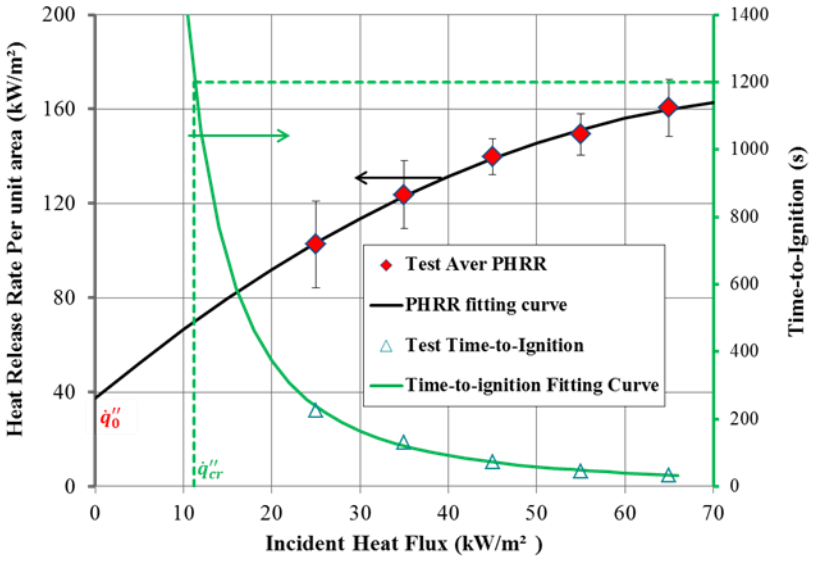

Figure 4.3: Estimation of flame heat flux base on HRR data

4.7 Results and Discussion

The heat transfer model (Equations (4.1)-(4.20)) was solved by commercial software COMSOL [88] for MLR, flame heat flux, including radiative heat flux and convective heat flux from flame, and net heat flux into specimens at the exposed surface of specimens.

The total heat flux and its radiation component are shown in Figure 4.4. The average total flame heat fluxes and the average radiation heat fluxes for incident heat fluxes from 35 to 65kW/m² are near constant values of 18.1 and 15.1 kW/m², respectively.

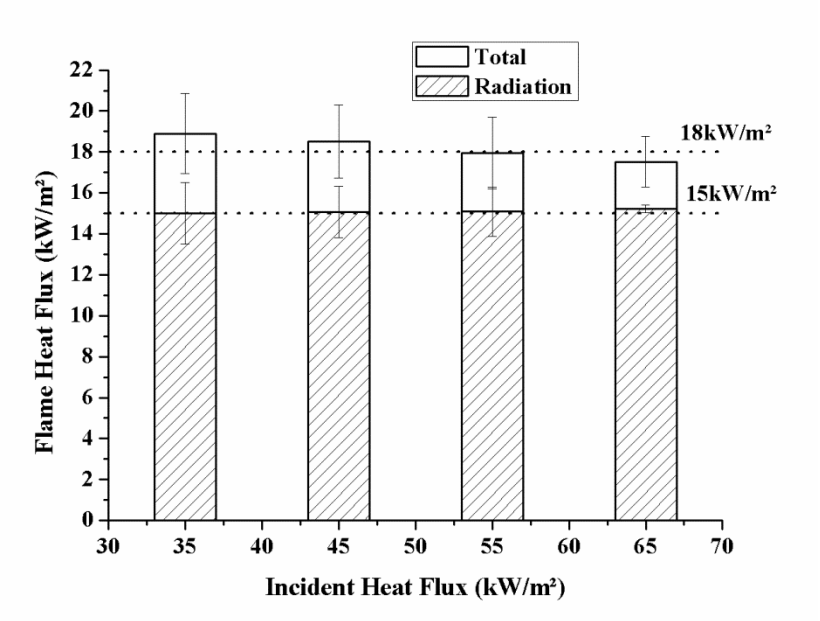

Figure 4.4: Flame heat flux by the two-layer model

Under incident heat flux levels of 15 and 25kW/m², the thermal model predicted that MLR per unit area was below 5g/m².s, an empirical threshold for flaming combustion [77], and therefore no flame heat flux (Equation (4.10)).The constancy of flame heat flux is due to the geometry of the cone flame [78]. A flame in a cone calorimeter test is tall and narrow. The flame shape makes that the lower part of the flame accounts for a determinant fraction of radiative heat flux back to the specimen.

The flame heat flux above was estimated based on the flame temperature of 1022ºC. Solid polymer flame temperature was reported in the range of 917-1127ºC [85-87], which suggests that the total heat flux lies in range of 19.1±6kW/m² based on the two-layer flame model. Thus when the variation of turbulent flame temperature is considered, the total flame heat flux from the model prediction is close to the estimation using experimental data (which is 23.2±4kW/m²).

The effect of flame on the net heat flux at the exposed surface of specimens is shown in Figure 4.5, which measures the actual contribution to the heat transfer process. The flame heat flux adds to net heat flux at the beginning of continuous flaming by 12-16kW/m², depending on the irradiance level, but decreases very quickly to about 3kW/m². This is because of the rapidly increasing the heat loss of the exposed surface due to the increasing surface temperature. It is noted that the value of flame heat flux is not equal to its actual contribution to net heat flux into specimens. The actual contribution of flame heat flux is the difference of net heat flux at the exposed surface of specimens between when flame heat flux is considered and when it is not.

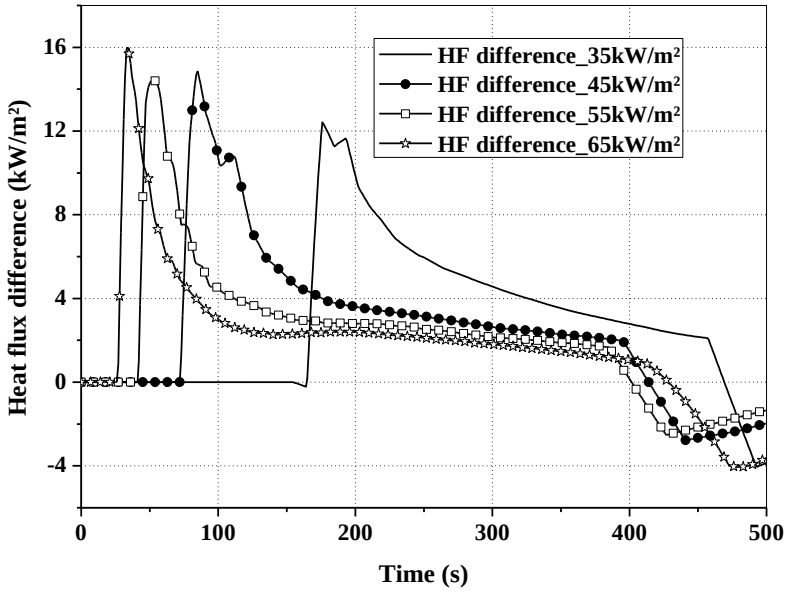

Figure 4.5: Flame's effect on net heat flux into specimens

The predictions of MLR per unit area with and without flame heat flux are compared to experimental data as shown in Figures 4.6(a)-(d). As expected, with consideration of flame heat flux the heat transfer model predicts MLR higher and better than without consideration of flame heat flux. The second MLR peak was not captured by

predictions, which was caused by the assumption in Henderson's model that states no mass loss through the back surface.

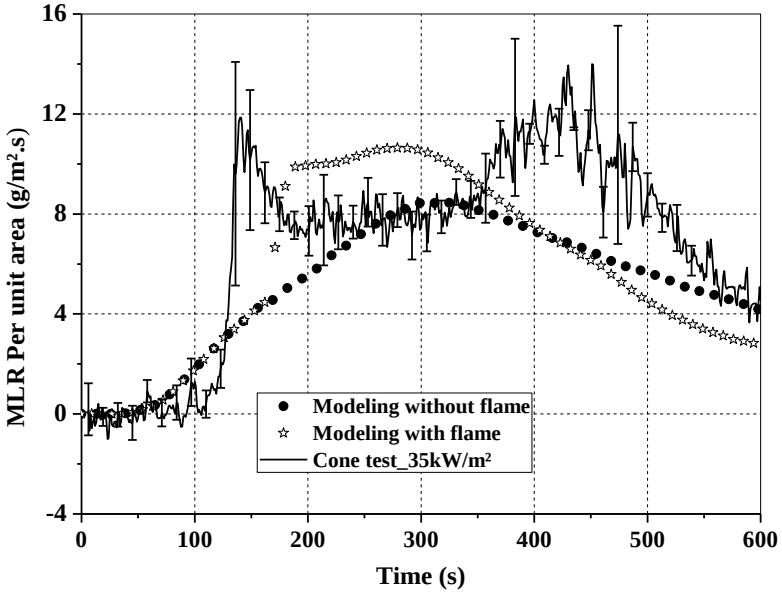

Figure 4.6(a): MLR predictions and cone calorimeter test results at 35kW/m²

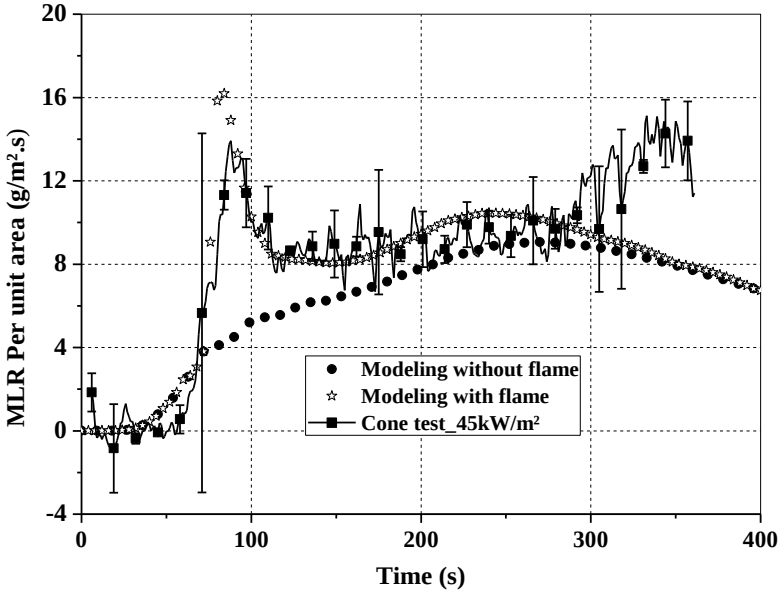

Figure 4.6(b): MLR predictions and cone calorimeter test results at 45kW/m²

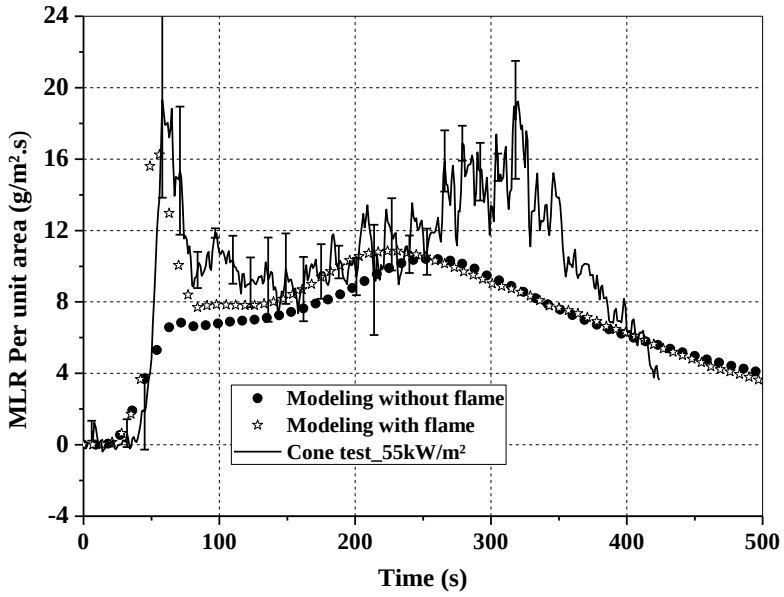

Figure 4.6(c): MLR predictions and cone calorimeter test results at 55kW/m²

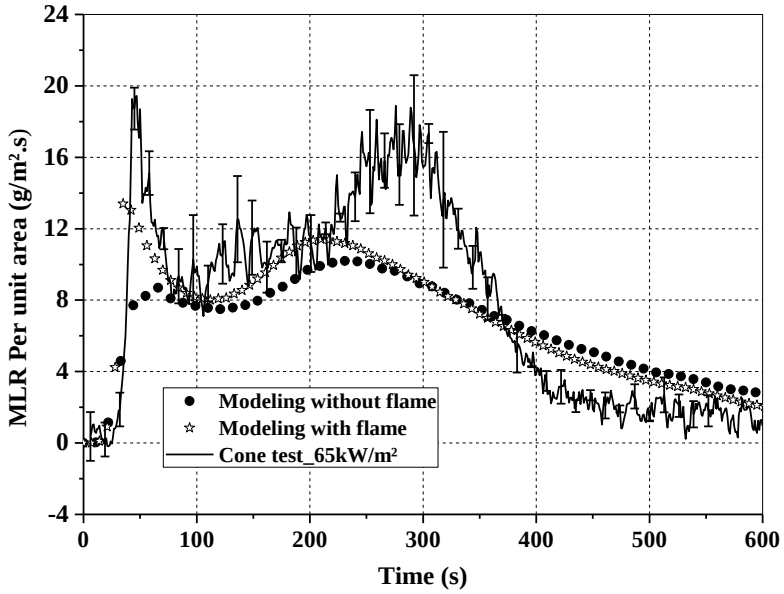

Figure 4.6(d): MLR predictions and cone calorimeter test results at 65kW/m²

Predicted (Equation (4.22)) and experimental HRR results are shown in Figures 4.7(a)-(d). When the effect of flame is included, the heat transfer model over-predicts the first HRR peak and then gives similar results to those without consideration of flame heat

flux. The use of a constant effective heat of combustion may cause the HRR over-prediction.

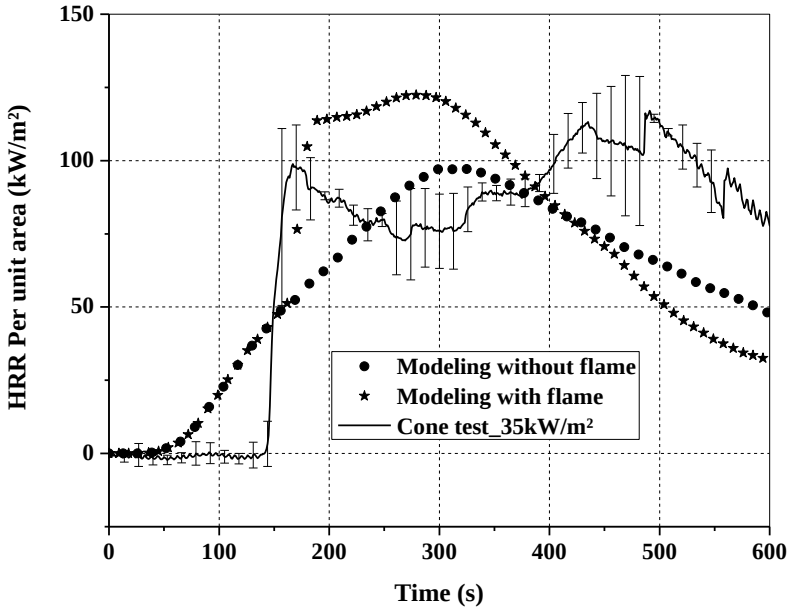

Figure 4.7(a): HRR predictions and cone calorimeter test results at 35kW/m²

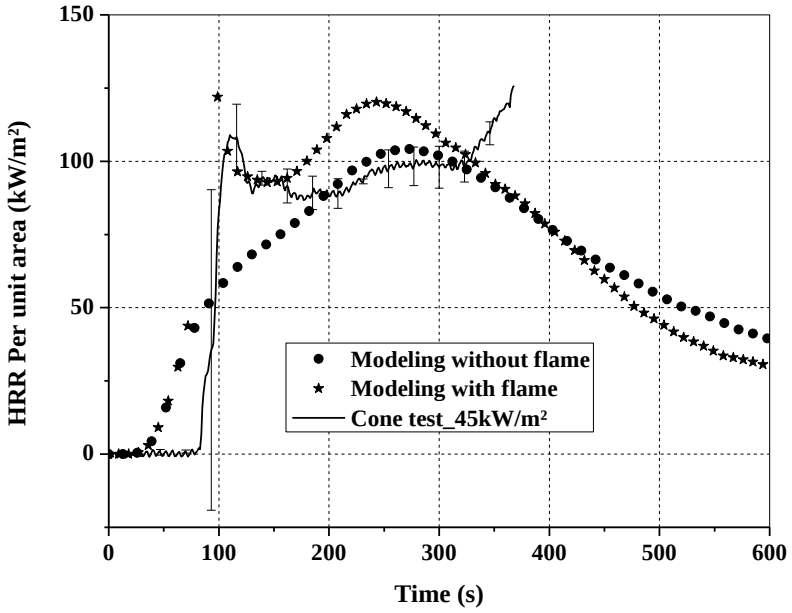

Figure 4.7(b): HRR predictions and cone calorimeter test results at 45kW/m²

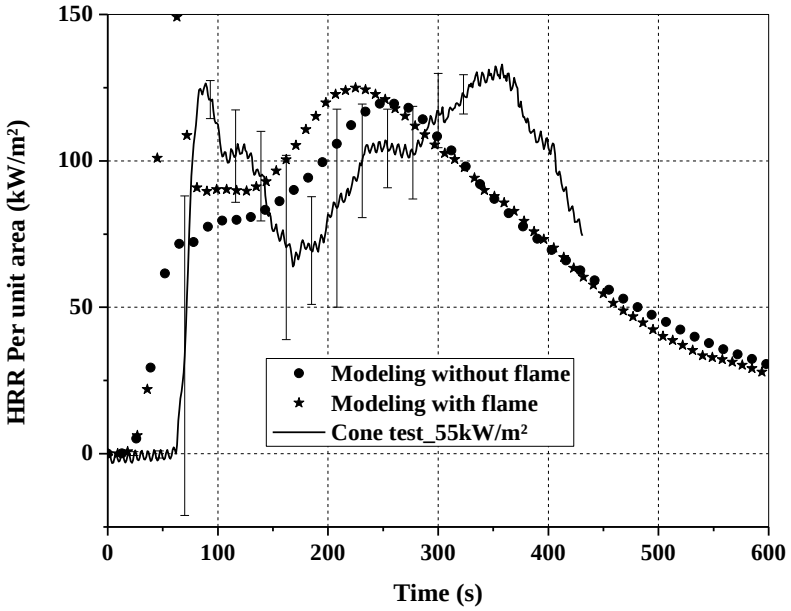

Figure 4.7(c): HRR predictions and cone calorimeter test results at 55kW/m²

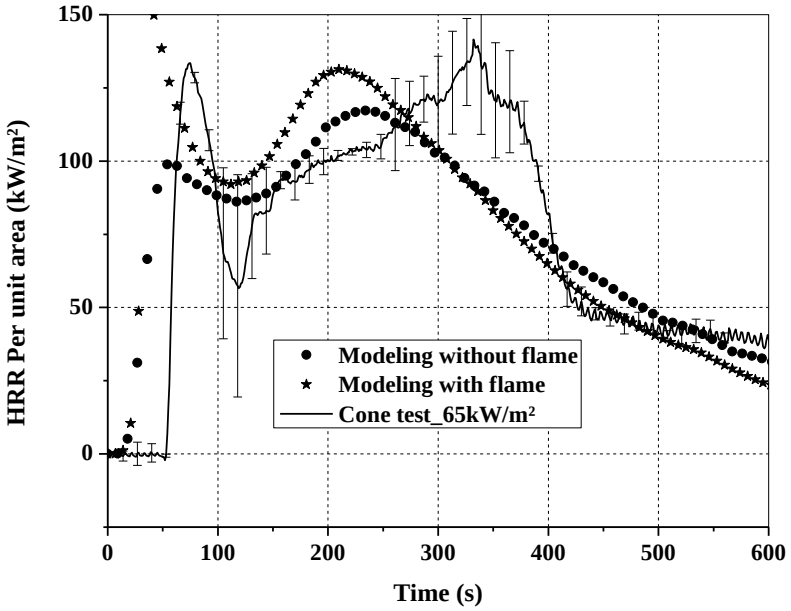

Figure 4.7(d): HRR predictions and cone calorimeter test results at 65kW/m²

From the comparisons of MLR and HRR between predicted and measured results, it can be seen that the flame heat flux has a significant effect only for very limited time

after ignition. Afterwards, the flame heat flux has little influence on both MLR and HRR predictions.

The heat of gasification is also determined with the heat transfer model as shown in Figures 4.8(a)-(d). It can be seen that the flame has little influence on the heat of gasification. The reason is that the heat of gasification is the ratio of net heat flux to MLR (Equation (4.27)) and while increasing the net heat flux the flame increases MLR.

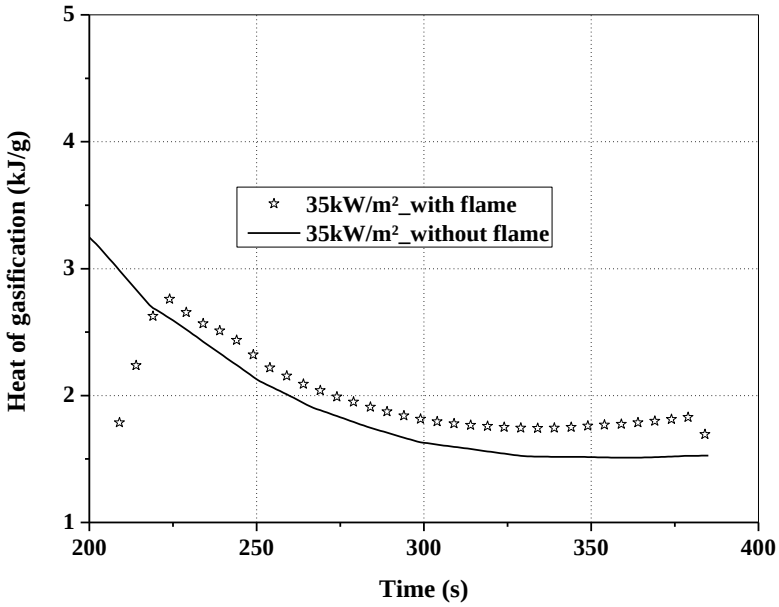

Figure 4.8(a): Determination of heat of gasification with and without flame heat flux at 35kW/m²

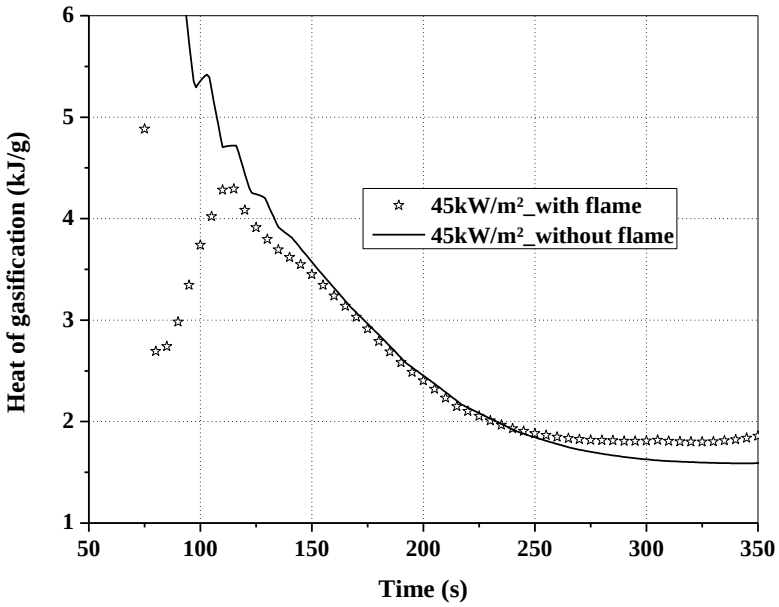

Figure 4.8(b): Determination of heat of gasification with and without flame heat flux at 45kW/m²

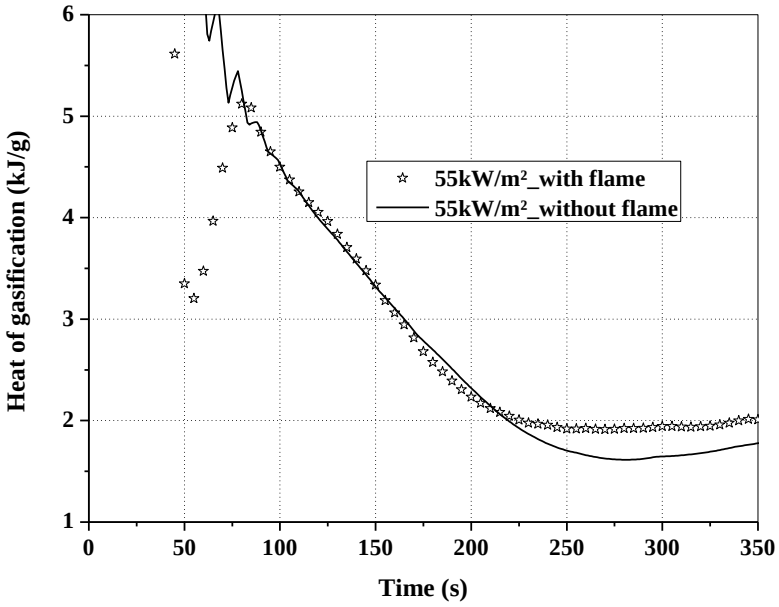

Figure 4.8(c): Determination of heat of gasification with and without flame heat flux at 55kW/m²

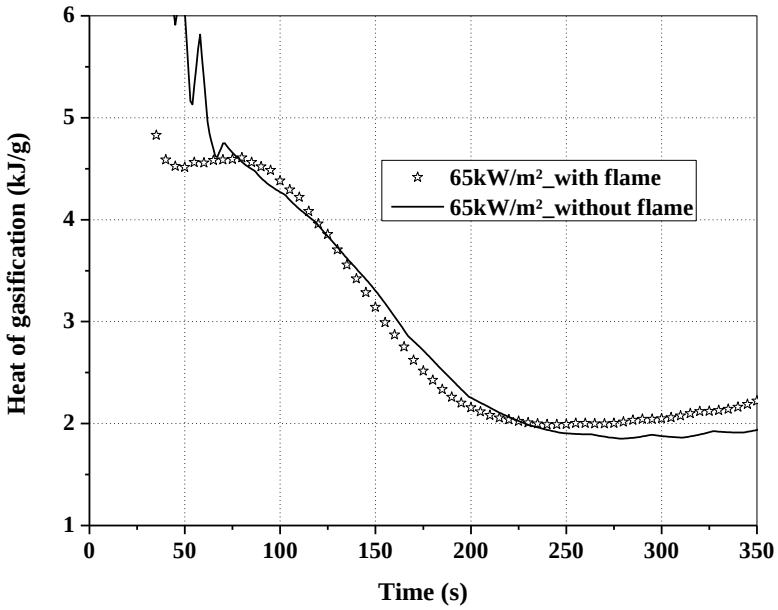

Figure 4.8(d): Determination of heat of gasification with and without flame heat flux at 65kW/m²

4.8 Conclusions

Experimental and modeling studies were conducted to investigate the effect of combustion flame on the thermal response and fire properties of char-forming composite in a cone calorimeter test setting. A simplified two-layer flame model was proposed to estimate the flame heat flux, and was used to predict the flame's effect on the predictions of MLR, HRR, and the heat of gasification of char-forming composite materials. Results from the model showed that the flame heat flux of the E-glass/polyester composite in a typical cone test was in the range of 19.1±6kW/m². While the flame heat flux obtained using experimental cone calorimeter data was determined as 23.2±4kW/m². Predictions from the model demonstrated that the flame heat flux significantly increased both MLR and HRR at the beginning of sustained flaming. However, the influence from flame heat flux on MLR and HRR reduced quickly shortly after flaming ignition. The predictions

further showed that the consideration of flame heat flux made little difference on the prediction of the heat of gasification.

CHAPTER 5: CONCLUSIONS AND FUTURE WORKS

5.1. Conclusions

This research focused on the investigation of the thermal and mechanical responses of fiber reinforced polymers exposed to one-sided heating. Based on the assumption that the decomposition of FRP composites occurs at an infinite rate at a single temperature point, an infinite-rate decomposition model was incorporated into a heat conduction model to predict the temperature profile and mass loss of FRP composites. The results were compared to those obtained from the decomposition described by the n^{th} Arrhenius equation.

To validate the model predictions, bench- and intermediate-scale fire tests were performed with a cone calorimeter and intermediate-scale calorimeter at a set of heat flux levels. It was showed by comparisons of temperature, mass loss, HRR, and char formation between the predictions and experimental data that:

(1) The finite-rate and infinite-rate pyrolysis models can give acceptable predictions,

(2) The infinite-rate model works well for both thermally-thin and thermally-thick conditions and is easier to implement with fewer parameters, and

(3) The effect of the internal gas convection is negligible when the external heat flux is low.

To simplify the prediction of mechanical response of FRP panels under one-sided heating and compressive loading, a plain-strain model was developed to predict

deformation and time-to-failure. In order to consider the effect of delamination on the mechanical response of FRP sandwich panels under the combined thermal and mechanical loading, cohesive elements in commercial finite element software ABAQUS were incorporated into a plane strain model. Based on the concept of fracture energy, a bilinear traction-separation law was assumed to model the constitutive response of the delamination interface. It was validated by furnace test results that:

(1) The plain-strain mechanical model worked well for both single FRP laminates and sandwich FRP structures, and

(2) The effect of delamination in a sandwich FRP structure can be considered with cohesive elements.

To evaluate the effect of thermal feedback of a FRP composite's own flame, a two-layer flame model was proposed to model total, radiation, and convection heat fluxes of the flame in a cone calorimeter testing condition. The flame model used solid polymer flame properties and provided a generalized procedure to estimate the thermal feedback of flame in a cone calorimeter test. It was shown that the flame heat flux significantly increases both MLR and HRR at the beginning of flaming combustion but appears little influence afterwards due to increasing heat loss from the exposed surface.

This research improved the predictions of thermal response of FRP composites by the consideration of flame heat flux, and simplified the predictions of mechanical response with a plain-strain model and introduction of cohesive elements for delamination. The main contributions of the research include (1) an original analytical method to characterize the decomposition of FRP composites, (2) detailed procedures to implement infinite-rate decomposition model with commercial software, (3) the

incorporation of delamination into the plain-strain mechanical model to predict the mechanical response of FRP sandwich structures, and (4) the incorporation of a two-layer flame model into heat transfer models to predict flame heat flux and its effects in a cone calorimeter test.

5.2 Future Work

The thermal feedback of an FRP composite's own flame has not been validated with direct measurements. The total flame heat flux can be measured with a heat flux gauge at heat flux levels of 25, 35, 45, 55, and 65kW/m² in a cone calorimeter. Further, the two-layer flame model was validated with experimental data from the applications of horizontal orientation. A flame at a vertically oriented surface exhibits more complicated fire behaviors. It is desirable and interesting to develop a flame model to predict the thermal feedback of a flame in a vertical surface of FRP composites.

In the prediction of the mechanical response of FRP panels under the combined thermal and compressive loading, the modeling of deformation and delamination can be expanded to three-dimensional applications in the future. Efforts also may be made to model other fire damages, such as matrix cracking.

REFERENCES

1. American Society for Testing and Materials (ASTM), E84-09: Standard Test Method for Heat and Visible Smoke Release Rates for Materials and Products Using an Intermediate Scale Calorimeter (ICAL), ASTM International, West Conshohocken, PA.

2. American Society for Testing and Materials (ASTM), ASTM E119-09: Standard Test Methods for Fire Tests of Building Construction and Materials, ASTM International, West Conshohocken, PA.

3. Sorathia U, Long G, Gracik T, Blum M, Ness J. Screening tests for fire safety of composites for marine applications. *Fire & Materials*, 2001; 25:215-222.

4. Allison DM, Marchand AJ, R.M. Morchat RM. Fire performance of composite materials in ships and offshore structures. Marine Structures, 1991; 4:129-140.

5. American Society for Testing and Materials (ASTM), ASTM 1269 Standard Test Method for Determining Specific Heat Capacity by Differential Scanning Calorimetry, ASTM International, West Conshohocken, PA.

6. American Society for Testing and Materials (ASTM), ASTM E1354-09: Standard Test Method for Heat and Visible Smoke Release Rates for Materials and Products Using an Oxygen Consumption Calorimeter, ASTM International, West Conshohocken, PA.

7. American Society for Testing and Materials (ASTM), ASTM E1623-09: Standard Test Method for Determination of Fire and Thermal Parameters of Materials, Products, and Systems Using an Intermediate Scale Calorimeter (ICAL), ASTM International, West Conshohocken, PA.

8. Janssens M, Parker WJ. Oxygen consumption calorimetry. In: Heat Release in Fires, ed. V. Babrauskas and S.J. Grayson, London: Elsevier Applied Science, pp. 31-59

9. Sultan MA. The effect of furnace parameters on fire severity in standard fire resistance tests. Fire & Materials, 1996; 20:245-252.

10. Mouritz AP, Gibson AG. Fire Properties of Polymer Composite Materials, Springer, Dordrecht, Netherlands, 2006.

11. Pering GA, Farrell PV, Springer GS. Degradation of tensile and shear properties of composites exposed to fire or high temperature. Journal of Composite Materials, 1980; 14:54-66.

12. Henderson JB, Wiebelt JA, Tant MR. A model for the thermal response of polymer composite materials with experimental verification. Journal of Composite Materials, 1985; 19:579-595.

13. Florio J, Henderson JB, Test FL, Hariharan R. A study of the effects of the assumption of local thermal equilibrium on the overall thermally-induced response of decomposition, glass-filled polymer composite. International Journal of Heat & Mass Transfer, 1991; 34:135-147.

14. McManus HL, Springer GS. High temperature behaviour of thermomechanical behaviour of carbon-phenolic and carbon-carbon composites, I. Analysis. Journal of Composite Materials, 1992; 26:206-229.

15. Mouritz AP, Mathys Z. Post-fire mechanical properties of marine polymer composites. Composite Structures, 1999; 47:643-653.

16. Budiansky B, Fleck NA. Compressive Failure of Fibre Composites. Journal of the Mechanics and Physics of Solids, 1993. 41(1): p. 183-211.

17. Boyd SE, Lesko JJ, Case SW. The Thermo-Viscoelastic, Viscoplastic Characterization of Vetrotex 324/Derakane 510A-40 through Tg. Journal of Engineering Materials and Technology, Transactions of the ASME, 2006. 128(4): p. 586-594.

18. International Code Council (ICC), International Building Code, International Code Council, Inc., Washington, DC, 2009.

19. Society of Fire Protection Engineers (SFPE), The SFPE Engineering Guide to Performance-Based Fire Protection (2nd edition), SFPE, Bethesda, Maryland, 2007.

20. American Society for Testing and Materials (ASTM), E1354-09: Standard Test Method for Heat and Visible Smoke Release Rates for Materials and Products Using an Oxygen Consumption Calorimeter, ASTM International, West Conshohocken, PA.

21. American Society for Testing and Materials (ASTM), E 1623-09: Standard Test Method for Heat and Visible Smoke Release Rates for Materials and Products Using an Intermediate Scale Calorimeter (ICAL), ASTM International, West Conshohocken, PA.

22. Blasi CD, The State of the Art of Transport Models for Charring Solid Degradation. Polymer International, 49(10), pp. 1133-1146, 2000.

23. Moghtaderi B. The state-of-the-art in Pyrolysis Modelling of Lignocellulosic Solid Fuels. Fire and Materials, 30(1), pp. 1-34, 2006.

24. Griffis CA, Masumura RA, Chang CI. Thermal Response of Graphite Epoxy Composite Subjected to Rapid Heating. Journal of Composite Materials, vol. 15, pp. 427-442, 1981.

25. Henderson JB, Wiecek TE. A Mathematical-model to Predict the Thermal Response of Decomposing, Expanding Polymer Composites. Journal of Composite Materials, 21(4), pp. 373-393, 1987.

26. Milke JA, Vizzini AJ. Thermal Response of Fire-exposed Composites. Journal of Composites Technology & Research, 13(3), pp. 145-151, 1991.

27. Sullivan RB, A Coupled Solution Method for Predicting the Thermostructural Response of Decomposing, Expanding Polymeric Composites. Journal of Composite Materials, 27(4), pp. 408-434, 1993.

28. Gibson AG, et al. The Integrity of Polymer Composites During and After Fire. Journal of Composite Materials, 38(15), pp. 1283-1307, 2004.

29. Krysl P, et al. Finite Element Modelling of Fibre Reinforced Polymer Sandwich Panels Exposed to Heat, International Journal for Numerical Methods in Engineering, vol. 61, pp. 49-68, 2004.

30. Looyeh MRE, et al. Modelling of Reinforced Polymer Composites Subject to Thermo-mechanical Loading. International Journal for Numerical Methods in Engineering, vol. 63, pp. 898-925, 2005.

31. Lua J. et al. A Temperature and Mass Dependent Thermal Model for Fire Response Prediction of Marine Composites, Composites Part A,37(7), pp. 1024-1039, 2006.

32. Trelles J, Lattimer BY. Modelling Thermal Degradation of Composite Materials, Fire and Materials, vol. 31, pp.147-171, 2007.

33. Bai Y, Vallee T, Keller T. Modeling of Thermal Responses for FRP Composites under Elevated and High Temperatures. Composites Science and Technology, 68(1), Pp. 47-56, 2008.

34. Galgano A, et al. Thermal Response to Fire of a Fibre-reinforced Sandwich Panel: Model formulation, selection of intrinsic properties and experimental validation. Polymer Degradation and Stability, 94(8), pp. 1267-1280, 2009.

35. Mouritz AP, Feih S, Kandare E, Mathys Z, Gibson AG, Des Jardin PE, Case SW, Lattimer BY. Review of fire structural modelling of polymer composites, Composites: Part A, vol. 40, pp. 1800–1814, 2009.

36. Lattimer BY, Ouellette J, Trelles J. Measuring Properties for Material Decomposition Modeling. Fire and Materials, 35(1), pp. 1-17, 2011.

37. Yu Z, Zhou A. Fiber Reinforced Polymer Composite Structures in Fire: Modeling and Validation, Mechanics of Advanced Materials and Structures (accepted for publication).

38. Galgano A, Blasi CD. Infinite- versus Finite-rate Kinetics in Simplified Models of Wood Pyrolysis, Combustion Science and Technology, 177(2), pp. 279-303, 2005.

39. Park WC, Atreya A, Baum HR. Determination of Pyrolysis Temperature for Charring Materials. Proceedings of the Combustion Institute, vol. 32, pp. 2471-2479, 2009.

40. Prime RB, Bair HE, Vyazovkin S, Gallagher PK, Riga A. Thermogravimetric Analysis (TGA), in Thermal Analysis of Polymers: fundamentals and applications, edited by J.D. Menczel and R.B. Prime, pp241-317, John Wiley & Sons, Hoboken, New Jersey, 2009.

41. Menczel JD, Judovits L, Prime RB, Bair HE, Reading M, Swier S. Differential scanning calorimetry (DSC), in Thermal Analysis of Polymers: fundamentals and applications, edited by J.D. Menczel and R.B. Prime, pp7-239, John Wiley & Sons, Hoboken, New Jersey, 2009.

42. Urbas J, Parker JW. Surface Temperature Measurements on Burning Materials Using Infrared Pyrometer: Accounting for Emissivity and Reflection External Radiation. Fire and Materials, vol. 28, pp. 33-53, 2004.

43. Yu Z, Zhou A. Mass Loss of Fiber Reinforced Polymer Composite Materials in Fire. Proceedings of the 2010 SAMPE Conference (CD-ROM), Seattle, Washington, May 17-20, 2010.

44. ASTM, ASTM E1591: Standard Guide for Obtaining Data for Deterministic Fire Models, ASTM International, West Conshohocken, PA, 2007.

45. Samanta A, Looyeh M, Jihan S, McConnachie J. Thermo-mechanical Assessment of Polymer Composites Subject to Fire. Report prepared for Robert Gordon University under EPSRC Project No. GR/N10271, Aberdeen, UK, 2004

46. Cernuschi F, Ahmaniemi S, Vuoristo P, Mantyla T. Modeling of Thermal Conductivity of Porous Materials: Application to Thick Thermal Barrier Coatings. Journal of the European Ceramic Society, vol. 24, pp. 2657–2667, 2004.

47. COMSOL AB, *COMSOL Multi-physics Modeling Guide V3.4*, COMSOL AB, 2007.

48. Bausano JV, Boyd S, Lesko J, Case S. Composite life under sustained compression and one sided simulated fire exposure: Characterization and prediction, Composites Part A: Applied Science and Manufacturing, vol. 37, pp. 1092-1100, 2006

49. Keller T, Tracy C, Zhou A. Structural response of liquid-cooled GFRP slabs subjected to fire: Part II. Thermo-chemical and thermo-mechanical modeling, Composites Part A, vol. 37(9), pp. 1296-1308, 2006

50. Zhou A, Keller T. Structural responses of FRP elements under combined thermal and mechanical loadings: experiments and analyses, 4th Int. Conf. on the Response of Composite Materials to Fire, Newcastle, U.K, 2005.

51. Lua J. Hybrid progressive damage prediction model for loaded marine sandwich composite structures subjected to fire, Fire Technology, DOI: 10.1007/s10694-009-0124-6, 2009.

52. Gu P, Asaro RJ. Structural buckling of polymer matrix composites due to reduced stiffness from fire damage, Composite Structures, vol. 69, pp. 65-75, 2005

53. Kim J, Lee SW, Kwon S. Time-to-failure of compressively loaded composite structures exposed to fire, Journal of Composite Materials, vol. 41(22), pp. 2715-2735, 2007.

54. **ABAQ**US (2007). ABAQUS Analysis User's Manual (v.6.7), Simulia Inc., Providence, RI.

55. Strauch EC, Strait LH. Characterization of strain energy release rate for primary and secondary scrimp bondlines in composite panels, Technical Memorandum, Applied Research Laboratory, Pennsylvania State University, PA, 1999.

56. ISO. (1999). Fire-resistance tests -Elements of building construction - Part 1: General requirements, ISO 834-1:1999, International Organization for Standardization (ISO), Geneva, Switzerland.

57. Feih S, Mathys Z, Gibson AG, Mouritz AP. Modeling the tension and compression strengths of polymer laminates in fire, Composites Science and Technology, vol. 67, pp 551–564, 2007.

58. Asaro RJ, Lattimer BY, Ramroth W. Structural response of fiber reinforced plastic composites during fires, Composite Structures vol. 87, pp. 382-393, 2005

59. Lattimer BY, Quellette J. Properties of composite materials for thermal analysis involving fires, Composites: Part A, vol. 37 (7), pp. 1068–1081, 2006.

60. Easterling KE, Harryson R, Gibson LJ, Ashby MF. On the mechanics of balsa and other woods, Proceeding of the Royal Society of London, Series A, Mathematical and Physical Sciences, The Royal Society, London, pp. 31-41, 1982.

61. Lattimer BY, Quellette J, Trelles J. Thermal response of composite materials to elevated temperatures." Fire Technology.DOI: 10.1007/s10694-009-0121-9, 2009.

62. Quintiere JG. A semi-quantitative model for the burning of solid materials. *NIST-4840*, National Institute of Standards and Technology, June 1992.

63. Beaulieu PA, Dembsey NA. Effect of oxygen on flame heat flux in horizontal and vertical orientations, *Fire Safety Journal* 2008;**43**: 410-428

64. Petrella RV. The mass burning rate of polymers, wood and organic liquids. *J Fire Flammability* 1980; **11**:3-20.

65. Azhakesan MA, Shields TJ, Silcock GWH. On the nature, influence and magnitudes of flame heat transfer during surface flame spread. Fire Safety Journal 2000; **35**:189-222

66. Rhodes BT, Quintiere JG. Burning rate and flame heat flux for PMMA in a cone calorimeter. *Fire Safety Journal* 1996; **26**: 221-240

67. Luo C, Xie W, DesJardin PE. Numerical simulation of composite structure response from a fire plume. *Proceedings of the SAMPE 2005 symposium & exhibition.*

68. Luo C, Xie W, DesJardin PE. Fluid–structure simulations of composite material response for fire environments. *Modeling of naval composite structures in fire.* Melbourne: Acclaim Printing; 2006.

69. Chen L, Luo C, Lua J, Shi J, A direct coupling approach for fire and composite structure interaction. *Proceedings of the 17th international conference on composite materials* 2009; 27–31, Edinburgh, UK; 2009.

70. Tant MR, Henderson JB, Boyer CT. Measurement and modeling of the thermochemical expansion of polymer composites. *Composites* 1985; **16**:121–6.

71. Henderson JB, Doherty MP. Measurement of selected properties of a glass-filled polymer composite. *High Temp–High Press* 1987; 19:95–102.

72. Florio J, Henderson JB, Test FL. Measurement of the thermochemical expansion of porous composite materials. *High Temp–High Press* 1989; **21**:157–65.

73. McManus HL, Springer GS. High temperature behavior of thermomechanical behavior of carbon–phenolic and carbon–carbon composites, II. Results. J Compos Mater 1992; **26**:230–55.

74. Gibson AG, Wu YS, Chandler HW, Wilcox JAD, Bettess P. A model for the thermal performance of thick composite laminates in hydrocarbon fires. *Rev L'Inst Franc Petrol* 1995; **50**:69–74.

75. Yu Z, Zhou A. Fiber reinforced polymer composite structures in fire: modeling and validation. *Mechanics of Advanced Materials and Structures*, 2011, in press.

76. Zhou A, Yu Z. Validating thermal response models using bench-scale and intermediate-scale fire experiment data. *Mechanics of Advanced Materials and Structures*, 2011, accepted for publication.

77. Quintiere J. burning rate, *Principles of fire behavior*, Delmar Publisher.

78. Braun E, Levin BC. Polyesters: a review of the literature on products of combustion and toxicity. *Fire and Materials* 1986; **10**: 107-123

79. Orloff L, Modak A, Alpert R. Burning of large scale vertical surfaces, in: the *16th International Symposium on Combustion*, Combustion Institute, The Combustion Institute, Pittsburg, PA, 1974

80. deRis JN. Fire Radiation-a Review, in: *Proceedings of the 17th International Symposium on Combustion*, pp. 1003-1016, 1979.

81. Orloff L. Simplified radiation modeling of pool fires, in: *Proceedings of* the 18th *International Symposium on Combustion*. 1981, pp. 549-562.

82. Shaddix C, Smyth K. Laser induced incandescence measurements of soot production in steady and flickering methane, propane and ethylene diffusion flames, *Combust, Flame* 1996; **107**: 418-452.

83. Jiang F. Flame Radiation from Polymer Fires, *Fire Safety Journal* 1998; **30:** 383-395.

84. Heskestad G. Luminous heights of turbulent diffusion flames, *Fire Safety Journal* 1983; **5**: 103-108.

85. Egglestone GT, Turley DM. Flammability of GRP for use in ship superstructures. *Fire and Materials* 1994; **18**: 255-260

86. Tewarson A. Flammability of polymers. *Plastics and the Environment*, Hoboken, NJ: John Wiley and Sons, 2003

87. Shields TJ, Azhakesan MA, Silcock GWH. The creation, development and application of a strategy for the classication of building materials using a cone calorimeter. FireSERT Centre, University of Ulster, Report to the DOE, UK. Project No: 7/6/709, December 1995.

88. *COMSOL Multiphysics Modeling Guide V3.5*, COMSOL AB, 2007.

89. Feih S, Mathys Z, Gibson AG, Mouritz AP. Modelling the compression strength of polymer laminates in fire. Composites: Part A 2007; **38**: 2354–2365

90. Tien CL, Lee KY, Stretton, AJ, *SFPE Handbook of Fire Protection Engineering*. National Fire Protection Association, 1988, pp. 1-92-1-105.

91. Holman JP, *Heat Transfer*. McGraw-Hill, Scarborough, CA, USA, 1976.